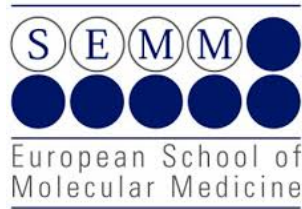PhD degree in Systems Medicine (curriculum in Molecular Oncology)
European School of Molecular Medicine (SEMM),
University of Milan and University of Naples "Federico II"

Settore disciplinare: MED/04

iNKT cells contribute to colorectal cancer progression

inducing neutrophils pro-tumorigenic functions

Georgia Lattanzi
Matricola: R12402

European Institute of Oncology (IEO), Milan

Tutor: Dr. Federica Facciotti
IEO and University of Milano-Bicocca

PhD Coordinator: Prof. Saverio Minucci

Internal examiner:
Prof. Massimiliano Pagani, IFOM, Milan

External examiner:
Dr. Patricia Barral, The Francis Crick Institute, London

Academic year 2021-2022

Table of Contents:

List of Abbreviations:

αGalCer: alpha Galactosyl Ceramide

AOM: Azoxymethane

APC: Adenomatous polyposis coli

APCs: Antigen presenting cells

APC$^{Min/+}$: Adenomatous polyposis coli-multiple intestinal neoplasia

ASV: Amplicon Sequence Variants

ATAC: Assay for Transposase-Accessible Chromatin

AUC: Area under the curve

Bft: *Bacteroides fragilis* toxin

BMDCs: Bone marrow derived dendritic cells

CAF: Cancer associated fibroblasts

CAR: Chimeric Antigen Receptor

CEACAM: CEA Cell Adhesion Molecule

CCL: C-C Motif chemokine ligand

CD: Cluster of differentiation

CD: Crohn's Disease

COAD: Colon adenocarcinoma

CRC: Colorectal Cancer

CXCL: Chemokine (C-X-C motif) ligand

DCs: dendritic cells

DNMT: DNA methyltransferases

DSS: Dextran sodium sulfate

EGFR: Epidermal growth factor receptor

ELISA: Enzyme-linked immunosorbent assay

EMT: Epithelial to mesenchymal transition

EOMES: Eomesodermin

FACS: Fluorescence activated cell sorting

FAP: Familial Adenomatous Polyposis

FasL: Fas ligand

FBS: Fetal bovine serum

FDA: Food and drug administration

FDR: False discovery rate

FMO: Fluorescent minus one

FMT: Fecal Microbiota transplantation

Fn: Fusobacterium nucleatum

GEO: Gene Expression Omnibus

GNLY: Granulysin

GrzA: granzyme A

GrzB: Granzyme B

GZM: Granzyme

HBSS: Hanks′ Balanced Salt Solution

HLA: human leukocyte antigen

HR: Hazard Ratio

IBD: Inflammatory Bowel Diseases

I.c.: Intracecally

ICAM1: Intercellular Adhesion Molecule 1

ICI: Immune checkpoint inhibitors

IEC: Intestinal epithelial cells

IEO: European Institute of Oncology

IFNγ: Interferon gamma

IL: Interleukin

ILCs: Innate lymphoid cells

iMFI: Integrated mean fluorescent intensity

iNKT: invariant Natural Killer T

I.p: Intraperitoneally

IVIS: *In vivo* imaging system

LDH: Lactate dehydrogenase

LPMC: Lamina propria mononuclear cells

LTB: Lymphotoxin-beta

MAIT: Mucosal-associated invariant T cells

MAPK: Mitogen-activated protein kinase;

MCT: Monocarboxylate transporters

MDSC: Myeloid derived suppressor cells

MHC-II: Major histocompatibility complex II

MMP: Matrix metalloproteinase

MMR: Mismatch repair

moDC: Monocytes-derived dendritic cells

NCT: Non-tumor colon tissue

NF-kB: nuclear factor 'kappa-light-chain-enhancer' of activated B-cells

NK: Natural Killer

NKG7: Natural Killer Cell Granule Protein 7

NET: Neutrophil extracellular trap

NS: Non-stimulated

OS: Overall survival

PBMC: Peripheral blood mononuclear cells

PBS: Phosphate buffered saline

PCA: Principal component analysis

PCR: Polymerase chain reaction

PD-1: Programmed cell death protein 1

PD-L1: Programmed death ligand 1

PI3K: Phosphoinositide 3-kinases

PPLZF: Promyelocytic leukemia zinc finger

RFS: Relapse-free survival

RNA: Ribonucleic acid

ROS: Reactive oxygen species

SCFA: Short chain fatty acids

siMFI: Scaled integrated mean fluorescent intensity

SMA: Smooth muscle actin

SNN: Shared nearest neighbour

SPF: Specific pathogen free

TAMs: Tumor-associated macrophages

TANs: Tumor-associated neutrophils

TBX21: T-box transcription factor21

TCGA: The Cancer Genome Atlas

TCR: T cell receptor

Tet: Tetramer

TGFβ: Transcription growth factor-β

Th1/Th2: T helper 1/T helper 2

TIGIT: T cell immunoreceptor with Ig and ITIM domains

TIM3: T cell immunoglobulin and mucin domain-containing protein 3

TLR: Toll-like receptor

TMB: tetramethylbenzidine

TME: Tumor microenvironment

TNFα: Tumor-necrosis factor alfa

TRAIL: Tumor necrosis factor-related apoptosis inducing ligand

TRAMP: Transgenic adenocarcinoma of the mouse prostate

t-SNE: t-Distributed stochastic neighbor embedding

TUM: Tumor lesion

UMI: Unique molecular identifier

VEGF: Vascular endothelial growth factor

ZBTB16: Zinc finger and BTB domain containing 1

List of Figures:

List of Tables:

Abstract

Colorectal cancer (CRC) is a multifactorial disease driven by genetic alterations, environmental factors and inflammation [1]. Inflammation is a hallmark of cancer with opposite roles in CRC [2]–[4]. Hyperactivation of immune cells can lead to chronic colitis and colitis-associated CRC [2], equally hyporesponsive immunity can promote disease progression [3], while anti-tumorigenic immunity efficiently limits tumor growth [4]. Mucosal immunity is involved in the patrolling of intestinal tissues and in the maintenance of homeostasis [5]. Disruption of intestinal homeostasis leads to different pathologies, among which CRC [6]. Invariant Natural Killer T (iNKT) cells are a lipid-specific, CD1d-restricted population of unconventional T cells [7] residing also in the intestinal mucosa [8]. Although their role in inflammation [9], infection [10] and in tumor immune surveillance [11] has been extensively elucidated, iNKT cells involvement in CRC progression remains controversial [12]–[15].

Here, by analyzing a cohort of 118 CRC patients we showed that human tumor-infiltrating iNKT cells acquire a pro-tumorigenic, exhausted phenotype characterized by high expression of PD-1, GM-CSF and IL17, while they maintain cytotoxic properties in the paired non-tumor tissue site. The phenotype of intra-tumor iNKT cells was induced by CRC-associated microbiota and *Fusobacterium nucleatum (Fn)*. Priming with *Fn* did not influence the killing capabilities of iNKT cells *in vitro*, while it induced their expression of GM-CSF, IL17 and neutrophil-chemotactic genes. The existence of an iNKT-neutrophil crosstalk was confirmed by *ex vivo* correlative analysis and *in vitro* functional assays. Three different murine models of CRC revealed that iNKT cells promote tumor growth inducing a pro-tumorigenic polymorphonuclear-myeloid derived suppressor cell (PMN-MDSC) gene signature in tumor associated neutrophils (TANs). Importantly, *in vivo* treatment with αGalCer restored tumor control and iNKT cell cytotoxic functions. Survival analyses of human CRC patients showed that co-infiltration by iNKT cells and TANs led to unfavorable prognosis.

Our results identified a functional role for iNKT cells in the pathogenesis of CRC, promoting pro-tumorigenic properties on TANs, and suggest a direct implication of the CRC-associated microbiota in the process. The targeted manipulation of iNKT cells restored their anti-tumorigenic properties, thus highlighting their potential use for novel cancer immunotherapies.

1 Introduction

1.1 Colorectal Cancer and its etiology

Colorectal cancer (CRC) is the third most prevalent cancer worldwide and the second leading cause of cancer-related death despite advances in its prevention and treatments [16]. By the end of 2030, CRC is estimated to be the leading cause of cancer related death in the population aged 20-49 [1]. Both genetic and environmental factors play a pivotal role in its etiology [1]. The vast majority of CRC cases are nonhereditary, sporadic tumors that originate from premalignant polyps within aberrant crypts [17]. The progression of CRC is provoked by the accumulation of genetic mutations and epigenetic alterations along with the activation of oncogenes and the inactivation of tumor suppressor genes, in the so-called adenoma to carcinoma sequence [17], [18] (Figure 1.1).
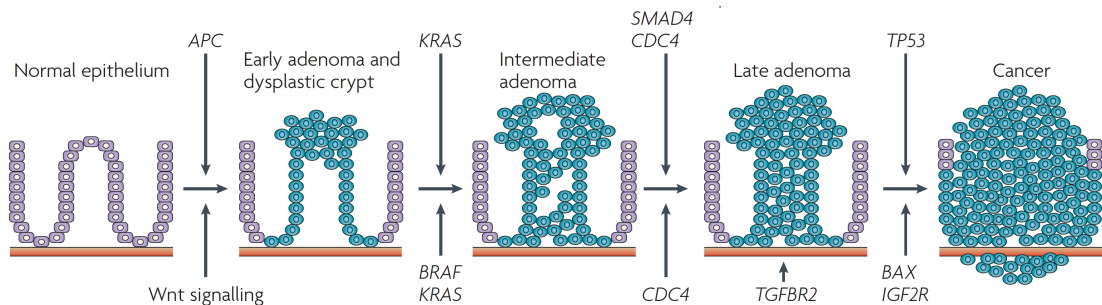
Figure 1.1: Representation of the Adenoma-Carcinoma sequence. The initial step of adenoma formation is associated with loss of APC, followed by mutations in the GTPase KRAS or BRAF and by loss of SMAD4 and CDC4. Mutations in the TP53 gene lead to carcinoma. In microsatellite instable tumors, mutations affecting microsatellites in TGFβ receptor 2 (TGFBR2), insulin-like growth factor 2 receptor (IGF2R) and BAX cause TP53-independent progression to carcinoma. Adapted from Axel Walther, et al., Nature Reviews Cancer, 2009, [18].

Early genetic mutations comprise genes such as adenomatous polyposis coli (*APC*) affecting the Wnt/β-catenin signaling pathway that regulates key cellular functions such as proliferation, genetic stability and stem cell renewal [17]. First genetic events are followed by deregulation of the MAPK (*KRAS* or *BRAF* mutations), PI3K and p53 signaling pathways [18], leading to uncontrolled cell growth. Whole exome sequencing on premalignant colorectal adenoma and serrated polyps was used to identify

carcinogenic driver mutations, and confirmed the presence of truncated *APC* [19]. The laboratory of William Dove exploited the effect of N-ethyl-N-nitrosourea, a potent mutagen, on the *APC* gene and generated the *APC*^*Min/+* mouse model of intestinal cancer [20], which is nowadays one of the most widely used preclinical model for this disease [21]. The adenoma-carcinoma sequence takes approximately 10-15 years [18], but it can be accelerated in certain settings of familial CRC such as Lynch syndrome and Familial Adenomatous Polyposis [22]. In addition to defined genetic mutations, CRC is characterized also by structural and chromosomal abnormalities [23] and by pervasive epigenetic alterations [24]. Although the heterogeneity of genetic alterations has been well described it fails to predict patient survival and therapy response [3].

Indeed, CRC formation, progression and treatment is highly dependent also on the activity of all the components of the surrounding tumor microenvironment (TME) and not only on the genetic background of neoplastic cells [25]–[27].

1.2 The tumor microenvironment in CRC

The TME is an active promoter of cancer progression and it consists of several cellular and non-cellular components summarized in Figure 1.2 [27].
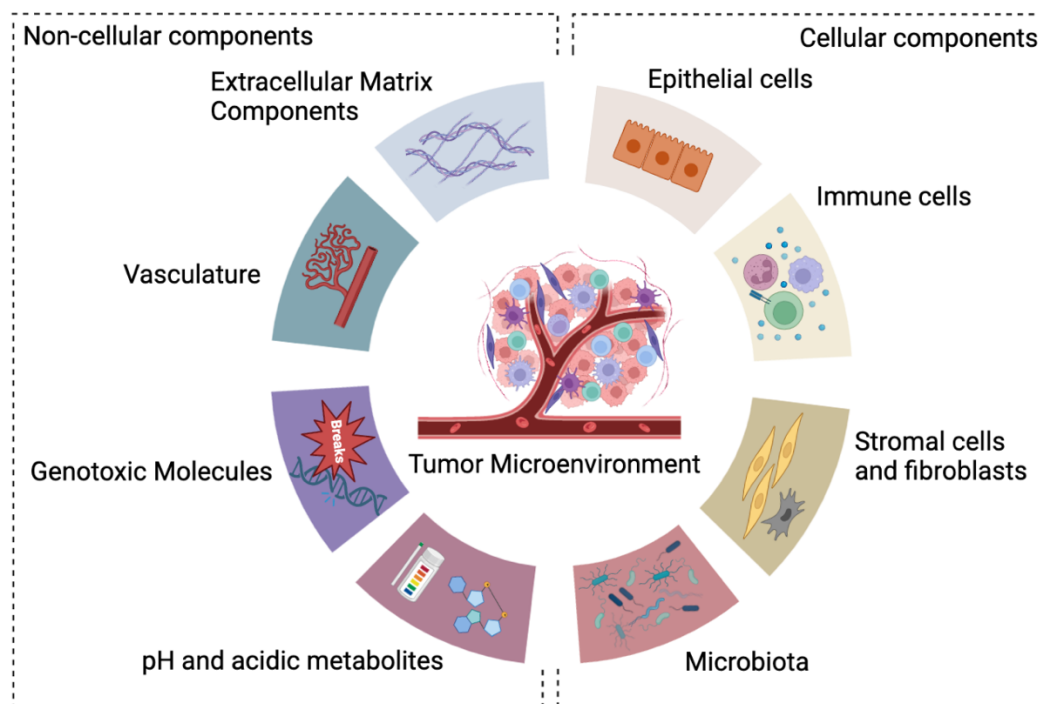
Figure 1.2*: Schematic representation of cellular and non-cellular components of the Tumor Microenvironment. Cellular components are: epithelial cells, immune cells, stromal cells, fibroblasts and the microbiota; while non-cellular components are: elements of the extracellular matrix, the*

Cancer development is accompanied by continuous changes in the extracellular matrix (ECM) composition, in the vasculature structure with the induction of angiogenesis, in the production of genotoxic molecules, in pH condition, in cell structure and composition (*i.e.* epithelial cells, stromal cells and fibroblasts) [28]–[30] and in the recruitment and differential activation of immune cells [2], [3] as well as in microbiota composition [31], [32].

Dysregulation of ECM remodeling and stiffness can favor tumor formation by direct release of angiogenic factors (*i.e.* Collagen IV-cryptic epitopes) [29], of ECM-anchored growth factors (*i.e.* Vascular endothelial growth factor VEGF or TGFβ) [33] and it can promote tumor metastasis by inducing epithelial to mesenchymal transition (EMT) of tumor cells [29]. EMT is a multifaceted and dynamic progress of epithelial cells remodeling. Epithelial cells lose their apical and basal polarity and acquire mesenchymal features, associated with loss of adhesion molecules, cytoskeleton remodeling and increased cell motility [34]. This phenomenon is at the basis of the multistep process of tumor invasion and metastasis and leads to the development of aggressive tumors with low survival probabilities [35]. Changes in oxygen and nutrient availability also influence tumor development. Hypoxia stimulates ECM stiffness to favor cancer progression and metastasis [27], by regulating the expression of collagen modifying enzymes, such as matrix metalloproteinase (MMP)-2 and MMP9 [36]. Tumor cells adapt to hypoxic conditions by upregulating the glucose-transporter GLUT-1 and shifting their energy metabolism toward anaerobic glycolysis [37]. The metabolic shift toward glycolysis is not only a consequence of hypoxia but it is a general hallmark of cancer [38]. Tumor cells undergo aerobic glycolysis in normoxia, as described by the Warburg effect [38], gaining proliferative advantages compared to normal cells. Moreover, the glycolytic shift leads to an elevated production of lactate to which tumor cells respond by upregulating the production of monocarboxylate transporters (MCT)-1, MCT-2 and MCT-4 [39], that are used to direct lactate in and out of the cell. This causes a strong acidification of the TME which induces the death of normal cells, the ECM remodeling and it promotes tumor invasion [39].

Along with structural and biochemical alterations, the TME undergoes cellular changes that can favor or hamper tumor development [26], [27]. CRC is defined as an

heterocellular system [40] meaning it is composed of multiple cell types (Figure 1.3) that are likely to affect each other.
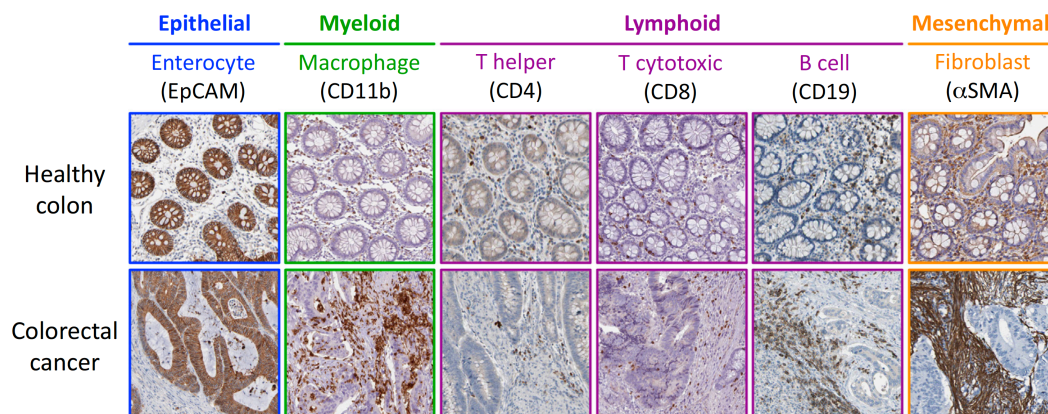
Figure 1.3: Different cellular components of CRC. Both Healthy colons (up) and Colorectal cancer (bottom) tissues contain EpCAM+ epithelial cells, CD11b+ myeloid cells, CD4+, CD8+ T cells and CD19+ B cells and αSMA+ (smooth muscle actin) mesenchymal fibroblasts. Adapted from Christopher J. Tape, Trends in Cancer, Opinion 2016. [40]

Immune cells, cancer associated fibroblasts (CAFs) and stromal cells infiltrate malignant lesions and have disparate roles [27]. For instance, CAFs are shown to promote CRC formation through paracrine activation of tumor-initiating stem cells and angiogenesis, and metastasis through stromal activation of the interleukin (IL)6-STAT3 signaling pathway [41]. CAFs in CRC are characterized by specific frequencies and patterns of somatic copy number alterations and functional transcriptomics as well as by upregulated transcription growth factor β (TGFβ) signaling [42], which induces CRC initiation and metastasis. Stromal cells promote tumor growth by providing structural and physical help to tumor cells [43]. For instance, they favored tumor establishment and growth in a 3D model of CRC, by promoting an immunosuppressive tumor microenvironment [44]. Immune cells of both the innate and the adaptive immunity, and their inflammatory functional responses actively shape the TME, dictating different disease developmental trajectories.

1.3 Immune cells and inflammatory cues of CRC

Inflammation can influence tumor development at all steps of carcinogenesis, having disparate and opposite roles in the pathophysiology of CRC [2]–[4]

Immune responses can cause tumor formation by direct DNA damage of intestinal epithelial cells (IEC) which promote tumor stem cell selection [45], or by causing epigenetic changes [46], chromosomal alterations and microsatellite instability [47]. Inflammation can influence the TME and promote pro-tumorigenic features such as angiogenesis, metabolic changes and the release of growth factors [29], [46]–[48] (Figure 1.4).
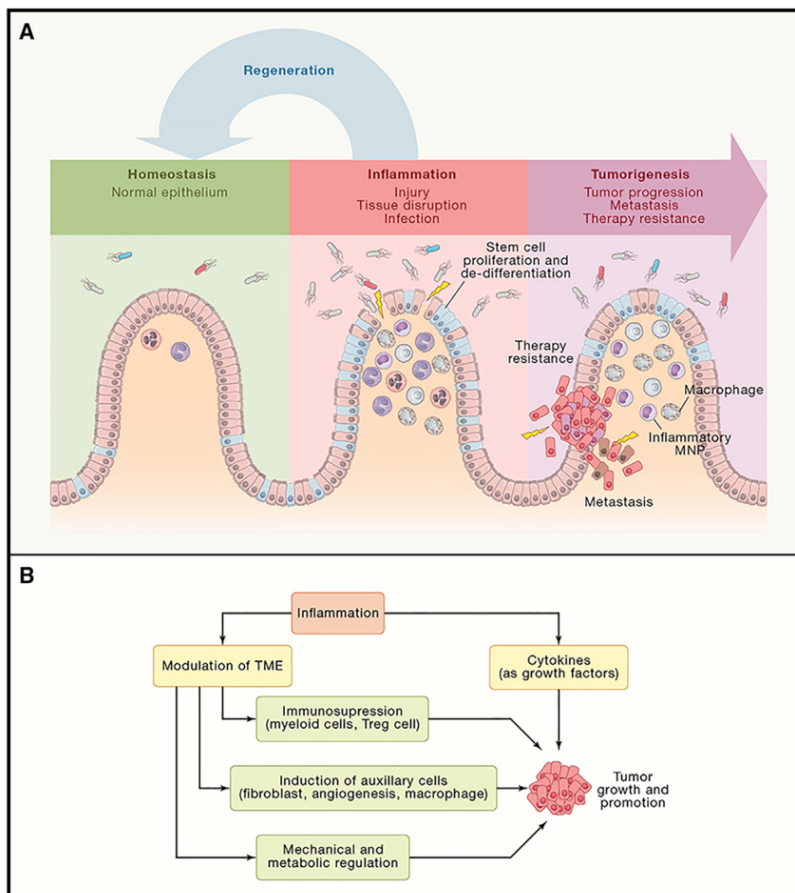
Figure 1.4: Pro-tumorigenic features of inflammation in CRC formation. A) Inflammatory processes following tissue injury or infection leading to tumor formation and progression through cancer stem-cell proliferation and epithelial cells de-differentiation. B) Schematic representation of TME modulation by inflammation. Adapted from Florian R. Greten and Sergei I. Grivennikov, Immunity Review, 2019 [2].

Inflammatory cytokines such as tumor necrosis factor α (TNFα), IL6, IL1β and IL17A can induce tumorigenesis by promoting NF-kB signaling pathway and βcatenin/Wnt-dependent transcription of intestinal stem cell genes [4], fostering de-differentiation and acquisition of stem cell properties on IEC. Specialized intestinal secretory cells, namely Paneth cells, can also undergo processes of de-differentiation and tumor promotion in inflammatory conditions through the Wnt signaling axis [49]. Inflammation, specifically high levels of IL6 and IL11, correlate with excessive activation of the STAT3 signaling pathway in solid tumors [50]. In murine models of CRC, IL6 and IL11 promote IEC survival, proliferation and hasten the onset of the disease by activating the Stat3 cascade [50], [51]. The arising of cancerogenic lesions in excessive inflammatory conditions is accompanied by differential pattern of DNA methylation in epithelial cells [52]. IL1β, IL6, IL22 and TNF activate DNA methyltransferases (DNMT)1 and 3, regulating gene expression and proliferative characteristics [53]. Microsatellite and chromosomal instability are also affected by inflammation [47]. For instance, mismatch repair proteins (MMR), involved in the maintenance of genetic stability, are downregulated by inflammatory messengers through several mechanisms. IL6, IL1β and reactive oxygen species (ROS) promote nuclear translocation of the MMR protein MSH2 into the cytosol, causing genetic alterations in CRC epithelial cell lines [54]. In different murine models of colitis-associated CRC the pro-inflammatory cytokine IL17A is associated with increased tumor burden, as its pharmacological blockade [55] or genetical ablation [56] reduce tumorigenesis through Stat3 activity.

Inflammatory mediators, cytokines and factors can be produced by immune cells belonging to the innate [48] and the adaptive immunity [46] as well as by CAFs [26], [27] and transformed epithelial cells [26], [27]. Additionally, each cell population can influence the functionalities of the other populations [40], thus indirectly influencing tumor development.

1.3.1 Innate immune responses in CRC

Upon tissue injury, infection or abnormal cell proliferation, innate immune cells are activated and promote recruitment of other immune cells to the site of interest [48]. The major effector cells of the innate immunity are: dendritic cells (DCs), monocytes, macrophages, neutrophils, natural killer (NK) cells and innate lymphoid cells (ILCs) [48].

In CRC, innate immune cells profoundly affect the TME, having the ability to directly attack tumor cells but also to initiate adaptive immune responses [57]. For instance, the lymphoid populations of NK cells and ILCs have been detected in human CRC biopsies and, due to their potent anti-tumorigenic functions are nowadays proposed as novel cellular immunotherapies [58]. However, based on transcriptomic and high-dimensional flow cytometry analysis, a high degree of functional innate immune cell plasticity is found in tumors [59], raising concerns regarding their unconditional use in cancer therapies and limiting their success in clinical trials [60].

Tumor associated macrophages (TAMs) are essential components of the TME and they can orchestrate T cell dependent tumor cell killing [4], or they can support tumor growth by secreting angiogenic, growth factors and by inducing suppression of antitumor immunity [61]. Myeloid derived suppressor cells (MDSC), which are pathologically activated neutrophils and monocytes endowed of immunosuppressive properties [62] can be rapidly recruited to the tumor site through the TNFα pathway. MDSC release copious amount of H_2O_2, inducing tumorigenesis even in the absence of other carcinogenic insults [45] and their abundance is associated with poor clinical outcomes in cancer patients [63]. Instead, neutrophils are an heterogenous cell population (reviewed in [64]) that can drive tumor progression through induction of DNA damage [65], immunosuppression [66] and netosis [67], but they can also oppose carcinogenesis via the establishment of an antitumor microenvironment [68]. In human CRC patients, neutrophils are generally considered a favorable prognostic factor [69]–[71], although their heterogeneity is associated with opposite roles in tumor immunology [72].

1.3.2 Adaptive immune responses in CRC

The understanding of CRC immunological landscape led to the discovery of anti-tumorigenic, cytotoxic, T-helper 1 (Th1) immune signatures as well as Th2, regulatory T cells and Th17 pro-inflammatory signatures associated with tumor progression [73] (Figure 1.5).
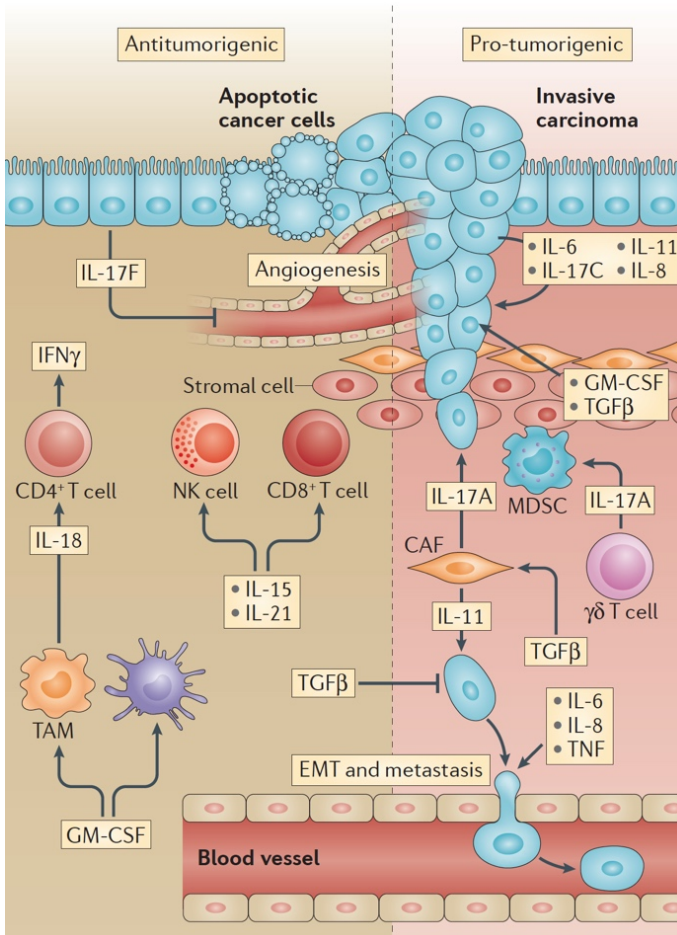
Figure 1.5: Cytokines produced in anti-tumorigenic or pro-tumorigenic inflammatory conditions. On one side, GM-CSF recruits macrophages and dendritic cells to activate cytotoxic CD4$^+$ T cells, sustaining anti-tumorigenic responses. IL15 and IL21 activate NK and CD8$^+$ T cells causing cancer apoptosis. Epithelial-derived IL17F and TGFβ, block angiogenesis and metastasis, respectively. On the other side, GM-CSF, IL17A and IL8 recruit protumor MDSC, while IL6 and TNF sustain tumor growth and metastasis. Adapted from Nathan R. West, et al., Nature Reviews Immunology, 2015. [4]

Tumor infiltration of Th1 cells and cytotoxic T lymphocytes (CTLs) is associated with favorable patient prognosis in CRC [73]. CTLs cause direct tumor cell lysis through the release of cytolytic effector molecules such as granzymes, perforin and granulysin and through the activation of death receptor signaling pathways [74]. IFNγ is the main Th1 associated cytokine and it is involved in cell cycle regulation, apoptosis and tumor suppression (reviewed in [75]). IFNγ signaling activates the JAK/STAT (Janus kinase/signal transducers and activators of transcription) pathway, leading to transcription of numerous genes and transcription factors on target cells [75]. In addition to tumor cell targeted effects, IFNγ affects the gene expression of immune cells residing in the TME [76]. IFNγ induces upregulation of the MHC-I and MHC-II molecules, promoting

antigenic presentation in DCs, macrophages and epithelial cells and enhance motility and the cytotoxic capability of CTLs [77]. IFNγ can reprogram macrophages toward an anti-tumorigenic M1 phenotype [78] and it induces recruitment of iNOS$^+$CD206$^-$ M1-macrophages and limits tumor growth in murine solid tumors [79]

Regulatory T cells (Treg) are a population of Th cells, which have major roles in suppressing autoimmune responses [80]. In cancer they are generally associated with adverse prognosis [73] with the notable exception of CRC, where they can exert divergent roles. For instance, a great heterogeneity of functional Treg subpopulations is found in CRC [81]. Treg-specific gene signatures correlate with patients' survival [82], whereas a population of clonally expanded effector regulatory T cells, highly enriched in primary CRC tumors and metastasis, is associated with disease progression [81]. Treg are immunosuppressive cells characterized by the expression of IL10 [80], however a population of Treg cells expressing inflammatory cytokines, such as granzyme K and IFNγ in addition to IL10 was detected in inflammatory bowel disease (IBD) patients [83], with potential implications also in the pathogenesis of CRC and in inflammation driven CRC.

The major sources of pro-inflammatory and pro-tumorigenic cytokines in the tumor microenvironment are Th17 cells, and specialized subsets of unconventional T cells [4]. IL22 and IL17, the most characteristics Th17 cytokines are associated with CRC progression [4]. IL22 promotes stem cell mediated tumorigenesis through STAT3 binding and protects stem cell from genotoxic stress [84], whereas IL17 activates the NF-kB pathway and promotes tumorigenesis in the $APC^{Min/+}$ and in the colitis-associated CRC mouse model [56].

Many of these cytokines are also involved in the recruitment of innate cells and MDSCs at tumor sites [4], promoting their interaction with the adaptive immune system. For instance, granulocyte macrophage colony stimulating factor (GM-CSF), IL17A and IL8 stimulate myelopoiesis, DCs, macrophages, neutrophils and MDSCs maturation and migration [85], influencing the TME.

1.3.3 Unconventional T cells in CRC

T lymphocytes are a major component of the TME. Different functional populations of conventional T cells (*i.e.* Th1, Th2, Th17 or regulatory T cells) are discussed in the previous Section1.3.2, however unconventional T cells have recently emerged as regulator of tissue homeostasis at mucosal sites [86]. Unconventional T cells comprehend: MHC class Ib-restricted T cells, CD1 and MR1-restricted T cells and γδ T cells [87] (Figure 1.6).
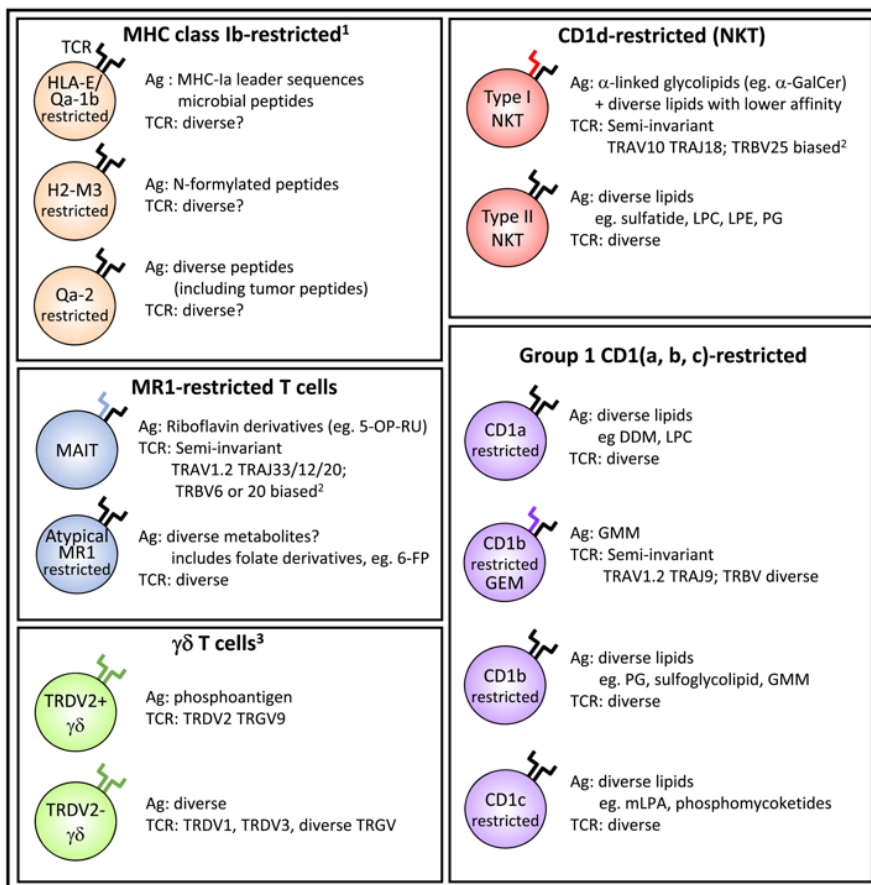
Figure 1.6: *Unconventional T cells grouped according to their restriction elements. 5-OP-RU: 5-(2-oxopropylideneamino)-6-D-ribitylaminouracil; 6-FP: 6-formylpterin; Ag: antigen; a-GalCer, a-galactosylceramide; DDM: dideoxymycobactin; GEM: germline-encoded mycolyl lipid-reactive; GMM: glucose monomycolate; LPC: lysophosphatidylcholine; LPE: lysophosphatidylethanolamine; mLPA: methyl lysophosphatidic acid; MAIT: mucosalassociated invariant T; NKT: natural killer T; PG: phosphatidylglycerol; PM: phosphomycoketide; ? = insufficient or very limited data; 1: H2-M3 and Qa-2 restricted T cells are mouse only; 2: human T cell receptor (TCR) sequences; 3: only human γδ T cells are shown. Adapted from Godfrey D. et al., Immunity Review, 2018.* [87]

Unconventional T cells accumulate in tissue during early life [88], mature before egressing the thymus [89] and are activated by monomorphic antigen presenting molecules, such as molecule of the CD1 family or MR1 [87]. Differently from conventional T cells, which must be recruited to tumor sites by innate immune responses and must be further activated in loco by recognizing peptide antigens presented by antigen presenting cells (APCs) [2], unconventional T cells are mainly mucosal tissue-resident cells with major roles in intestinal homeostasis [86]. Additionally, bacterial lipids and their derivatives are among the most common antigens for unconventional T cells [90]. Although unconventional T cells are understudied compared to conventional T cells, they are shown to interact with epithelial cells and other immune cells, having potential roles in tumor immunity and in tumor evolution [91].

For instance, MHC-Ib restricted unconventional T cells are strongly inhibited by binding with the MHC-Ib molecule human leukocyte antigen-G (HLA-G) [92] and CRC samples upregulate the expression of the HLA-G molecule [93], suggesting that HLA-G overexpression could be used as tumor immune evasion mechanism in CRC.

MR1-restricted T cells, or mucosal associated invariant T (MAIT), are present in the lamina propria of CRC patients. However, their role in tumor surveillance is still debated [94]; MAIT cells infiltration correlates with poor clinical outcome in CRC patients and tumor-infiltrating MAIT exhibit dysfunctional phenotype with impaired production of IFNγ [95]. On the contrary, circulating MAIT cells in CRC patients are decreased in frequency but retain strong cytotoxic properties [96]. In allogeneic hematopoietic cell transplantation, MAIT cells promoted by microbial diversity, are associated with favorable patients' outcome [97].

Humans γδ T cells can be divided into two classes depending on their T cell receptor (TCR) δ-chain V region usage: TRDV2$^+$ and TRDV2$^-$ cells (Figure 1.6). Both γδ T cells classes show antitumor properties *in vitro* [98] and γδ T cells infiltration is correlated with patient survival in many cancer types, such as melanoma [99], leukemia [100] and bladder cancer [101]. In rectal cancer TRDV2$^+$ and TRDV2$^-$ (specifically TRDV1$^+$) γδ T cells have opposite correlations with tumor burden [102], suggesting a differential role for these populations. Indeed, a recent work identified distinct profiles of intestinal γδ T cells dependent on the TCR-Vγδ, in human and murine CRC tissues [103]. Intestinal-resident Vγ1 and Vγ7 γδ T cells have antitumor activity, restraining tumor formation in the

inflammation-driven AOM/DSS model of CRC, whereas tumor-infiltrating Vγ4 and Vγ6 γδ T cells have protumor functions linked to the production of IL17 [103].

CD1-restricted T cells recognize lipid antigens [87] and are classified into two groups: Group 1 cells are restricted to CD1a, CD1b and CD1c while group 2 are CD1d-restricted T cells. Group 1 are generally autoreactive cells with main functions in tissue homeostasis maintenance at the epidermal site (specifically CD1a-restricted T cells) [87], with no described functions in tumor immunity. Group 2, CD1d-restricted T cells, namely invariant natural killer T cells (iNKT), have been extensively investigated in human and murine contexts, due to their relevant role in homeostasis, inflammation and cancer. iNKT cells are discussed in detail in the next section1.4.

1.4 Invariant natural killer T cells

iNKT cells are a unique subset of evolutionary conserved unconventional T cells [7]. They were first identified in the mid-90s as mature T cells with restricted TCR and NK markers [104]. iNKT cells harbor a semi-invariant αβ TCR, comprising of an invariant α chain (Vα14-Jα18 in mouse and Vα24-Jα18 in human) and limited β chain rearrangements (Vβ2, Vβ7 or Vβ8 in mouse and Vβ11 in human) [7], through which they recognize glycolipid antigens presented by the MHC class I-like molecule CD1d (Figure 1.7) [105]. CD1d is a non-polymorphic molecule that presents foreign and self-lipids to iNKT cells, mediating innate-adaptive immune responses [106].

Two broad group of CD1d-restricted T cells exist: type I or iNKT cells with a restricted TCR and type II NKT cells, which have a more diverse TCR [7]. Type I iNKT cells recognize glycolipids and can be precisely detected with the use of ligand-loaded tetramers [107] , while type II NKT cells have a more promiscuous TCR with different affinities toward several ligands [7]. Notably, there is not univocal ligand for type II NKT cells to be used for their identification [7], only a subset of type II NKT cells reactive to sulfatide antigens [108] can be faithfully identified using ligand-loaded tetramers.
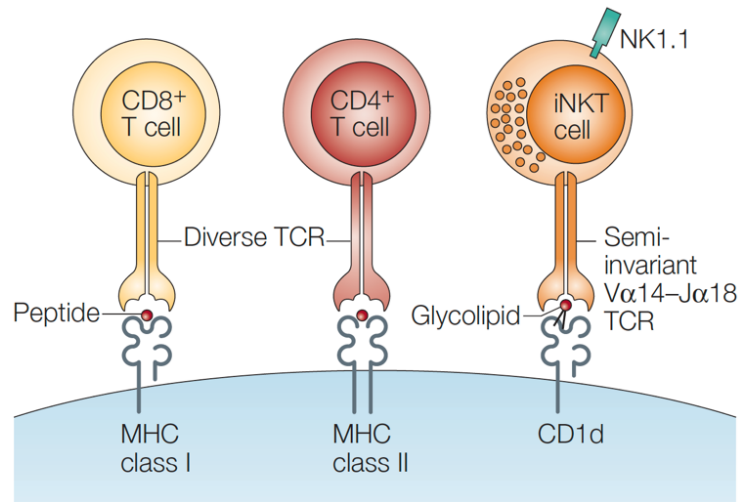
Figure 1.7*: Schematic view of conventional and iNKT cells.* CD8^{+} *and CD4*^{+} *T cells express diverse TCRs through which they recognize peptide antigens on the MHC-I and MHC-II antigen presenting molecule, respectively. iNKT cells express a semi-invariant TCR (Vα14-Jα18 in human) through which they recognize glycolipids presented by the CD1d antigen presenting molecule. iNKT cells possess also NK-like marker (NK1.1) and pre-formed granules. Adapted from Luc Van Kaer, Nature Reviews Immunology, 2005* [105]*.*

The prototype ligand for iNKT cells is the bacteria-derived lipid αGalactosyl-Ceramide (αGalCer) [7], originally discovered in a marine sponge. αGalCer binds with high affinity the TCR on iNKT cells and thus it is employed to target iNKT cells using αGalCer-loaded tetramers [107]. αGalCer binding induces clonal expansion and iNKT cell activation, with the massive production of Th1 and Th2 cytokines (*i.e.* IFNγ or IL4) [105].

Similar antigens, able to activate iNKT cells, are present in the cell wall of Gram-negative bacteria *Sphingomonas spp.* [109], in members of the *Bacteroidetes* phylum [110], in the Gram-positive *Streptococcus pneumoniae* and in *Lactobacillus casei* [111], or they can be produced by the bacteria *Borrelia burgdorferi*, the causative agent of Lyme disease [112], or by mycobacteria [113]. Self-antigens as well can activate iNKT cells, although they bind the TCR with lower affinity [113]. Peroxisome-derived lysophosphatidylethanolamine are important for positive thymic selection [114] and ER stress induces the production of neutral endogenous lipids in APCs [115], which have important implications in the sterile activation of iNKT cells. iNKT cells can be activated also in a CD1d-independent manner [7]. For instance, IL12 and IL18 are able to potently activate iNKT cells *in vivo*, without antigen presentation and in the absence of APCs [116]. Moreover, iNKT cells bear on their surface many natural killer markers such as

NK1.1 (human CD161), NKG2D and NKp46 and are rich in cytokines storing granules, accounting for their immediate and massive activation [116].

iNKT cells acquire their characteristics in a multi-step maturation process, that involve thymic and post-thymic selection [89]. In the thymus, iNKT cells develop in an unconventional mechanism of B7-CD28 co-stimulation [117] and mature into different functional subsets; iNKT1, iNKT2, iNKT17 (Figure 1.8) [89]. Functional subsets are differentiated by the expression of transcription factors and cytokines. All iNKT cells populations express the promyelocytic leukaemia zinc-finger protein (PLZF) transcription factor at certain levels [89]. iNKT1 are characterized by the expression of the T-bet transcription factor and by the production of cytotoxic cytokines such as IFNγ, whereas iNKT2 produce Th2-associated cytokines, predominantly IL4, and iNKT17 express RORγt and produce IL17, IL22, GM-CSF and TNFα [8].
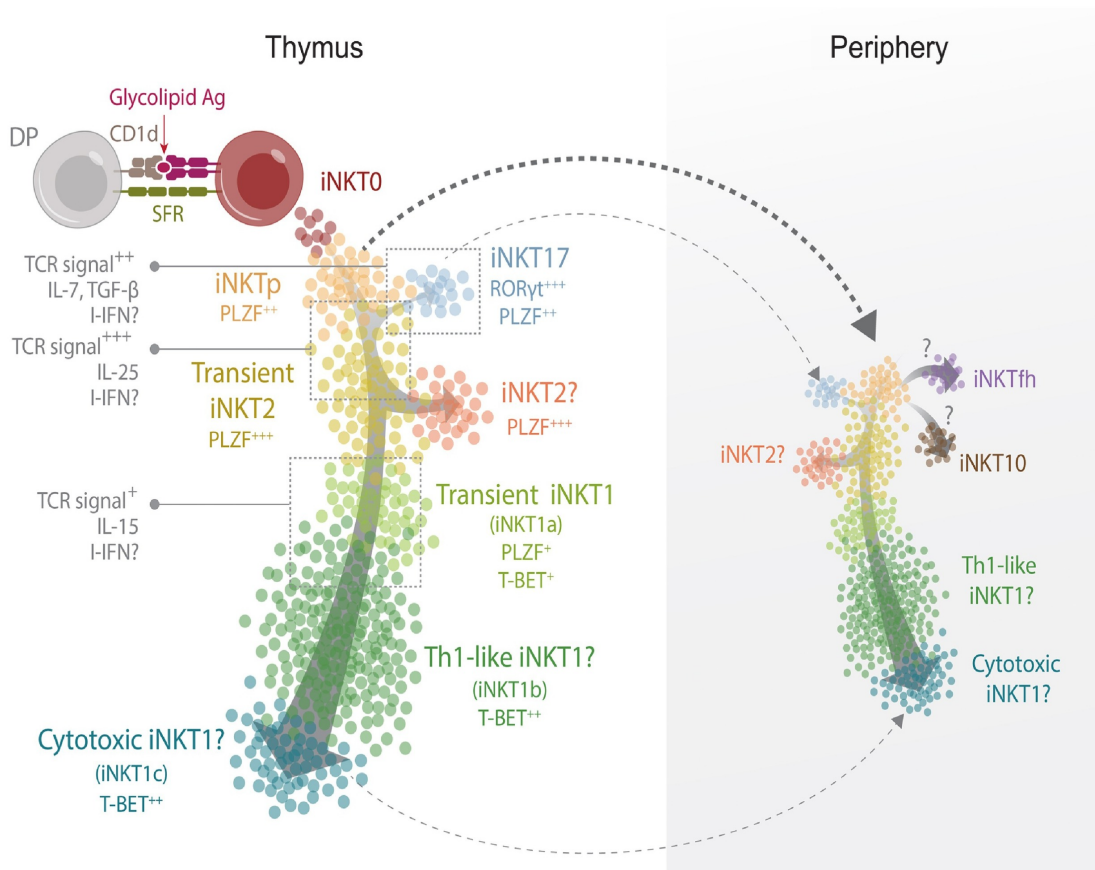
Figure 1.8: _Thymic developmental and effector differentiation of murine iNKT cells._ On the left panel thymic development: Positive selection of iNKT0 upon CD1d and SLAM family receptor (SFR) binding with CD4/CD8 double positive (DP) cortical thymocytes. Maturation of iNKT0 into iNKT precursor (iNKTp) expressing high levels of the transcription factor PLZF. Maturation of thymic iNKT17, iNKT2, Th1-like iNKT1 and cytotoxic iNKT1 upon differential TCR binding strength and cytokines

Upon thymic maturation the majority of iNKT cells egress and reach peripheric lymphoid and non-lymphoid organs, although a certain amount of them stays in the thymus and influence the establishment of "natural memory" affecting eomesodermin (EOMES)-expressing CD8$^+$ T cells [118]. Mature iNKT cells reach the periphery following chemokine recruitment and homing receptors expression and become mainly tissue-resident cells [8]. At sites, iNKT cells can undergo a further step of post-thymic induction with the surrounding environment determining iNKT cell phenotype [8], suggesting a certain degree of plasticity in their activation.

Therefore, iNKT cells are defined as tissue-resident cells expressing tissue-specific functions and frequency. In mice, iNKT cells frequency is 30% of lymphocytes in liver, 1-3% in spleen, 5-10% in lungs and approximately 1% in the intestine [8]. In human, iNKT cell frequency is slightly less abundant, although fewer studies are available [8]. However, the functional impact of iNKT cells in mucosal and in tumor immunity has great potential, as they can rapidly skew their cytokines production and influence the inflammatory state of the surrounding environment.

1.4.1 iNKT cells and cancer

The capability of iNKT cells to rapidly respond to different stimuli and to bridge innate and adaptive immune responses, make them one of the first players in tumor immunity [116]. iNKT cells are found in several tumor types such as breast cancer [119], [120], melanoma [121], [122], lymphomas [123]–[125], osteosarcoma [126], neuroblastoma [127], [128], glioma [129], lung [130], pancreatic [131], [132], prostate [133], [134], intestinal [12], [135]–[140] and gastrointestinal cancers [141]–[149] (Table 1.1). However, their roles in disease formation and evolution are not fully elucidated yet.

In *in vivo* models of melanoma and breast cancer iNKT cells show an activated phenotype, differently from type II NKT and NK cells [150], however tumor downregulation of the CD1d molecule inhibit iNKT-dependent antitumor responses [119]. iNKT cells reduce the growth of T-cell lymphoma through the release of perforin

[124], whereas they favor B-cell lymphoma suppressing cytotoxic antitumor responses [125]. The absence of iNKT cells in the transgenic adenocarcinoma of the mouse prostate (TRAMP) model of prostate cancer, result in premature and more aggressive tumors [134]. iNKT cells impair prostate cancer by reducing pro-tumorigenic M2 macrophages and promoting anti-tumorigenic M1 macrophages [133].

In gastric and intestinal cancers, iNKT cells show disparate effects [146]; they hamper gastric and pancreatic cancers [131], whereas they promote intestinal cancer formation [139]. In the $APC^{Min/+}$ model of CRC, polyps-infiltrating iNKT cells have regulatory functions and suppress antitumor Th1 immunity, promoting polyps' formation [139]. On the contrary, human iNKT cell lines efficiently kill CRC cells *in vitro,* through the perforin/granzyme axis [151]. Several preclinical and clinical studies investigated the role of iNKT cells in liver cancer [143], [148], [152], however, the direct comparison of murine and human hepatic iNKT cells is not so straight forward. The abundance of murine hepatic iNKT cells is ~ 30% of lymphocytes, while human hepatic iNKT cells account for ~ 0.05 and 1%. Moreover, murine and human hepatic iNKT cells show different pattern of activation upon αGalCer stimulation [149]. For instance, human hepatic iNKT cells release IFNγ but not IL4 upon αGalCer stimulation, while murine hepatic iNKT cells release both IFNγ and IL4 [153]. In a murine model of liver cancer, iNKT cells are recruited by microbiota-derived modified bile acids and exerted anti-tumorigenic functions, limiting tumor growth and metastasis formation [152], whereas iNKT metabolic activation drive hepatocarcinoma through the canonical NF-κB signaling in a murine model of nonalcoholic steatohepatitis and liver cancer [143]. In human colon cancer, tumor infiltration of Vα24 NKT cells was defined as positive prognostic factor [12], however, more recently the abundance of circulating NKT-like cells in CRC patients was found to be a negative prognostic factor for patients' recurrence [154]. Based on *in vivo* studies on murine models of CRC, iNKT cells are thought to inhibit antitumor immunity, behaving like regulatory and Th2 cells [139], however their antitumor activity can be restored by treatment with the ligand αGalCer [140].

CANCER	TREATMENT METHOD	FUNCTION	REFERENCES
LEUKEMIA	-	-	Gorini F. et al., 2017
T – CELL LYMPHOMA	αGalCer	Antitumor	Bassiri H. et al., 2014
B – CELL LYMPHOMA	-	Protumor	Bjordahl R. et al., 2012
NEUROBLASTOMA	CAR-IL15-iNKT	-	Heczey A. et al., 2020 Metelitsa L. et al., 2004

GLIOMA	αGalCer-DCs	Antitumor	Dhodapkar K. et al., 2004
MELANOMA	αGalCer	Antitumor	Kawano T. et al., 1999 Wingender G. et al., 2010
OSTEOSARCOMA	-	Antitumor	Fallarini S. et al., 2012
BREAST CANCER	- CD1d-binding glycolipid	Antitumor Antitumor	Laura M. et al., 2011 Seki T. et al., 2019
LUNG CANCER	αGalCer	Antitumor	Konishi J. et al., 2004
GASTRIC CANCER	αGalCer-DCs αGalCer -	- Antitumor -	Yanagisawa K. et al., 2022 Xu Q. et al., 2018 Melo A. et al., 2020
PANCREATIC CANCER	$CD1d^{-/-}$ mice αGalCer-DCs	Antitumor Antitumor	Janakiram N. et al., 2017 Nagaraj S. et al., 2006
LIVER CANCER	- αGalCer - - - αGalCer	Protumor Antitumor Protumor Protumor Antitumor Antitumor	Kenna T. et al., 2003 Mayagy T. et al., 2003 Bricard G. et al., 2009 Wolf MJ. Et al., 2014 Ma C. et al., 2018 Sicheng F. et al., 2020
PROSTATE CANCER	$J\alpha 18^{-/-}$ mice -	Antitumor Antitumor	Bellone M. et al., 2010 Cortesi F. et al., 2018
INTESTINAL CANCER	- αGalCer/antiPD-1	Protumor Antitumor	Wang Y. et al., 2017 Wang Y. et al., 2020
COLORECTAL CANCER	$CD1d^{-/-}$ mice - αGalCer αGalCer -	Protumor Protumor Antitumor Antitumor Antitumor	Myun Park J. et al., 2004 Darcy P. et al., 2020 Ambrosino E. et al., 2007 Hattori T. et al., 2007 Tachibana T. et al., 2005

Table 1.1*: List of studies investigating the role of iNKT cells in different cancers.*

In cancer, iNKT cells have divergent functionalities. Their activation status, cytokines production and killing capabilities are organ-cancer specific [8] and can influence and be influenced by all the different components of the TME.

1.4.2 Interactions between iNKT cells and the TME

The interaction between iNKT cells and the TME can influence iNKT cells recruitment, activation and functional skewing, affecting iNKT-direct and indirect mechanisms of tumor control [155] (Figure 1.9).

For instance, iNKT cells are recruited by tumor-derived CCL2 in neuroblastoma [127]. CCL2 is shown to recruit also macrophages and precursor of tumor associated macrophages (TAMs) in several malignancies [156], suggesting an interaction between these two cell populations in the TME. Indeed, iNKT cells reduce tumor growth in neuroblastoma by killing monocytes pulsed with tumor cell lysates and TAMs [157]. In pancreatic and prostate cancer, iNKT cells limit tumor progression by inhibiting M2 macrophages and by polarizing them toward an anti-tumorigenic M1 phenotype [131], [133]. On the contrary, in intestinal cancer, iNKT cells induce M2 TAMs along with recruitment of regulatory T cells and polyps' formation [139]. Potentially, iNKT cells can interact, by direct binding, with all cells expressing the CD1d molecule. CD1d has a wide tissue distribution and it can be found on all APCs and also on IECs [106], [158]. Elevated expression of CD1d in lung cancer correlates with favorable patients' outcome and $CD1d^+$ DCs potently induce iNKT cells degranulation and IFNγ production [159]. CRC epithelial cell lines also express CD1d and its upregulation, induced by Thymosinα1 treatment enhanced iNKT cells cytotoxicity *in vitro* [160]. CD1d-dependent lipid uptake by B cells induces iNKT cells recruitment and establish a crosstalk between the two cell populations that provide help for B cells antibodies production [161]. iNKT cells can interact also with neutrophils [162]–[164]. On one side, iNKT cells limit the suppressive activity of neutrophils, with important implications in the clinical treatment of melanoma patients [162]. On the other side, neutrophils influence iNKT cell responses in mice and humans and regulate the expression of death receptors on iNKT cells [163], suggesting the existence of an iNKT-neutrophils axis, with relevant functionalities in cancer.

Another important constituent of the TME, with high relevance in gastro-intestinal tumors and specifically in CRC is the gut microbiota (Section1.5). iNKT cells can be rapidly shaped by different microbial lipids [88] and germ-free mice have less mature iNKT cells that can be functionally activated by *Sphingomonas* bacteria [165]. Microbial exposure during early life is indeed an important factor for iNKT cells imprinting and proper development [88]. Additionally, we have recently demonstrated that not only the absence of microbiota, but also its alteration can influence iNKT cells functional phenotype. Mucosa-associated microbiota drove differential cytokine expression in human iNKT cell

lines, contributing to the fueling of inflammation in IBD patients [166]. Dysbiosis, namely the alteration of gut microbiota, caused by short term oral antibiotics administration induce inflammatory activation of iNKT cells [167]. On the contrary, iNKT cells priming with metronidazole-treated *Lactobacillus*-enriched feces drove their production of the immunoregulatory molecule IL10 [168]. Microbiota-derived metabolites influence iNKT cells recruitment and activation in hepatocellular carcinoma. *Clostridium scindens* causes primary to secondary bile acid metabolism, which induces overexpression of iNKT cell chemokine recruiting molecule (CXCL16) by endothelial cells, resulting in iNKT cell infiltration and antitumor activation [152].
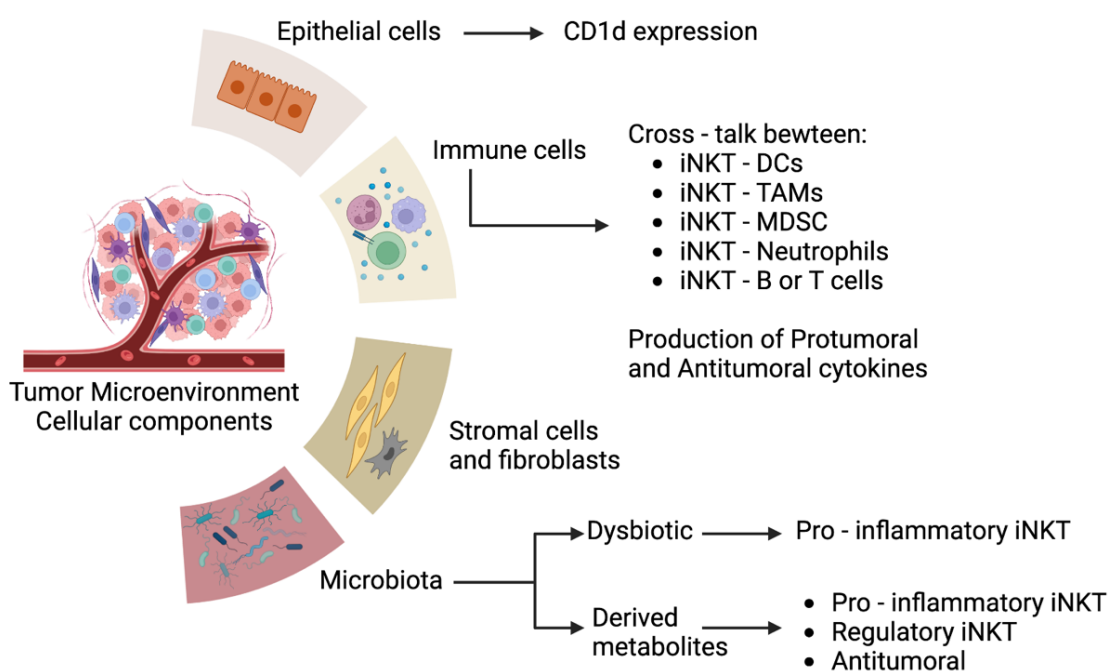
Figure 1.9: *Interactions between the cellular compartment of the TME and iNKT cells. Epithelial cells express CD1d and influence the cytotoxic capacity of iNKT cells. iNKT cells influence several immune cells of the TME. Microbiota can directly or indirectly influence iNKT cell functional phenotype. DCs, Dendritic cells; TAMs, Tumor associated macrophages; MDSC, myeloid derived suppressor cells. This figure was created in BioRender.com.*

Although bacterial metabolites and lipid antigens have the potential to drive iNKT cells, the identification of iNKT reactive gut microbial lipids is still largely undefined. Some commensal species discussed in Section1.4 harbor glycosylceramides on their cell wall, however it is likely that many more species can differentially influence iNKT cells. Generally, the gut microbiota can activate or inhibit iNKT cells [9], [166]–[168], thus it is plausible it may play a role in the iNKT-dependent immunological shaping of the TME in CRC.

1.5 The gut microbiota in CRC

The gut microbiota is an important player of the TME in CRC [31]. The composition of the gut microbiota consists of bacteria, eukaryotic fungi, protozoa and viruses which live in symbiosis with the host, collaborating in digestive, metabolic and homeostatic processes in exchange to a favorable, nutrient-rich environment where to live in [32]. If this homeostatic condition is compromised the integrity of the mucosal epithelial barrier is lost, inflammation is exacerbated and cancer can arise [169].

Tumor-associated bacteria have been identified and can impact the TME and influence cancer progression at all steps of carcinogenesis, through the mechanisms illustrated in Figure 1.10 [32].

Helicobacter pylori is a known carcinogen in gastric cancer and it induces chronic inflammation promoting Th1 and Th17 responses and recruiting innate immune cells such as NK cells [170]. *Fusobacterium nucleatum (F. nucleatum)*, a pathobiont associated with CRC lesions [31], can activate the β-catenin pathway through direct binding of the virulence factor FadA, affecting the EMT process and tumor proliferation [32]. *F. nucleatum* sustains tumor cell extravasation, migration and metastasis formation by specifically activating the NF-kB pathway, that results in the overexpression of Intercellular Adhesion Molecule 1 (ICAM1) on tumor cells [171]. ICAM1 promotes EMT, angiogenesis and malignancy potential in CRC [172]. *F. nucleatum* sustains tumor proliferation and migration in pancreatic cancer [173] and in CRC [174] by inducing autocrine and paracrine GM-CSF, CXCL1 and IL8 signaling. These cytokines are also relevant for the recruitment of myeloid derived immune cells. Indeed, *F. nucleatum* induces expansion of myeloid derived immune cells in the $APC^{Min/+}$ model of intestinal cancer [175]. *F. nucleatum* metabolites, specifically short chain fatty acids (SCFA), mediate immunomodulatory effects *in vivo,* promoting IL17 production and enhancing tumorigenesis [176]. *F. nucleatum* derived extracellular vesicles activate innate immune responses through the toll-like receptor 2 (TLR2) [177], however *F. nucleatum* inhibits NK cell cytotoxicity by binding the immune inhibitory receptor TIGIT (T cell immunoreceptor with Ig and ITIM domains) with the Fap2 virulence factor [178], suggesting the existence of bacteria immunomodulatory capabilities. In human metastatic CRC patients, infiltration of *F. nucleatum* is associated with low progression-free survival [179], however it correlates with improved response to immunotherapies [180], generating concerns regarding its effects on CRC development.

Bacteria can also promote mutations and genomic instability in epithelial cells by causing DNA damages. The toxin colibactin, produced by *Escherichia coli* and the cytolethal distending toxin produced by several ε- and γ-proteobacteria, are shown to cause double-strand DNA damages, while the *Bacteroides fragilis* toxin (Bft) causes indirect DNA damages, by promoting chronic production of ROS and it recruits pro-inflammatory IL17-producing immune cells [31], [32].
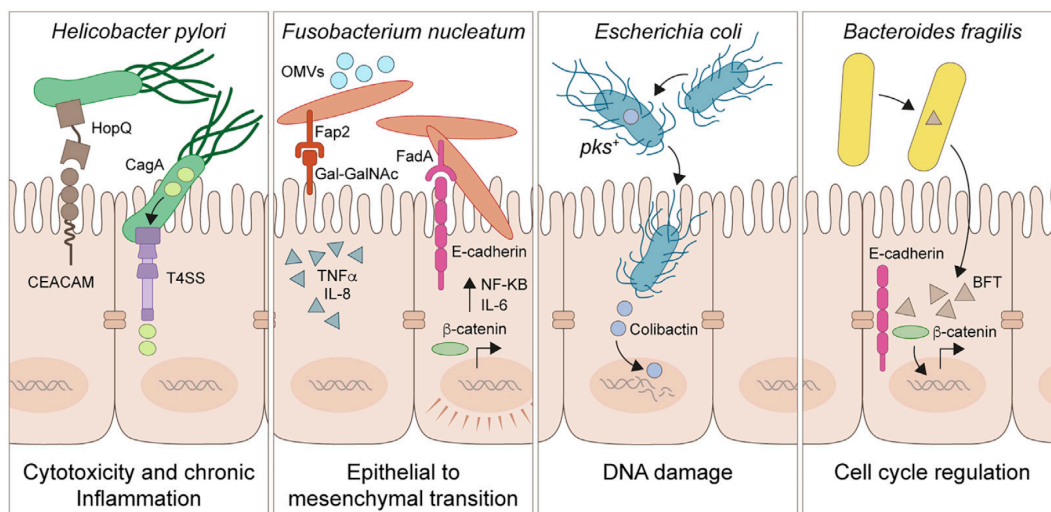
Figure 1.10*: Mechanisms of tumor induction by microbiota. Helicobacter pylori binds to epithelial cells through the adhesin HopQ and inject its virulence factor CagA into the epithelial cell through the T4SS, activating the Wnt/β-catenin pathway. Fusobacterium nucleatum trigger tumorigenesis through the binding between the adhesion molecule Fap2 and D-galactose-β (1–3)-N-acetyl-D-galactosamine (Gal-GalNAc) carbohydrate moieties on epithelial cells which contribute to inflammation and EMT remodeling, or by cellular internalization, through FadA-E-cadherin binding, and activation of the NF-kB cascade. Escherichia coli release the genotoxic molecule colibactin into the cell and cause double-strand DNA breaks with protumor effects. Bacteroides fragilis produce the toxin BFT that interfere with the production of E-cadherin and its cleavage promoting intestinal permeability and inflammation. Adapted from Cullin N., et al, Cancer Cell Review 2021* [32]*.*

Not only flourishing of single species, but general alteration of the microbiota and their derivatives, sustain tumor formation by hindering antitumor immunity and promoting chronic inflammation [169]. Moreover, differential bacterial composition is associated with immunotherapy responses in melanoma patients [181], highlighting a role for the microbiota in cancer treatments and in the mechanisms of immune evasion.

1.6 Standard treatment of CRC

Although many advances in the understanding of the genetic background of CRC and in its immunological landscape, an efficient therapy for the treatment of the disease has not been defined yet. The goal of cancer treatment is improving patients' survival with high life quality, reaching maximal shrinkage of the tumor and suppression of further tumor growth or metastasis. The standard treatments for CRC comprehend surgical resection of the primary tumor and regional lymph nodes in localized disease, followed by adjuvant chemotherapy in TNM Stage III and IV patients [182].

Targeted therapies aimed at inhibiting cancer cell proliferation, differentiation and migration have been developed. Epidermal growth factor receptor (EGFR) inhibitor therapy (Cetuximab and Panitumumab) is used to limit the uncontrolled cancer cell growth and monoclonal antibodies directed toward VEGF (Bevacizumab and Ramucirumab) are used to inhibit angiogenesis [183]. Immunotherapy, or immune checkpoint inhibitors (ICI) therapy, are part of the standard treatment for metastatic CRC [182] and it consists in the use of monoclonal antibodies toward immune checkpoint proteins with the aim to reactivate the antitumor immune system. In 2017 the federal agency of Food and Drug administration (FDA) approved Pembrolizumab, a monoclonal antibody for PD-1 (programmed cell death protein 1), as second-line treatment of metastatic microsatellite instability high (MSI-H) CRC [183]. However, only a small portion of CRCs are MSI-H and they rapidly enter the phase of immune remission [184]. Thus, novel therapies exploiting combinatorial treatments (*i.e.* targeted therapy + ICI) or the use of engineered immune cells (*i.e.* chimeric antigen receptor, CAR-T cells) are under active investigation.

1.6.1 iNKT cells as novel therapy in cancer

The antitumor functions of iNKT cells are ascribed to their potent release of cytotoxic molecules and IFNγ [11]. iNKT cell stimulation with αGalCer has proved significant efficacy in preclinical studies (reviewed in [185]) and it showed clinical safety in human treatments; however, it failed to generate tumor regression in clinical trials (reviewed in [155]). Administration of αGalCer loaded DCs or APCs result in stable disease in a small fraction of solid tumors, among which lung cancer and head and neck squamous cell carcinoma [186]. The limited efficacy of iNKT cell-based immunotherapies can be due to the anergic state induced on iNKT cells by αGalCer stimulation [187], suggesting that approaches limiting iNKT cells anergy could be employed for efficient iNKT cell-based immunotherapies. Indeed, combinatorial treatment of αGalCer and immune checkpoint inhibitors (*i.e.* anti-PD-1) synergize to reduce tumor development *in vivo* [140].

In addition to their rapid production of cytotoxic molecules iNKT cells possess other advantages that make them highly suitable for adoptive immunotherapies in cancer. As already discussed in Section1.3.3-1.4, iNKT cells are CD1d-restricted unconventional T cells. CD1d is a monomorphic molecule, shared among individuals, which avoid the risk of alloreactivity in adoptive immunotherapy [155]. Due to the lack of toxicity iNKT cells are ideal for adoptive immunotherapy, however they do express MHC molecules and could cause treatment rejection by the allogeneic host immune system. To this purpose, iNKT cells were expanded *in vitro* from human hematopoietic stem cells expressing undetectable levels of HLA-I and HLA-II [188] and could be further engineered with chimeric antigen receptors (CAR) Figure 1.11 [189]. CAR-iNKT cells efficiently kill antigen-presenting tumor cell lines or patient-derived plasma cells *in vitro* and *in vivo* [190]. Moreover, promising results were obtained in an interim analysis of a phase I clinical study of CAR-NKT treatment in children with relapsed or resistant neuroblastoma (NCT03294954; [128]). Other two phase I clinical trials aimed at assessing safety, toxicity and effectiveness of CAR19-iNKT cells treatment in CD19$^+$ leukemia are nowadays in the recruiting phase (NCT03774654, NCT04814004, first results expected by mid 2023.). iNKT cells can be engineered also to express recombinant TCRs [191], allowing the detection of neoantigens and tumor associated antigens. Genetically engineered iNKT cells with TCRs specific for *Mycobacterium tuberculosis* have directed antigen recognition *in vitro* retaining also responsiveness toward αGalCer [192]. A recent study shows that TCR-engineered iNKT cells migrate into solid tumors *in vivo* and lead to prolonged antitumor effects and tumor rejection in some mice [193].

| iNKT cell therapies | CAR-T and rTCR-T therapies | CAR-iNKT and rTCR-iNKT therapies |

Endogenous iNKT- TCR
mediate killing

Endogenous T-TCR
No function or GvHD

Chimeric antigen receptor
mediates killing

iNKT-TCR & Chimeric antigen receptor
Both receptors mediate killing

T-TCR   CAR

iNKT cell

CAR-T cell

iNKT-TCR   CAR

CAR-iNKT cell

| Endogenous anti-tumor | Potential GvHD + anti-tumor activity (allogeneic setting) | Enhanced activity with exogenous antigen receptor |

Figure 1.11: *Schematic representation of T cells and iNKT cells immune therapies. iNKT cells possess endogenous antitumor properties (left side). T cells do not possess endogenous antitumor properties, only CAR or TCR-engineered T cells possess antitumor properties, but cause graft versus host disease (GvHD) syndrome (middle panel). CAR or TCR-engineered iNKT cells enhance their endogenous antitumor properties (right panel). Adapted from Wolf et al., Frontiers in Immunology, 2018* [189].

In conclusion, iNKT cells are promising candidates for novel "off the shelf treatments" in cancer immunotherapies, due to their lack of toxicity and their robust antitumorigenic responses. Understanding of their functional role in human tumor samples can help to rationalize efficient immune treatments.

Aims

CRC patients display deregulated inflammatory responses and an altered, dysbiotic microbiota [4], [31], which are known etiological causes for the onset and progression of the disease [3]. Here, we aimed at characterizing the mucosal immunological landscape and the tumor-associated microbiota of human and experimental models of CRC.

We investigated the role of a unique subset of unconventional T lymphocytes, namely iNKT cells, and their crosstalk with different players of the tumor microenvironment from the gut microbiota to myeloid cells. During this work we focused on:

- The identification and phenotypical characterization of iNKT cells in surgical specimens of human CRC and in different murine models of CRC
- The characterization of the inflammation-driven properties of the tumor microenvironment
- The taxonomic bacterial identification of CRC-associated microbiota
- The study of the functional crosstalk among CRC-associated microbiota, iNKT cells and tumor-associated neutrophils
- The clinical relevance of iNKT cells in CRC

2   Materials and Methods

2.1 Mice

2.1.1 Strains used in the study

C57BL/6J mice (Charles River, IT, JAX stock: 000664) from 6 weeks of age were housed at the European Institute of Oncology (IEO, Italy) or at the Bios$^+$ (Switzerland) animal facility in SPF conditions. *CD1d$^{-/-}$* (JAX stock: 008881) and *Traj18$^{-/-}$* (JAX stock: 030524) and *APC$^{Min/+}$* (JAX stock: 002020) animals were bred and maintained at the IEO animal facility in SPF conditions. *CD1d$^{-/-}$* and *Traj18$^{-/-}$* animals were kindly gifted from Dr. Paolo Dellabona, San Raffaele Scientific Institute, Milan. Both male and female mice, aged matched, were used for experiments. Animal experimentations were approved by the Italian Ministry of Health (Auth. 10/21, Auth. 1217/20), by the animal welfare committee (OPBA) of the IEO, Italy and by the Swiss Animal Welfare office (National no. 34368 and Cantonal n. TI54/2021).

2.2 Murine experimental model of colon cancer

2.2.1 AOM/DSS model

Co-housed mice at 7 weeks of age were injected intraperitoneally (i.p) with 10 mg/kg body weight Azoxymthane (AOM, Merck), dissolved in isotonic saline solution. After 7 days, mice were given 1 % (w/v) dextran sodium sulfate (DSS MW 40 kD; TdB Consultancy) in their drinking water for 7 days followed by 14 days of recovery. The cycle was repeated once or twice and mice sacrificed at day 49 (T1) or day 70 (T2). Colons were opened and their length was measured using an electronic caliper (2Biological). Tumors were counted and measured as well. Tumor's volume was calculated using the formula: Volume (mm^3) = (Length (mm) X Width^2 (mm^2))/2, while the area of tumors was calculated using the formula: Area (mm^2) = Length (mm) X Width (mm).

2.2.2 Subcutaneous MC38 model

Co-housed mice at 7 weeks of age were subcutaneously injected with 4×10^5 MC38 cells in 200µl of sterile phosphate buffered saline (PBS, Microgem S.R.L.) either alone or with 1×10^5 of freshly sorted splenic iNKT cells (CD45$^+$CD3$^+$Tet$^+$). Mice were weight every two days, tumors measured using an electronic caliper and tumor volumes were calculated as described above. For αGalCer treatment mice were injected i.p. with 2µg of αGalCer at day 0, 3 and 6. iNKT reconstitution in *Traj18$^{-/-}$* mice was performed co-inoculating freshly sorted splenic iNKT with MC38 cells at 1:4 ratio. Animals were sacrificed after 15 days from the injection or earlier if they showed signs of discomfort.

2.2.3 Intracecal (I.c.) MC38-Luc model

Co-housed C57BL/6J mice at 7 weeks of age were intracecally injected with 3×10^5 MC38 cells in 30µl of sterile solution of Matrigel matrix (Corning) and PBS (Microgem S.R.L.) in a 1:1 ratio. 30 minutes prior to surgery mice were administered subcutaneously a combination of the analgesic drugs rimadyl (5mg/Kg of mouse, Zoetis) and buprenorphine (0.1 mg/Kg of mouse, ZooPharm). Surgery was performed under isoflurane (Sigma Aldrich) anesthesia (1.5-3%, monitoring based on respiratory rate and reflex) upon local administration of lidocaine (10mg/Kg of mouse, Streuli) and bupivacaine (4mg/Kg of mouse, Sintetica). The abdomen of the mouse was shaved, cleaned and disinfected using an iodine-based disinfectant. Firstly, the skin was incised and then the abdominal membrane was cut. The cecum was exteriorized and cell injected with the help of a stereomicroscope using a 30-gauge needle. The cecum was reinternalized and both abdominal cavity and skin were sewed using absorbable filaments (Coated Vicryl, Ethicon). Mice were weight once a week, starting from day 15 and tumor growth was measured on the IVIS Spectrum (Caliper LifeSciences) upon administration of D-luciferin (GoldBio). For αGalCer treatment mice were injected i.p. with 2µg of αGalCer at day 7, 10 and 13. For direct comparison of i.p and i.c. MC38 injected mice they were all injected with 3×10^5 MC38-Luc cells in a solution of Matrigel and PBS in 1:1 ratio. Animals were sacrificed after 30 days from the injection or earlier if they showed signs of discomfort.

2.3 Murine colonoscopy

Colonoscopy in AOM/DSS treated animals was performed twice a week for tumor monitoring using the Coloview system (TP100 Karl Storz, Germany) [194]. The procedure was performed under 3% isoflurane (Sigma Aldrich) anesthesia.

2.4 Murine cell isolation

AOM/DSS treated mice were euthanized and bled for further colon resection. Colons were opened; feces were collected and immediately frozen in a sterile eppendorf, mucus was collected in TES buffer (50 mM Tris HCl, 10 mM NaCl, 10 mM EDTA) using a sterile scraper. Tumors were measured and tissue samples of both the tumor and the healthy, most-distal part (toward the ileum) were collected directly in RNAprotect Cell Reagent (QIAGEN) for further RNA extraction or they were fresh frozen for further protein extraction. The rest was kept in cold PBS for single cell processing of lamina propria mononuclear cells (LPMC) and cytofluorimetric analysis. To reach single cells suspension colons were incubated with 5mM EDTA in RPMI-1640 medium (Microtech S.R.L.) with 2% FBS (Microtech S.R.L.) and 100 units of penicillin and streptomycin (pen/strep) per ml in agitation at 37 °C for 30 min, followed by mechanical digestion using the gentleMACS™ Dissociator (Miltenyi Biotec) pre-installed m_intestine_01 protocol, for three times. Cell solution was filtered through a 100μm, a 70μm filter, washed with PBS, centrifuged at 300g for 5min, resuspended and counted for further staining.

MC38 inoculated mice were euthanized at day 15 (for subcutaneously injected mice) or at day 35 (for intracecally injected mice), or earlier if they showed any sign of discomfort. Tumors were weight, minced in small pieces < 1mm and incubated in RPMI-1640 2% FBS pen/strep with the addition of collagenase D (0.75mg/ml, Merck) and Dnase I (0.1mg/ml, Merck) on a rotating wheel at 37 °C for 45 min. Cell solution was filtered through a 100μm, a 70μm filter, washed with PBS, centrifuged at 300g for 5min, resuspended and counted for further staining.

2.5 Murine neutrophil sorting

AOM/DSS treated C57BL/6 and *Traj18*^{-/-} mice were sacrificed at day 49 post-treatment (T1). Tumors and distal tissue sites were processed to reach single cell suspension as described above (Section2.4). Neutrophils were sorted using a FACS Aria (BD) machine as CD45^{+}, Lin^{-} (CD19 and CD11c), CD11b^{+} and Ly6G^{+} cells directly in RNAprotect Cell Reagent (QIAGEN).

2.6 Human samples

Surgical resections of intestinal tumors (n=118) were obtained from the IRCCS Policlinico Ospedale Maggiore, Milan, Italy. Tumor samples were taken transversally to collect both marginal and core tumor zone. Normal adjacent samples were taken 10 cm away from the tumor toward the Ileum. Buffy coat of healthy donors were obtained from Fondazione IRCCS Policlinico San Matteo, Pavia, Italy.

2.7 Feces and Mucus collection from human samples

Feces were freshly collected from the surgical specimen and fresh frozen in aliquots of 1g each. The mucus lining on tumor lesions and on adjacent non-tumor colon tissue was collected by its mechanical scraping. It was then resuspended in 5ml of TES buffer (50 mM Tris HCl, 50 mM NaCl, 10 mM EDTA) and centrifuged at 200g for 3min for fibers and tissue removal. The supernatant was collected and centrifuged at 3500g for 10min. Pellet was resuspended in 1ml of 20% glycerol and stored at -80 °C.

2.8 CRC cell lines

MC38 and MC38-Luc murine cancer cell lines (from Kerafast) were cultured using DMEM (Microgem S.R.L.) medium with 10% FBS, pen/strep and split when they reached confluence. MC38-Luc were cultured using blasticidin (Sigma Aldrich) as selection antibody.

Human colorectal cancer cells Colo 205 and RKO (from American Type Culture Collection, ATCC) were cultured in RPMI-1640, 10% FBS, pen/strep and MEM, 20% FBS, pen/strep, respectively. Cells were maintained for a maximum of 8 passages.

2.9 *Fusobacterium nucleatum* culture condition

Fusobacterium nucleatum (strain ATCC25586, DSMZ #DSM15643) was cultured in Columbia agar with 5% sheep blood or in Columbia broth (Difco, Detroit, MI, USA) under anaerobic conditions at 37 °C. Columbia broth was supplemented with menadione at 1 μg·mL−1 and hemin at 5 μg·mL−1 and. Bacterial cells were heat-killed (HK) at 95°C for 15min and density was adjusted to 1×10^7 CFU·mL−1. HK bacteria were stored at −80 °C and used in further experiments.

2.10 Murine cellular biology and *in vitro* experimentation

2.10.1   Murine bone-marrow derived dendritic cells (BMDCs)

Bone marrow cells were isolated from femur and tibia of the animals. The bone marrow was smashed and filtered through a 70μm filter. $2x10^6$ cells were seeded in a sterilin-plate (Thermo Fisher) in 10ml of RPMI-1640, 10% FBS, 20μg/ml gentamycin and 20ng/ml of mouse recombinant GM-CSF (Miltenyi Biotec). After 3 days 10ml of fresh medium was added to the culture. On day 6 and 8 the culture was replenished with 10ml of fresh medium. At day 10 non-adherent cells were collected, checked at FACS for DCs markers, such as CD11c and used in further experiments.

2.10.2   Gut microbiota priming of murine iNKT cells

iNKT cells were sorted from B cell depleted (negative selection with Mouse CD19 microbeads, Miltenyi) spleen of C57BL/6 animals. Sorting strategy is shown in Figure 2.1. 1×10^5 BMDCs were primed with 1×10^6 CFU of heat-inactivated fecal microbiota of controls or AOM/DSS treated C57BL/6, *Traj18*-/- and *CD1d*-/- animals. Primed BMDCs were cultured with 2×10^5 splenic sorted iNKT cells in RPMI-1640 with 10%FBS, pen/strep for 24h. Upon stimulation iNKT cells activation was measured by FACS analysis. As negative control endogenous activation of BMDCs alone was tested. Fluorescent minus one (FMO) served as negative controls.
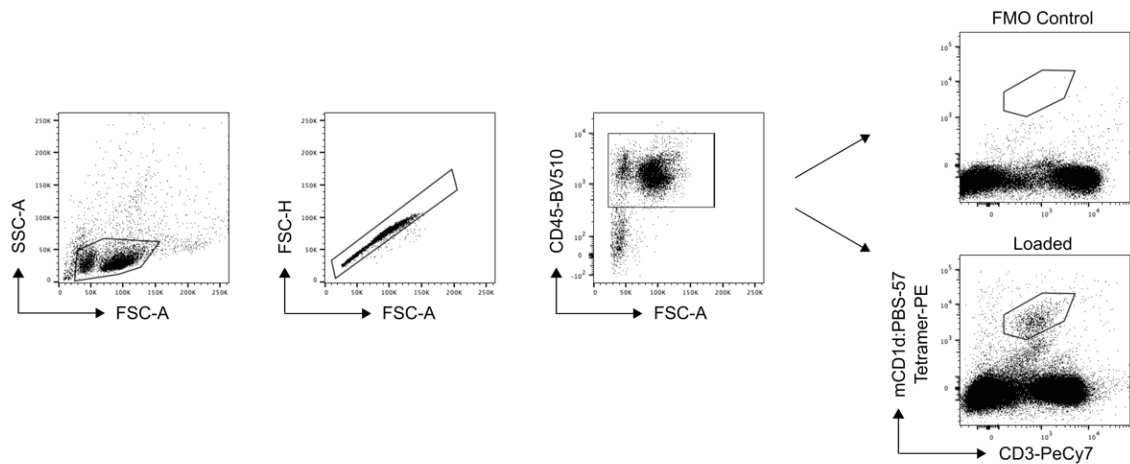
Figure 2.1*: Gating strategy for iNKT cells sorting from murine splenocytes.*

2.11 Human cellular biology and *in vitro* experimentation

2.11.1 Peripheral blood mononuclear cells isolation (PBMCs) and irradiation

Human peripheral blood mononuclear cells were isolated by Ficoll-Hypaque gradient (Sigma-Aldrich). Briefly, 20ml of blood were centrifuged at 300g for 10min with no brake on the centrifuge and plasma was collected. It was heat-inactivated for 30min at 56 °C and centrifuged at 1500g for 20min. The supernatant was collected, filtered through a 0,22μm filter and store at – 20 °C. Cells were resuspended in 20ml of PBS and it was layered on top of 15ml of Ficoll-Hypaque and centrifuged at 300g for 20min with no brake on the centrifuge. The ring formed between the two solutions, containing PBMCs, was collected using a Pasteur pipette (BD). cells were centrifuged, resuspended, counted and further used. For feeders' generation PBMCs were irradiated 2.5Gy/min per 5min.

2.11.2 Human monocytes-derived dendritic cells generation (moDCs)

CD14$^+$ cells were isolated from PBMCs by magnetic separation using CD14 MicroBeads (Miltenyi Biotec) following manufacturer instructions. 9x10^6 CD14$^+$ cells were seeded in a six-well plate (EuroClone) per well. Cells were cultured in RPMI-1640 with 5% of autologous plasma, 100μg/ml of gentamycin (Himedia), 1000IU/ml of recombinant human rhGM-CSF (Miltenyi Biotec) and 400 IU/ml of rhIL4 (Miltenyi Biotec). On day

3 and 5 after seeding the same amount of rhGM-CSF and rhIL4 was added to cells. At day 6 after seeding cells were checked at the flow cytometry for extracellular marker expression. For being used as moDC cells must be Cd14$^-$, CD11c$^+$ and CD86$^+$.

2.11.3   Peripheral blood neutrophils isolation

Human peripheral neutrophils were isolated by dextran (Merck) gradient and subsequent Percoll-Plus gradient. Briefly, 15 ml of blood were centrifuged at 400g per 10min. Supernatant was discarded and pellet resuspended to a volume of 25ml with cold Hank's balanced salt solution (HBSS, Himedia). 25 ml of sterile filtered 3% dextran in HBSS were added to the solution and gently mixed by inversion. The solution was left 30min to sediment. Supernatant was collected and centrifuged at 300g for 10min, pellet was lysed using 1ml of ACK lysis buffer (life Technologies) for 5min. The reaction was stopped adding 20ml of HBSS. The solution was centrifuged at 300g for 10min and pellet was resuspended in 2ml of HBSS. A Percoll-Plus gradient of 51% and 42%, in HBSS, was layered. Cell solution was layered on top of the Percoll-Plus gradient and centrifuged at 400g for 10min without brake. Cell pellet, containing neutrophils, was collected, counted and used in *in vitro* assays.

2.11.4   Human lamina propria mononuclear cells isolation

Human lamina propria mononuclear cells were isolated by enzymatic digestion and Percoll-Plus gradient. Briefly, the dissected intestinal mucosa was freed of mucus and epithelial cells in sequential steps with DTT (0.1 mmol/l) and EDTA (1 mmol/l) (both from Sigma-Aldrich) in HBSS with pen/strep and gentamycin. If needed epithelial cells were recovered from the EDTA washing steps, counted and used for further analysis. Samples were then digested with collagenase D (400 U/ml) (Worthington Biochemical Corporation) in RPMI-1640 pen/strep and gentamycin for 5 h at 37 °C in agitation. Cell solution was filtered through a 70μm and a 100μm filter and centrifuged at 300g for 5min. Cells were resuspended in Percoll-Plus 40% and a Percoll-Plus gradient of 100%, 60%, 40% and 30% was layered and centrifuged 1200g for 20min with no brake. The white ring formed at the interface between the 60% and the 40% phase was carefully collected using Pasteur pipettes. Cells were washed with RPMI-1640 10%FBS pen/strep and gentamycin, counted and used for further analysis.

2.11.5   Generation of human iNKT cell lines

Human iNKT cell lines (CD45$^+$CD3$^+$CD1d:PBS57Tet$^+$) were sorted using a FACSAria (BD) machine from either PBMCs or LPMCs. Sorted iNKT cells were expanded *in vitro* for 2 weeks in the presence of irradiated peripheral blood feeders, hIL2 (100 U/ml; Proleukin), and PHA (1μg/ml; Sigma-Aldrich). The gating strategy for the identification of human iNKT cells is shown in Figure 2.2. Unloaded tetramers are used as controls.
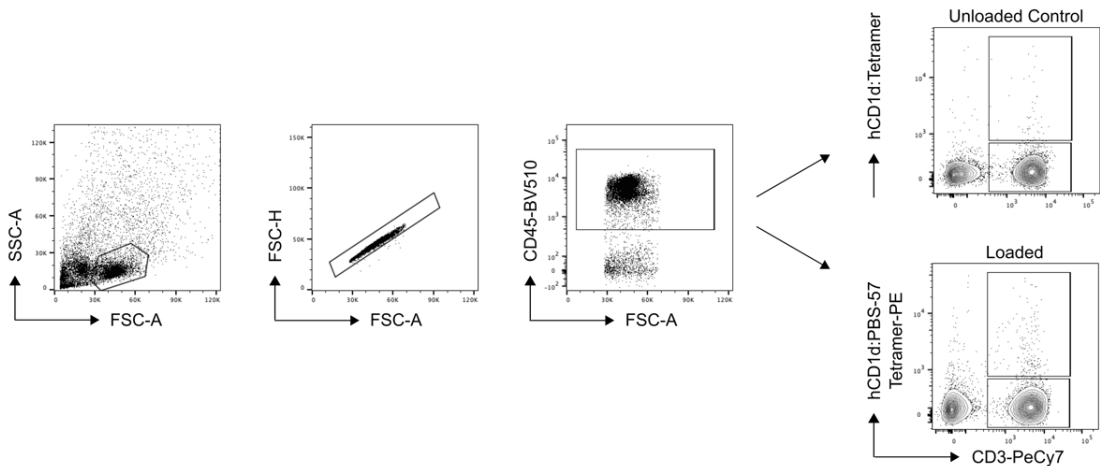
Figure 2.2: *Gating strategy to identify human iNKT cells.*

2.11.6   Human iNKT cells in vitro priming

1×10^5 proficient moDCs were primed with either 4×10^5 CFU of HK *Fusobacterium nucleatum* (strain ATCC25586, DSMZ #DSM15643) or 100ng/ml of αGalCer and then cultured with 1×10^5 human iNKT cells in RPMI-1640 10% FBS, pen/strep. After 24h, iNKT cells were analyzed at FACS by intracellular staining or used in *in vitro* functional experiments. As negative control endogenous activation of moDC alone was tested (NS). When iNKT cells were used for further RNA extraction they were depleted of any remaining moDC by staining with CD86-PE and negative selection with anti-PE microbeads (Miltenyi Biotec).

2.11.7   *In vitro* cytotoxicity assay

Cytotoxicity was assessed using the cytotoxicity lactate dehydrogenase (LDH) Assay Kit-WST (nonhomogeneous assay, Dojindo, EU) following the manufacturer's instructions and as previously described [151]. All experimental conditions were performed in duplicate. 2.5×10^4 Colo 205 and RKO cells were incubated at 37 °C for 4 hours with bacterial primed iNKT cell lines at a 8:1 ratio. Supernatants were collected in optically-cleared 96 well plate and absorbance was measured at 490nm using a GloMax Microplate Reader (Promega, Madison, WI, USA) after the colorimetric reaction for LDH. The percentage of cytotoxicity was calculated as follows: (test well – spontaneous release control)/(maximal release control – spontaneous release control) × 100.

2.11.8   iNKT-Neutrophil co-culture assay

Bacteria or αGalCer primed iNKT cells (2×10^5) were co-cultured with freshly isolated neutrophils in a 1:1 ratio, in RPMI-1640, 10% FBS and pen/strep. After 24 hours cells were stained for cytokine, extracellular molecule expression and respiratory burst capacity.

2.11.9   Neutrophil survival assay

Freshly isolated neutrophils were cultured with RPMI-1640 + 10% FBS with culture supernatants at 10% volumes of NS, αGalCer or *Fn*-primed iNKT cells for 16h at 37°C. After culture cells were then stained for apoptosis and necrosis using the FITC Annexin V Apoptosis Detection Kit with 7-AAD (Biolegend) following manufacturer's instruction and acquired at a FACS Celesta flow cytometer (BD Biosciences, Franklin Lakes NJ, USA).

2.11.10   Neutrophil migration assay

2.5×10^4 of freshly isolated neutrophils were seeded on a 3μm-pore transwell (SARSTEDT) in RPMI-1640 + 2% FBS. Culture supernatants of NS or αGalCer or *Fn*-primed iNKT cells diluted 10% in RPMI-1640 + 2% FBS was used as chemoattractant on the bottom of the transewll. When needed neutrophils were pre-incubated for 20 min

at 37°C with Reparixin (20 μM, MedChemExpress), to block the IL8-CXCR1/2 pathway. RPMI supplemented with 10% FBS was used as positive control. Migration was left for 4 hours and then the total number of cells on the bottom of the plate were stained and counted using plate-acquisition mode with maximum cell counts and fixed volumes on a FACS Celesta flow cytometer (BD Biosciences, Franklin Lakes NJ, USA).

2.11.11 Naïve CD4$^+$ T *in vitro* proliferation assay

Naïve CD4$^+$T cells were isolated from PBMCs of healthy donors using CD4 näive human microbeads (Miltenyi Biotech). Naïve CD4$^+$ T (2.5 x 10^4 cells/well) were labelled with 1 nM Far Red CellTrace (ThermoFisher) and cultured in medium with hIL2 (Proleukin) and anti-CD28 antibody (2 μg/ml, Tonbo) and they were plated in anti-CD3 antibody (2 μg/ml, Tonbo) pre-coated 96-well plates (NUNC Maxisorp) pre-coated with anti-CD3 antibody (2 μg/ml, Tonbo). 2.5 x 10^4 of freshly isolated neutrophils were co-cultured with naïve CD4$^+$ T cells in the presence of 10% supernatant from NS, αGalCer or *Fn*-primed iNKT cells. After 5 days cells were labelled with Zombie vital dye (Biolegend) and analyzed with FACS Celesta flow cytometer (BD Biosciences, Franklin Lakes NJ, USA). Proliferation index is calculated with the FlowJo Proliferation Modeling tool and normalized on minimal proliferation.

2.11.12 Respiratory burst assay

Respiratory burst capacity and so ROS production was detected using the Neutrophil/Monocyte Respiratory Burst assay (Cayman) following manufacturer's instructions.

2.12 Molecular Biology

2.12.1 RNA extraction and reverse transcription quantitative real time PCR

RNA was isolated from 0.5g human colonic tissues by homogenization, using an Ultra-Turrex T25 homogenizer (Janke & Kunkel IKA-Labortechnik) in 300µl of TriFast (Euroclone). RNA was extracted using Direct-zolTM RNA Miniprep Plus (ZymoResearch) according to manufacturer's instructions. cDNAs were generated from 1µg of total RNA with OneScript® Plus cDNA Synthesis Kit (abm) according to manufacturer's instructions. Gene expressions were measured by qPCR using BlasTaqTM 2X qPCR MasterMix (abm), following manufacturer's instructions, on a Viia7 machine (life technology). Human genes were normalized to *GAPDH* expression. Primers used in this study are listed in Table 2.1.

HUMAN PRIMERS	VENDOR
ACVRIL1 FWD : 5' - CGAGGGATGAACAGTCCTGG - 3'	(Romano G et al., 2016)
ACVRIL1 REV: 5' - GTCATGTCTGAGGCGATGAAG - 3'	(Romano G et al., 2016)
BCL2; QUANTITECT PRIMER ASSAY	QIAGEN, Cat. #: QT00025011
BCL2L1 FWD: 5' - GAGCTGGTGGTTGACTTTCTC - 3'	(Zhao S et al., 2016)
BCL2L1 REV: 5' - TCCATCTCCGATTCAGTCCCT - 3'	(Zhao S et al., 2016)
CASP3; QUANTITECT PRIMER ASSAY	QIAGEN, Cat. #: QT00997997
CCL2 FWD: 5' - AAGATCTCAGTGCAGAGGCTCG - 3'	(Nam J et al., 2006)
CCL2 REV: 5' - *TTGCTTGTCCAGGTGGTCCAT - 3'*	(Nam J et al., 2006)
CCL20; QUANTITECT PRIMER ASSAY	QIAGEN, Cat. #: QT00012971
CD274 (PDL1); QUANTITECT PRIMER ASSAY	QIAGEN, Cat. #: QT00082775
CRLF2 (TSLPR); QUANTITECT PRIMER ASSAY	QIAGEN, Cat. #: QT00210987
CXCL16A FWD: 5' - GCCATCGGTTCAGTTCA - 3′	(Mei J et al., 2019)
CXCL16A REV: 5' - CAATCCCCGAGTAAGCAT - 3'	(Mei J et al., 2019)
CXCL8; QUANTITECT PRIMER ASSAY	QIAGEN, Cat. #: QT00000322
FN1 FWD: 5' - AGGAAGCCGAGGTTTTAACTG ' 3'	(D. Britt R et al., 2015)
FN1 REV: *5′ - AGGACGCTCATAAGTGTCACC - 3′*	(D. Britt R et al., 2015)
FOXP3 FWD: 5' - CAGCACATTCCCAGAGTTCCTC - 3'	(Yuan X et al., 2011)
FOXP3 REV: 5' - GCGTGTGAACCAGTGGTAGATC - 3'	(Yuan X et al., 2011)
GAPDH FWD: 5' - CTGCTCTACGACATGAACGG - 3'	(Thanseem I et al., 2011)
GAPDH REV: 5' - TGGCATGGACTGTGGTCATG - 3'	(Thanseem I et al., 2011)
GAPDH; QUANTITECT PRIMER ASSAY	QIAGEN, Cat. #: QT00079247
GATA3 FWD: 5' - TCTGACAGTTCGCACAGGAC - 3'	This work
GATA3 REV 5' - *AAAATGAACGGACAGAACCG - 3′*	This work

ID1 FWD: 5'- CTGCTCTACGACATGAACGG - 3'	(Yang Y et al., 2008)
ID1 REV: 5'- GAAGGTCCCTGATGTAGTCGAT - 3'	(Yang Y et al., 2008)
IFNG FWD : 5 ' - GAGTGTGGAGACCATCAAGGA - 3'	(Pinto J et al., 2010)
IFNG REV: 5 ' - GTATTGCTTTGCGTTGGACA - 3'	(Pinto J et al., 2010)
IL10 FWD: 5' - AACAAGTTGTCCAGCTGATCC - 3'	(Burrello C et al., 2022)
IL10 REV 5' - *CAACCTGCCTAACATGCTTC - 3'*	(Burrello C et al., 2022)
IL13 FWD: 5' - CTGGTCAACATCACCCAGAAC - 3'	(Souza PPC et al., 2013)
IL13 REV: 5' - *CTGTCAGGTTGATGCTCCATAC - 3'*	(Souza PPC et al., 2013)
IL17A; QUANTITECT PRIMER ASSAY	QIAGEN, Cat. #: QT00009233
IL22; QUANTITECT PRIMER ASSAY	QIAGEN, Cat. #: QT00034853
IL23P19 FWD: 5' - TGTTCCCCATATCCAGTGTG - 3'	This work
IL23P19 REV 5' - *GCAAGCAGAACTGACTGTTG - 3'*	This work
IL4; QUANTITECT PRIMER ASSAY	QIAGEN, Cat. #: QT00012565
IL5; QUANTITECT PRIMER ASSAY	QIAGEN, Cat. #: QT00001435
PDCD1 (PD1); QUANTITECT PRIMER ASSAY	QIAGEN, Cat. #: QT01005746
RORG FWD: 5' - TTTTCCGAGGATGAGATTGC - 3'	(Yu S et al., 2015)
RORG REV: *5′ - CTTTCCACATGCTGGCTACA - 3′*	(Yu S et al., 2015)
TBET FWD: 5' - GATGCGCCAGGAAGTTTCAT - 3'	(Alvarez-Rodriguez et al., 2019)
TBET REV: 5' - *GCACAATCATCTGGGTCACATT - 3'*	(Alvarez-Rodriguez et al., 2019)
TGFB1 FWD: 5' - GAGCCTGAGGCCGACTACTA - 3'	(Esebanmen G et al., 2017)
TGFB1 REV: 5' - *GGGTTCAGGTACCGCTTCTC - 3'*	(Esebanmen G et al., 2017)

Table 2.1:*Human primers for qPCR.*

2.12.2 RNA extraction and sequencing of sorted murine neutrophils

Neutrophils were sorted from tumors, adjacent non-tumor tissues and healthy colons as described in Paragraph2.5. RNA was isolated from ~ 5×10^5 neutrophils per group, using the RNeasy Micro Kit (QIAGEN) following manufacturer's instruction. Carrier RNA was not used. RNA quality was checked on the Agilent 2100 Bioanalyzer (Agilent Technologies). Sequencing libraries were prepared with NEBNext® rRNA Depletion Kit v2, the NEBNext® Ultra™ II Directional RNA Library Prep kits and the NEBNext® Multiplex Oligos for Illumina® (96 Unique Dual Index Primer Pairs), following manufacturer's instructions. Libraries were sequenced on the Illumina NovaSeq platform at the genomic unit of IEO. 4 different sample per group were sequenced.

2.12.3   RNA sequencing of human iNKT cells

RNA was extracted from 1×10^6 moDC-depleted primed-iNKT cells using the RNeasy kit (Qiagen). RNA quality was checked at the Agilent 2100 Bioanalyzer (Agilent Technologies). 1µg of RNA was used for libraries generation using the Illumina TruSeq RNA Library Prep Kit v2 following the manufacturer's instructions. Libraries were sequenced as pair-end on the Illumina NovaSeq platform at the genomic unit of IEO. Three different priming experiments were sequenced together.

2.12.4   16S rRNA gene sequencing of human and murine mucosal samples

Mucus was scraped from the human and murine colons (tumor and non-tumor adjacent site) in TES buffer and stored at -80°C until DNA extraction. DNA was extracted using G NOME DNA isolation kit (Thermo Fisher) following manufacturers' instructions. Libraries were prepared by firstly amplifying the 16S rRNA using interest-specific primers for:

V3 (5′-TCGTCGGCAGCGTCAGATGTGTATAAGAGACAGCCTACGGGNGGCWGCAG-3′),

V4 (5′-TCGTCGGCAGCGTCAGATGTGTATAAGAGACAGCCTACGGGNGGCWGCAG-3′) regions, together with overhang adapters, using 2x KAPA HiFi HotStart ReadyMix (Roche). The Amplicon PCR program used is depicted in Figure 2.3. DNA resulting from the Amplicon PCR were subsequently amplified with dual-index primers using Nextera Xt Index Kit V2 Set A (Illumina). Libraries were checked for quality on the Agilent 2100 Bioanalyzer (Agilent Technologies) and sequenced pair-end using the Illumina Miseq Reagent Nano Kit V2 500 cycles at the genomic unit of IEO.
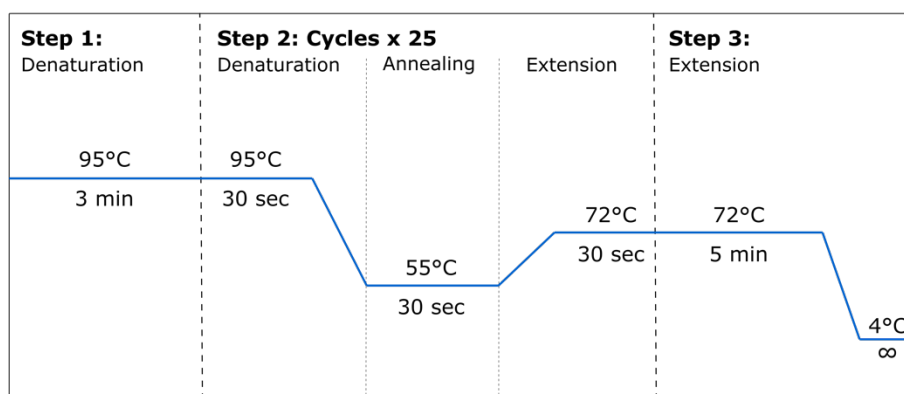
Figure 2.3: *Schematic representation of the Amplicon PCR program for 16S rRNA.*

2.12.5   Protein lysates

Proteins were extracted from 0.5g of human colonic tissues. They were homogenized using an Ultra-Turrex T25 homogenizer (Janke & Kunkel IKA-Labortechnik) in 300μl of RIPA buffer (Cell Signaling Technology) supplemented with phosphatase inhibitors (Sigma) and protease inhibitors (Complete Ultra tablets, Roche). Samples were then incubated at 4 °C for 30min under slow rotation and centrifuged at 25000g for 15 min at 4 °C. The supernatant was quantified at the Spectrophotometer (NanoDrop ND-1000) with Bradford Assay (BioRad).

2.13 ELISA assay

2.13.1   Cytokines detection in supernatant

Cytokines in supernatants were detected by coating maxisorp immuno plate (thermofisher) with anti-human capturing antibody for GM-CSF, IL17 and IFNγ (Biolegend) at 2μg/ml in carbonate coating buffer (11.9% $NaHCO_3$, 28% Na_2CO_3 in H_2O at pH 9.5) at 4°C overnight. Plates were blocked with PBS/Bovine Serum Albumin 2% for 1 hour at room temperature, while sample incubation was performed for 2 hours at room temperature. Standards and samples were analyzed in duplicates. Protein detection was performed with 2μg/ml of biotin anti-human detection antibody for GM-CSF, IL17 and IFNγ (Biolegend) for 1 hour at room temperature. Streptavidin-HRP conjugate (Biolegend) and tetramethylbenzidine (TMB) chromogen solution (ThermoFisher) were used to develop the assay, according to manufacturer's instruction. Reaction was blocked using sulfuric acid 1 N (Sigma-Aldrich).). Detection of human IL8 was performed using OptEIA Human IL-8 (BD) according to manufacturer's instruction. Plates were red at a wavelength of 450nm using Glomax (Promega).

2.13.2   Tissue ELISA

Detection of human IL8 and CXCL16 was performed on 200μg of protein lysate using OptEIA Human IL-8 (BD) and CXCL16 DuoSet ELISA kit (R&D), according to manufacturer's instruction. Plates were red at a wavelength of 450nm using Glomax (Promega).

2.14 Flow Cytometry

iNKT cells were stained and identified using human or mouse CD1d:PBS57 Tetramer (NIH Tetramer core facility) diluted in PBS with 1% FBS for 30 min at 4°C. For intracellular cytokine detection cells were previously incubated for 3 hours at 37°C in RPMI-1640 10% FBS pen/strep with PMA (50ng/ml, Merck), Ionomycin (1µg/ml, Merck) and Brefeldin A (10 µg/ml, Merck). Firstly, blocking of non-specific binding of immunoglobulin to Fc receptors (CD16/32, Biolegend) was performed for 20 min in PBS. Then extracellular staining and Zombie vital dye (Biolegend) were performed in PBS for 30 min. Cells were then fixed and permeabilized using Cytofix/Cytoperm (BD). Samples were analyzed with a FACS Celesta flow cytometer (BD Biosciences, Franklin Lakes NJ, USA). Gating strategy for unconventional T cells and ILCs is depicted in Figure 2.4. For the multi-dimensional analysis using t-Distributed Stochastic Neighbor Embedding (t-SNE) visualization and Phenograph clustering refer to the dedicated paragraph (Section2.15.1). The list of dyes and antibodies used in the study are listed in Table 2.2.
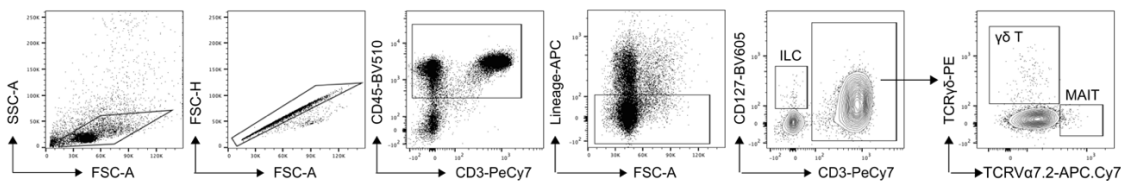
Figure 2.4: *Gating strategy for human unconventional T cells and ILCs.*

REAGENT	SOURCE	IDENTIFIER
Anti-human CD10 BV650	BD Biosciences	Cat. #: 563734; Clone: HI10a; RRID: AB_2738393
Anti-human CD103 BV421 c	Biolegend	Cat. #: 350214; Clone: Ber-ACT8 ; RRID: AB_2563514
Anti-human CD11c BV605	Biolegend	Cat. #: 301636; Clone: 3.9; RRID: AB_2563796
Anti-human CD127 Super Bright 600	ThermoFisher Scientific	Cat. #: 63-1278-42; Clone: eBioRDR5; RRID: AB_266260
Anti-human CD137 (4-1BB) Super Bright 600	ThermoFisher Scientific	Cat. #: 63-1379-42; Clone: 4B4; RRID: AB_2717053
Anti-human CD14 APC	Biolegend	Cat. #: 301808; Clone: M5E2; RRID: AB_314190
Anti-human CD15 BV785	Biolegend	Cat. #: 323044; Clone: W6D3; RRID: AB_2632921
Anti-human CD152 (CTLA-4) APC	BD Biosciences	Cat. #: 560938; Clone: BNI3; RRID: AB_398615
Anti-human CD16 APC-H7	BD Biosciences	Cat. #: 560715; Clone: 3G8; RRID: AB_1727432

Anti-human CD161 FITC	TONBO	Cat. #: 35-1619-T100; Clone: HP-3G10
Anti-human CD178 (FasL) APC	TONBO	Cat. #: 20-9919-T100; Clone: NOK-1
Anti-human CD184 (CXCR4) APC	Miltenyi Biotec	Cat. #: 130-098-357; Clone: 12G5
Anti-human CD19 APC	TONBO	Cat. #: 20-0198-T100; Clone: SJ25C1
Anti-human CD19 BV650	Biolegend	Cat. #: 302238; Clone: HIB19; RRID: AB_2562097
Anti-human CD1d APC	Miltenyi Biotec	Cat. #: 130-099-978; Clone: 51.1
Anti-human CD1d BV421	Biolegend	Cat. #: 350316; Clone: 51.1; RRID: AB_2687379
Anti-human CD253 (TRAIL) BV786	Biolegend	Cat. #: 743723; Clone: JRIK-2; RRID: AB_2741699
Anti-human CD261 (Trail R1) BV605	BD Biosciences	Cat. #: 745103; Clone: S35-934; RRID: AB_2742711
Anti-human CD262 (Trail R2) BV510	BD Biosciences	Cat. #: 745057; Clone: B-K29; RRID: AB_2742678
Anti-human CD274 (PDL1) PE	Biolegend	Cat. #: 393608; Clone: MIH2; RRID: AB_2749925
Anti-human CD274 (PDL1) PE-Cy7	BD Biosciences	Cat. #: 558017; Clone: MIH1; RRID: AB_396986
Anti-human CD279 (PD1) BV650	BD Biosciences	Cat. #: 564104; Clone: EH12; RRID: AB_2738595
Anti-human CD3 APC-Cy7	TONBO	Cat. #: 25-0038-T100; Clone: UCHT1
Anti-human CD3 PE-Cy7	TONBO	Cat. #: 60-0038-T100; Clone: UCHT1
Anti-human CD326 (EpCAM) PerCP-eFluor™ 710	eBiosciences	Cat. #: 46-9326-42; Clone: 1B7; RRID: AB_1834413
Anti-human CD33 BV510	Biolegend	Cat. #: 366610; Clone: P67.6; RRID: AB_2566403
Anti-human CD366 (Tim-3) BV785	Biolegend	Cat. #: 345032; Clone: F38-2E2; RRID: AB_2565833
Anti-human CD4 APC-Cy7	TONBO	Cat. #: 25-0049-T100; Clone: RPA-T4
Anti-human CD4 BV605	Biolegend	Cat. #: 300556; Clone: RPA-T4; RRID: AB_2564391
Anti-human CD4 PerCP-Cy5.5	Biolegend	Cat. #: 317428; Clone: OKT4; RRID: AB_1186122
Anti-human CD4 PerCP-Cy5.5	Biolegend	Cat. #: 317428; Clone: OKT4; RRID: AB_1186122
Anti-human CD45 BV510	BD Biosciences	Cat. #: 563204; Clone: HI30; RRID: AB_2738067
Anti-human CD45 FITC	BD Biosciences	Cat. #: 560976; Clone: HI30; RRID: AB_395874
Anti-human CD56 APC	BD Biosciences	Cat. #: 555518; Clone: B159; RRID: AB_398601
Anti-human CD62L PE	Miltenyi Biotec	Cat. #: 130-113-620; Clone: 145/15
Anti-human CD66b PerCP-Cy5.5	BD Biosciences	Cat. #: 562254; Clone: G10F5; RRID: AB_11154419
Anti-human CD68 APC-Cy7	Biolegend	Cat. #: 333822; Clone: Y1/82A; RRID: AB_2571965
Anti-human CD69 Alexa Fluor-700	BD Biosciences	Cat. #: 560739; Clone: FN50; RRID: AB_1727505
Anti-human CD69 PE-Cy7	BD Biosciences	Cat. #: 560712; Clone: FN50; RRID: AB_1727509

Anti-human CD8a Alexa Fluor-700	Biolegend	Cat. #: 344724; Clone: SK1; RRID: AB_2562790
Anti-human CD86 Pacific Blue	BD Biosciences	Cat. #: 305418; Clone: IT2.2; RRID: AB_493663
Anti-human CD86 PE	BD Biosciences	Cat. #: 557344; Clone: 2331; RRID: AB_396652
Anti-human CD95 (Fas) BV650	Biolegend	Cat. #: 305642; Clone: DX2; RRID: AB_2632622
Anti-human GM-CSF PerCP-Cy5.5	Biolegend	Cat. #: 502312; Clone: BVD2-21C11; RRID: AB_11147946
Anti-human GranzymeA PeCy7	ThermoFisher Scientific	Cat. #: 25-9177-41; Clone: CB9; RRID: AB_2573537
Anti-human GranzymeB eFluor450	ThermoFisher Scientific	Cat. #: 48-8896-41; Clone: JN4TL33; RRID: AB_2724391
Anti-human HLA-DR FITC	Miltenyi Biotec	Cat. #: 130-095-295; Clone: REA805
Anti-human HLA-DR SB780	eBiosciences	Cat. #: 78-9956-42; Clone: LN3; RRID: AB_2724457
Anti-human IFNg FITC	BD Biosciences	Cat. #: 554551; Clone: 4S.B3; RRID: AB_395473
Anti-human IL13 PE-Cy7	Biolegend	Cat. #: 501914; Clone: JES10-5A2; RRID: AB_2616746
Anti-human IL17A APC	ThermoFisher Scientific	Cat. #: 11-7179-42; Clone: eBio64DEC17; RRID: AB_1582221
Anti-human IL17A FITC	ThermoFisher Scientific	Cat. #: 11-7179-42; Clone: eBio64DEC17; RRID: AB_10805390
Anti-human IL22 PerCP-Cy5.5	Biolegend	Cat. #: 366710; Clone: 2G12A41; RRID: AB_2566794
Anti-human IL4 BV510	Biolegend	Cat. #: 500836; Clone: MP4-25D2; RRID: AB_2650993
Anti-human Ki67 Alexa Fluor 647	BD Biosciences	Cat. #: 558615; Clone: B56; RRID: AB_647130
Anti-human Ki67 BV510	BD Biosciences	Cat. #: 563462; Clone: B56; RRID: AB_2738221
Anti-human Perforin BV510	Biolegend	Cat. #: 308120; Clone: dG9; RRID: AB_2563829
Anti-human TCR gamma/delta PE	ThermoFisher Scientific	Cat. #: MHGD04; Clone: 5A6.E9; RRID: AB_10374518
Anti-human TCR Vα7.2 APC-Cy7	Biolegend	Cat. #: 351714; Clone: 3C10C; RRID: AB_2561996
Anti-human TIGIT eFluor 450	ThermoFisher Scientific	Cat. #: 48-9500-42; Clone: MBSA43; RRID: AB_2637414
Anti-human TNF-α BV785	Biolegend	Cat. #: 502948; Clone: MAb11; RRID: AB_2565858
Human CD1d:BV421	NIH Tet facility	-
Human CD1d:PBS57 Tet-BV421	NIH Tet facility	-
Human CD1d:PBS57 Tet-PE	NIH Tet facility	-
Human CD1d:PE	NIH Tet facility	-
Anti-mouse CD11b APC-Cy7	TONBO	Cat. #: 25-0112-U100; Clone: M1/70
Anti-mouse CD274 (PDL1) BV786	BD Biosciences	Cat. #: 741014; Clone: MIH5; RRID: AB_2740636
Anti-mouse CD11c FITC c	TONBO	Cat. #: 35-0114-U500; Clone: N418

Anti-mouse CD19 FITC	TONBO	Cat. #: 35-0193-U500; Clone: 1D3
Anti-mouse CD279 (PD1) APC	Biolegend	Cat. #: 562671; Clone: J43; RRID: AB_2737712
Anti-mouse CD3 FITC	Biolegend	Cat. #:100204; Clone: 17A2; RRID: AB_312661
Anti-mouse CD3 PE-Cy7	Biolegend	Cat. #: 100220; Clone: 17A2; RRID: AB_1732057
Anti-mouse CD4 BV650	Biolegend	Cat. #: 100545; Clone: RM4-5; RRID: AB_11126142
Anti-mouse CD4 PE/Dazzle594	Biolegend	Cat. #:100455; Clone: GK1.5; RRID: AB_2565844
Anti-mouse CD45 Alexa Fluor 700	Biolegend	Cat. #: 103127; Clone: 30-F11; RRID: AB_493714
Anti-mouse CD45.2 APC-Cy7	Biolegend	Cat. #: 109824; Clone: 104; RRID: AB_830789
Anti-mouse CD45.2 BV510	Biolegend	Cat. #: 109838; Clone: 104; RRID: AB_2650900
Anti-mouse CD8a APC-Cy7	BD Biosciences	Cat. #: 557654; Clone: 53-6.7; RRID: AB_396769
Anti-mouse CD8a Super Bright 600	ThermoFisher Scientific	Cat. #: 63-0081-82; Clone: 53-6.7; RRID: AB_2637163
Anti-mouse F4/80 PE	TONBO	Cat. #: 50-4801-U025; Clone: BM8.1
Anti-mouse GM-CSF FITC	Biolegend	Cat. #: 505404; Clone: MIP1-22E9; RRID: AB_315380
Anti-mouse GranzymeB PerCP-Cy5.5	Biolegend	Cat. #: 372212; Clone: QA16A02; RRID: AB_2728379
Anti-mouse IL4 PE-Cy7	Biolegend	Cat. #:504118; Clone: 11B11; RRID: AB_10898116
Anti-mouse IL10 PE	Biolegend	Cat. #:554467; Clone: JES5-16E3; RRID: AB_395412
Anti-mouse IL13 PerCP-eFluor710	Thermo Fisher Scientific	Cat. #:46-7133-82; Clone: eBio13A; RRID: AB_11218496
Anti-mouse IL17A Alexa Fluor-700	Biolegend	Cat. #: 506914; Clone: TC11-18H10.1; RRID: AB_536016
Anti-mouse IL17A BV605	BD Biosciences	Cat. #:564169; Clone: TC11-18H10
Anti-mouse IL22 Alexa Fluor 647	Biolegend	Cat. #:516406; Clone: Poly5164; RRID: AB_2280206
Anti-mouse Ly6G APC	TONBO	Cat. #: 20-1276-U025; Clone: 1A8
Anti-mouse Ly6G eFluor450	ThermoFisher Scientific	Cat. #: 48-9668-82; Clone: 1A8; RRID: AB_2637124
Anti-mouse Perforin PE	Biolegend	Cat. #: 154306; Clone: S16009A; RRID: AB_2721639
Anti-mouse TNFa BV711	Biolegend	Cat. #:506349; Clone: MP6-XT22; RRID: AB_2629800
CD16/32 purified	TONBO	Cat. #: 70-0161-U500; Clone: 2.4G2
Mouse CD1d:BV421	NIH Tet facility	-
Mouse CD1d:PBS57 Tet-BV421	NIH Tet facility	-
Mouse CD1d:PBS57 Tet-PE	NIH Tet facility	-
Mouse CD1d:PE	NIH Tet facility	-
Zombie Yellow™ Fixable Viability Kit	Biolegend	Cat. #: 423104

Table 2.2: *Antibodies and dye used in the study.*

2.15 Analysis

2.15.1 Multi-dimensional flow cytometry analysis

FCS files of TUM and NCT immune infiltrate were upload in FlowJo software (Version 10.8) and compensated according to the software usage. Irregularities on the flow stream were checked by querying a single color-parameter per each laser on the time-parameter. If variations in the flow stream were detected, they were excluded from the analysis. Data were accurately checked for antibodies aggregates by analyzing each parameter in a bimodal plot. Morphological gates on viable lymphocytes, singlets and subsequently CD3$^+$ cells were applied. To create uniform size populations CD3$^+$ populations of each sample were downsampled to 5000 events with the DownSample plugin (Version 3.3.1) of FlowJo. CD3$^+$ downsampled populations were exported as FCS files with applied compensation correction, excluding FSC-A, FSC-H, SSC-A, SSC-H parameters. Files were uploaded in the RStudio environment (Version 3.6.2) and analyzed with the flowCore package (Version 1.38.2). Data were transformed using logicleTransform() function present in the flowCore package. To correct for batch effects each marker was carefully interrogated for its density distribution using the densityplot() function present in the flowViz package (Version 1.36.2). If needed, markers were normalized using the Per-channel normalization based on landmark registration, so the gaussNorm() function of the flowStats package (Version 3.30.0). Peak.density, peak.distance and number of peaks were chosen according to each marker expression. Normalized files were analyzed using the cytofkit package through the cytofkit_GUI interface. For data visualization we used the t-SNE method (perplexity=50, iterations=1000, seed=42, k=50), while clustering was achieved using the Phenograph algorithm [195]. t-SNE plots were visualized on the cytofkitShinyAPP. Clusters FCS were generated, re-imported in FlowJo and manually analyzed to determine their integrated Mean Fluorescence Intensity (iMFI) [196]. To equalize the iMFI of different markers, it was scaled from 0 to 1 [196]. scaled iMFI values were used to define Phenograph clusters and were presented as heatmaps using the heatmap.2() function of the ggplots package (Version 3.1.1). For meta-clustering analysis, the identified cluster of iNKT cells was split into its composing subset and single FCS, each one relative to a single sample (NCT o TUM), were created. FCS were then used again for a new Phenograph run.

2.15.2   16S rRNA data analysis

Reads were pre-processed using the MICCA pipeline (v.1.5) (http://www.micca.org) [197]. Firstly, data were processed for primers trimming and quality filtering with micca trim and micca filter, respectively. Secondly, they were de-noised with the UNOISE61 algorithm implemented in micca out. This generates amplicon sequence variants [ASVs], allow the determination of true biological sequences. ASVs sequences were taxonomically classified using micca classify with the Ribosomal Database Project classifier v2.11 [198]. Nearest Alignment Space Termination [199] was used to perform ultiple sequence alignment of 16S rRNA gene sequences.

Samples were rarefyied at the depth of the less abundant one using micca tablerare. The phyloseq R package [200] was used to estimate alpha (intra-sample richness) and beta-diversity (inter-sample dissimilarity). Permutational multivariate analysis of variance (PermANOVA) test was performed with the adonis() function in the R package vegan with 999 permutations. Differential abundance was tested with the R package DESeq267 using non-rarefied data [201] and the Benjamini-Hochberg procedure was used for false-discovery rate (FDR) corrected pvalues.

2.15.3   Bulk RNA sequencing

RNA-seq reads were pre-processed using the FASTX-Toolkit tools and quality checked were performed with FastQC. Primary analysis (filtering and alignment to the reference genome of the raw reads) and secondary analysis (expression quantification and differential gene expression) have been run in the integrated HTS-flow system [202]. Bioconductor Deseq2 package was used to detect differentially expressed genes and only Benjamini-Hochberg-FDR corrected pvalues are shown [203]. Functional enrichment analyses, Gene Ontology determination and KEGG pathways were performed taking advantage of the DAVID Bioinformatics Resources (DAVID Knowledgebase v2022q2) (https://david.ncifcrf.gov) [204].

2.16 Single cell RNA sequencing

2.16.1 Dataset of immune cells in human CRC (Pelka K. et al., 2021)

Raw count matrices were downloaded from the Gene Expression Omnibus (GEO): accession number GSE178341. Data processing and analysis were performed using the Seurat workflow [205]. Counts were normalized and log-transformed using sctransform [206], while regressing out unique molecular identifier (UMI) counts and the percentage of mitochondrial counts. Highly variable genes were used to perform principal component analysis (PCA) and principal components (PCs) covering the highest variance in the dataset. The selection of these PCs was based on the elbow plot. Clusters were identified using the shared nearest neighbour (SNN) modularity optimization-based clustering algorithm, followed by Louvain community detection, and were visualised using the UMAP dimensional reduction method. iNKT cells were identified as *ZBTB16*$^+$ cells, based on the annotation from the original authors [207].

2.16.2 Dataset of murine polymorphonuclear cells (Veglia F. et al., 2021)

Raw count matrices were downloaded from the GEO: accession number GSE163834. Tumor (n=3) and splenic polymorphonuclear cells (PMNs) from control (n=3) and tumour-bearing mice (n=3) were sequenced, giving a total of 66,854 single cells. Seurat workflow was used for data processing and analysis [205]. Counts were normalized and log-transformed with sctransform [206], regressing out UMI counts and percentage of mitochondrial counts. Principal component analysis (PCA) and principal components (PCs) covering the highest variance in the dataset were performed on highly variable genes. PCs were given to Harmony [208] for batch correction. Shared nearest neighbour modularity optimization-based clustering algorithm and Louvain community detection was used to identify 14 different clusters. Two of them were defined as B cells and macrophages (*Cd79a*, *Cd79b* for B cells, and *Csf1r*, *Mafb*, *Adgre1* for macrophages) and were excluded for further analysis. The remaining clusters were annotated as PMN1, PMN2, and PMN3, according to the expression levels of the markers identified in [209]. The module score of signatures of the C57BL/6 and *Traj18*$^{-/-}$ bulk RNA-sequence of interest was calculated using the AddModuleScore function. Signatures of interest were

defined using genes upregulated in C57BL/6 mice (FDR $p < 0.1$ e $\log_2 FC < -1$) and in *Traj18*^{-/-} mice (FDR $p < 0.1$ e $\log_2 FC > 1$).

2.16.3 Survival and multivariate analysis

We investigated the relevance of iNKT cells and neutrophils co-infiltration on relapse-free survival (RFS) in our cohort of CRC patients. Relapse was defined by the oncologists during period check visit, upon disease reappearance. The clinical importance of neutrophils and iNKT cells transcription factors co-expression, *CEACAM8* and *ZBTB16* respectively, was investigated on overall survival (OS) in the adenocarcinoma cohort (COAD) of The Cancer Genome Atlas (TCGA). Samples were divided in two groups according to the infiltration of neutrophils or to the expression of *CEACAM8*. Similarly, samples were divided in two different groups according to the infiltration of iNKT cells or to the expression of *ZBTB16*. The intersection between neutrophils high infiltration (TANs[High]) and iNKT infiltration, as well as the intersection between *CEACAM8* high expression (*CEACAM8*[High]) and *ZBTB16* expression was also investigated for RFS and OS, respectively. Kaplan-Meier and multivariate analysis were carried out using the R packages *survival* (version 3-2-11) and *survminer* (version 0.4.9) as described in [210]. Multivariate analysis were performed by using the Cox-Log-Rank test and Hazard Ratio using relapse as censor and % of iNKT cells tumor infiltration, % tumor neutrophils, age, gender, MMR status, size of primary tumor (T), involvement of regional lymph nodes (N), tumor grading (G) and tumor location as confounders.

2.16.4 Statistical analysis

Statistical analysis was performed using Prism software (Version 8.2.0, GraphPad) or the R software (version 3.6.2). Paired Wilcoxon test was used to compute NCT and TUM comparisons, both for human and murine experiments, while for unpaired comparisons Mann-Whitney U test was used. Correlation analysis were performed with the two-tailed Spearman's correlation coefficient. Statistical analyses were always performed as two-tailed and pvalues were considered statistically significant when pvalue < 0.05. When pvalues approached significance but did not reach it, the value is explicity shown in the figure. ***pvalue < 0.001; **pvalue < 0.01; *pvalue < 0.05.

2.17 Data availability

16S rRNA gene sequencing data generated in this work can be found in the European Nucleotide Archive (https://www.ebi.ac.uk/ena) with accession number PRJEB56178. RNA-seq data of primed iNKT cell lines and murine neutrophils are deposited at the ArrayExpress database (http://www.ebi.ac.uk/arrayexpress), accession numbers E-MTAB-12278 and E-MTAB-12281, respectively. The scRNA-seq dataset of CRC immune infiltration taken from Pelka K. et al. [207], is publicly available at GEO (https://www.ncbi.nlm.nih.gov/geo/) with accession number GSE178341 The PMN-MDSC scRNA-seq dataset taken from Veglia F. et al. [209], is publicly available at GEO (https://www.ncbi.nlm.nih.gov/geo/) with accession number GSE163834.

3 Results

3.1 Characterization of tumor-infiltrating immune cells in human CRC, with a focus on iNKT cells

During the last decades tumor immunology is under extensive investigation as its understanding could be useful for novel therapeutical approaches. Immunological signatures and cytokines networks are relevant factors of CRC pathology, with cells of the mucosal immunity having a major role as first responders [4]. iNKT cells are unconventional T cells, present at mucosal surfaces, endowed of pro-tumorigenic and anti-tumorigenic functions [8], [15]. Since iNKT cells have pleiotropic roles at the intestinal site, supporting inflammation but also immune regulation in IBD patients [9], we aimed to assess their role in the pathophysiology of CRC.

3.1.1 Study design and patients' characteristics

In order to define the role of iNKT cells in CRC we designed a study (Figure 3.1) and (1) collected paired surgical specimens from tumor lesions (TUM) and non-tumor colonic tissues (NCT) from CRC patients (n=118). Multiparameter flow-cytometry was used to immunophenotype tissue-infiltrating cells and to characterize in detail tumor-infiltrating iNKT cells. From the same patients we also collected feces and the mucosal microbiota of either TUM or NCT for taxonomy identification. (2) iNKT cells were evaluated for their functionalities *in vitro* and, (3) their cellular interactions were tested in two different *in vivo* models of CRC. Finally, (4) the clinical relevance of tumor infiltrating iNKT cells was defined with survival and multivariate analysis using the internal CRC cohort and the COAD-TCGA dataset as validation cohort.
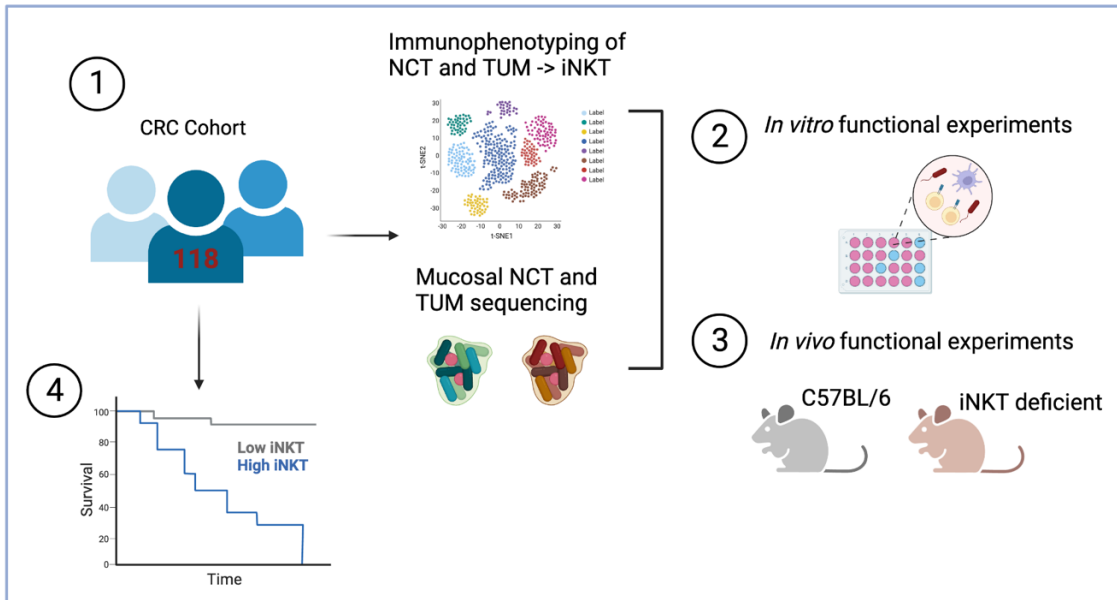
Figure 3.1: *Study design.* ***1)*** *Immunophenotyping and mucosal transcriptomic of CRC cohort (n=118),* ***2)*** *In vitro functional experiments of selected bacteria on human iNKT cell lines,* ***3)*** *In vivo experiments in C57BL/6 wild-type and TRAJ18$^{-/-}$ and CD1d$^{-/-}$ iNKT deficient animals.* ***4)*** *Clinical outcome of iNKT infiltration in CRC.*

Patients recruited in the study underwent surgery for TNM stage 0-III of CRC at the IRCCS Policlinico Ospedale Maggiore, Milan, Italy. Clinical and histopathological characteristics as well as patients' therapies are summarized in Table 3. We intentionally excluded Stage IV patients because of their metastatic condition associated with lower survival probability and altered immune infiltrate [182] thus representing a potential confounding factor for the analyses.

	All patients [n=118]	**Stage 0/I** [n=4/25]	**Stage II** [n=38]	**Stage III** [n=51]
Male/Female, n	64/54	14/15	24/14	25/26
Age at enrolment, mean ± SD	70 [±12.5]	71.7 [±12.5]	71.8 [±10.9]	67.7 [±14.1]
Male	69 [±12.7]	72.6 [±10.4]	71.3 [±11]	68.5 [±14.2]
Female	69.5 [±13]	71.2 [±13.8]	72.75 [±10.2]	66.8 [±14.3]
Disease Location				
Left-side colon (CSX)	66	20	18	28
Right-side colon (CDX)	52	9	20	23
MMR status				
Proficient/Deficient	103/15	27/2	32/6	44/7
Therapy				
Neoadjuvant				
Chemotherapy-Radiotherapy	9	5	1	3
Adjuvant CT	21	1	6	14
CAPOX	13	1	1	11
Capecitabine	6	-	5	1
Relapse	8	1	-	7

Table 3: *Clinical parameters of CRC patients enrolled until August 2022.*

3.1.2 iNKT cells infiltrate human CRC lesions showing an exhausted Th17 phenotype

To determine the infiltration and phenotype of iNKT cells in CRC tissues we first used an unbiased approach, analyzing high dimensional flow cytometry data using the Phenograph clustering algorithm [196]. The analysis of tissue-infiltrating $CD3^+$ T cells identified 18 clusters (C) differentially distributed in NCT and TUM (Figure 3.2A). NCT was mainly infiltrated by $CD4^+$ T cells producing TNFα, IFNγ and GM-CSF (C15), as well as by a group of proliferating, $Ki67^+$, $CD4^+$ T cells that overexpressed the checkpoint inhibitor PD-1 (C10, Figure 3.2A-C). TUM was characterized by $CD8^+$ T cells expressing TNFα, IFNγ, GM-CSF and PD-1 (C3, C5 and C1, Figure 3.2A-C), but also by double positive $CD4^+$, $CD8^+$ T cells expressing IL17, TNFα, and PD-1 (C6, Figure 3.2A-C). Cluster C16, representative of iNKT cells, was enriched in tumor tissues (Figure 3.2A-C). We confirmed the significant infiltration of iNKT cells in colorectal lesions by manual gating analysis (Figure 3.2D-E). Gating strategy of iNKT cells is shown in Figure 2.2.
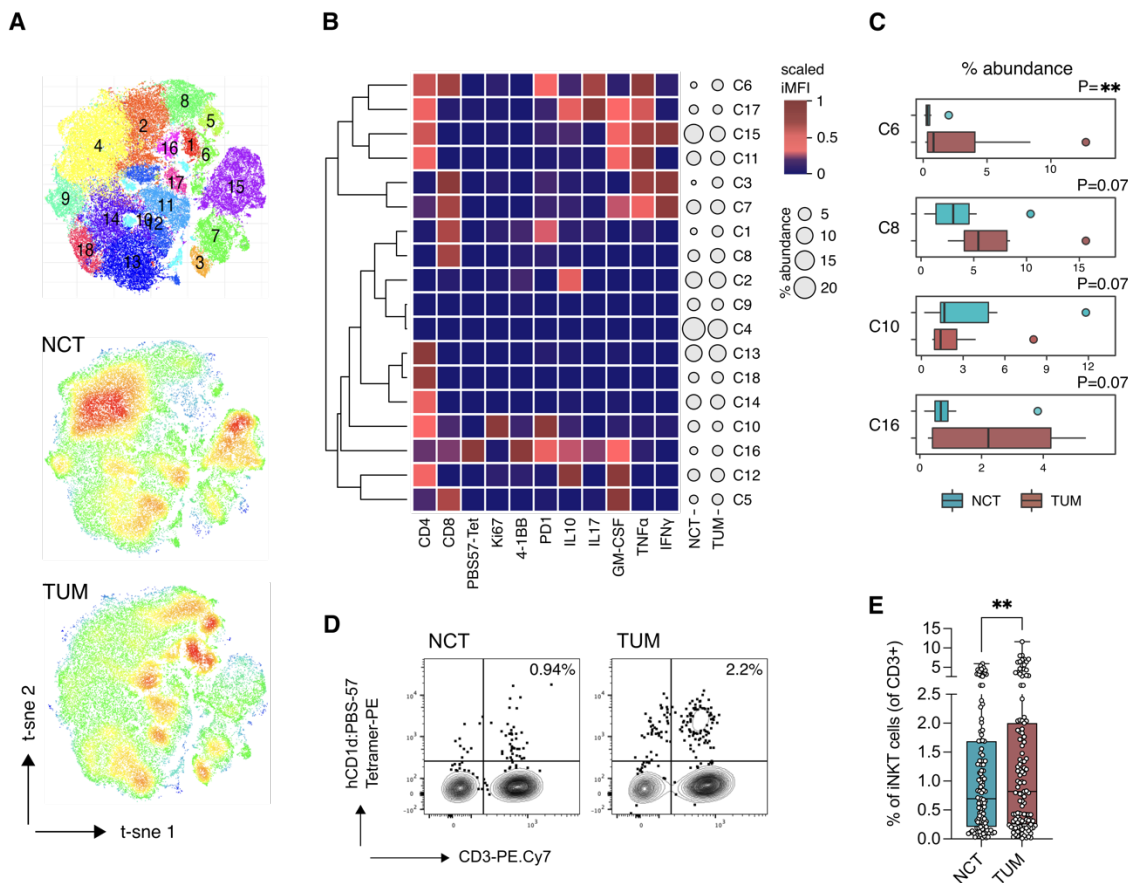

Figure 3.2: iNKT cells infiltrate CRC tumor lesions. (A) t-SNE map and Phenograph clustering of $CD3^+$ T cells infiltrating adjacent non-tumor colonic tissues (NCT) and tumor lesions (TUM). (B) Heatmap of scaled integrated MFI data from Phenograph clustering analysis; relative abundance of

To further validate our findings, we evaluated iNKT infiltration in publicly available dataset of single-cell sequencing in CRC. We used scRNA-seq data from the work of Pelka K. et al 2021. First, we defined the cell distribution between NCT and TUM (Figure 3.3A) and then we checked for the expression of *ZBTB16* (Figure 3.3B). *ZBTB16* is the gene encoding for PLZF the transcriptional factor regulating mainly NKT cell development. We observed that *ZBTB16$^+$*, NKT-like cells significantly infiltrate CRC lesions (Figure 3.3C), validating our previous results of flow cytometry data (Figure 3.2).
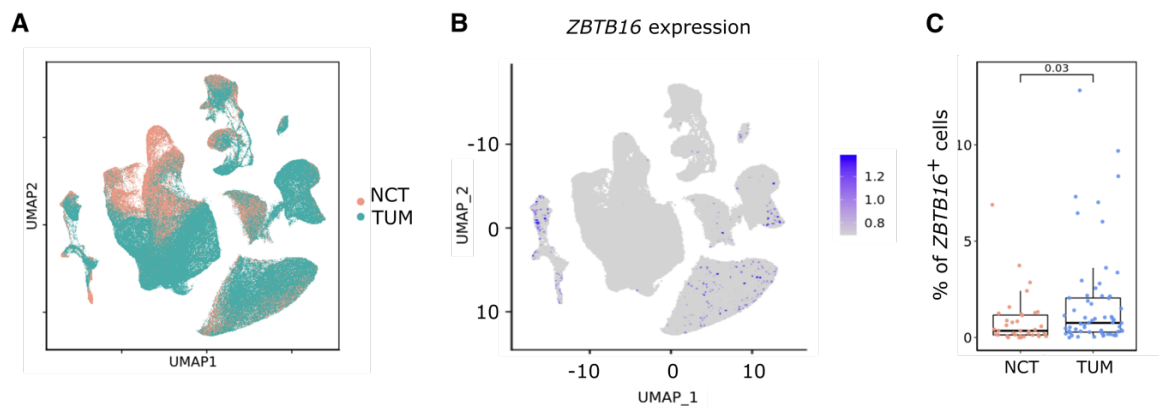
Figure 3.3: *ZBTB16$^+$ cells infiltrate tumor CRC tissues. (**A**) UMAP representative of single cells in Pelka K. et al., 2021, color coded by tissue of origin (cells n. = 328,265). (**B**) UMAP of ZBTB16 expression level in A. (**C**) Percentage of ZBTB16$^+$ cells in NCT and TUM. Wilcoxon matched-pairs signed rank test.*

To fine-tune the characterization of tumor infiltrating iNKT cells, we performed a meta-clustering analysis of cluster 16 (C16) (Figure 3.2A-B). C16 expressed several markers of activation, exhaustion (4-1BB and PD-1) as well as an array of different cytokines, including IL10, IL17, GM-CSF, TNFα and IFNγ (Figure 3.2B). We identified 7 distinct clusters of tissue infiltrating iNKT cells (Figure 3.4A). Clusters distribution was different between NCT and TUM, as shown by density plots (Figure 3.4A). TUM infiltrating iNKT cells were characterized by the production of GM-CSF, IL17 and the expression of PD-1 (C1, Figure 3.4A-B). On the other hand, NCT infiltrating iNKT cells were associated to a cytotoxic phenotype with the production of IFNγ and to a lesser extent of GM-CSF (C3

and C4, Figure 3.4A-B). By manual gating analysis we confirmed that tumor infiltrating iNKT cells upregulated the production of GM-CSF and IL17 while decreased that of IFNγ compared to their paired healthy site (Figure 3.4C-D). No difference was detected in other Th1-, Th2- or regulatory-associated cytokines (TNFα, IL13, IL22, IL10), although tumor infiltrating iNKT cells showed decreased expression of IL4 compared to NCT (p-value=0.06) (Figure 3.4D). Of note, the production of IL17 alone was upregulated by tumor infiltrating iNKT cells, but not that of GM-CSF (Figure 3.4D).
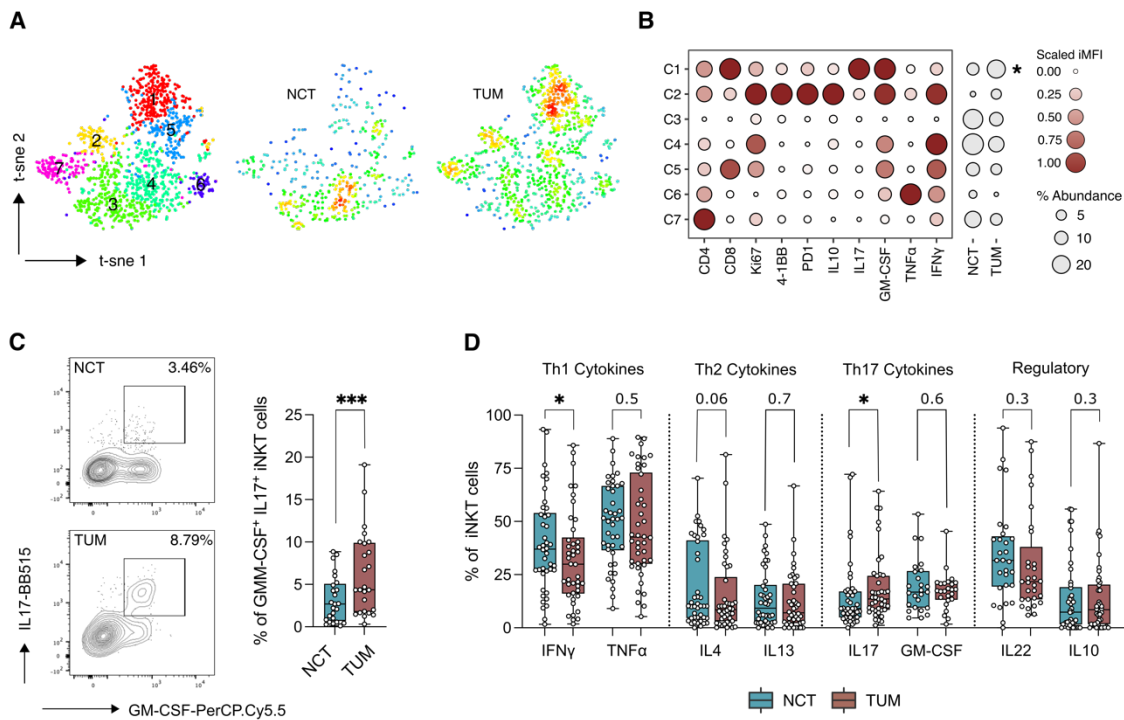
Figure 3.4: Tumor infiltrating iNKT cells have a Th17 like phenotype. (A) t-SNE map of iNKT cells based on Phenograph meta-clustering analysis of C16 in NCT and TUM. (B) Balloon plot of the scaled integrated MFI of Phenograph clusters generated in A. (C) Frequency of IL17$^+$GM-CSF$^+$ iNKT cells in NCT and TUM lesions (n = 25), with representative plots. (D) Frequency of IFNγ$^+$ TNFα$^+$, IL4$^+$, IL13$^+$, IL17$^+$, GM-CSF$^+$, IL22$^+$ and IL10$^+$ iNKT cells in NCT and TUM (n = 42, n = 25 for GM-CSF$^+$ cells). P < 0.05 (*), P < 0.001(***), Wilcoxon matched-pairs signed rank test, perplexity = 50, iterations = 1000, seed = 42, k = 50.

Tumor iNKT cluster 1 expressed also the inhibitory molecule PD-1 (Figure 3.4B), prompting us to further investigate their activation and exhaustion status. Tumor-infiltrating iNKT cells upregulated the co-inhibitory markers PD-1, CTLA-4, TIGIT and TIM3, (Figure 3.5A) while manifested a downregulation of the activation markers CD69, CD161 and 4-1BB (Figure 3.5B).
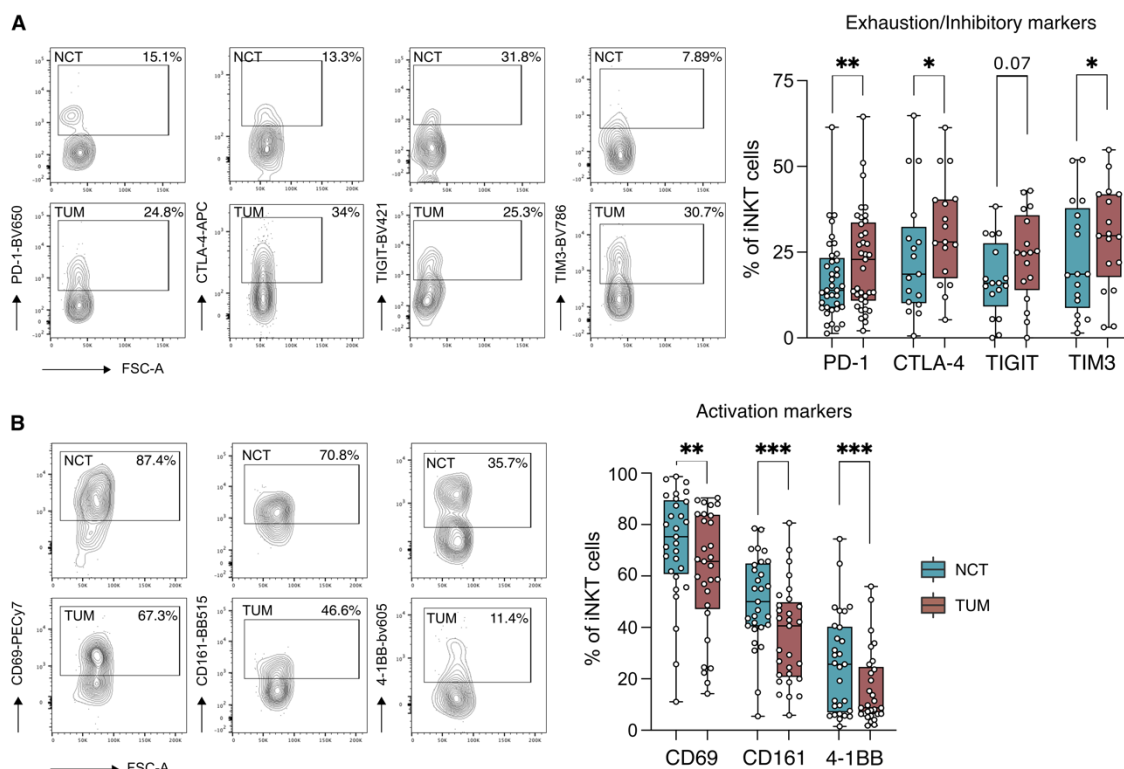
Figure 3.5: *Tumor infiltrating iNKT cells have an exhausted phenotype. (**A-B**) Frequency of PD-1$^+$, CTLA-4$^+$, TIGIT$^+$, TIM3$^+$ (**A**), CD69$^+$, CD161$^+$ and 4-1BB$^+$ (**B**) iNKT cells in NCT and TUM (n = 37, n = 16 for TIGIT$^+$ and TIM3$^+$ cells), with representative plots. P < 0.05 (*), P < 0.01(**), P < 0.001(***), Wilcoxon matched-pairs signed rank test.*

iNKT cells in mice have transcriptional programs associated with tissue residency and express the integrin CD103 [8], suggesting their tissue-residency at mucosal sites. We observed that also human iNKT cells expressed CD103, upregulating it in tumor tissues (Figure 3.6A-C). In addition, CD103$^+$ iNKT cells had an increased proliferation activity, as shown by the upregulated Ki67 expression in comparison to the CD103$^-$ counterpart (Figure 3.6D).
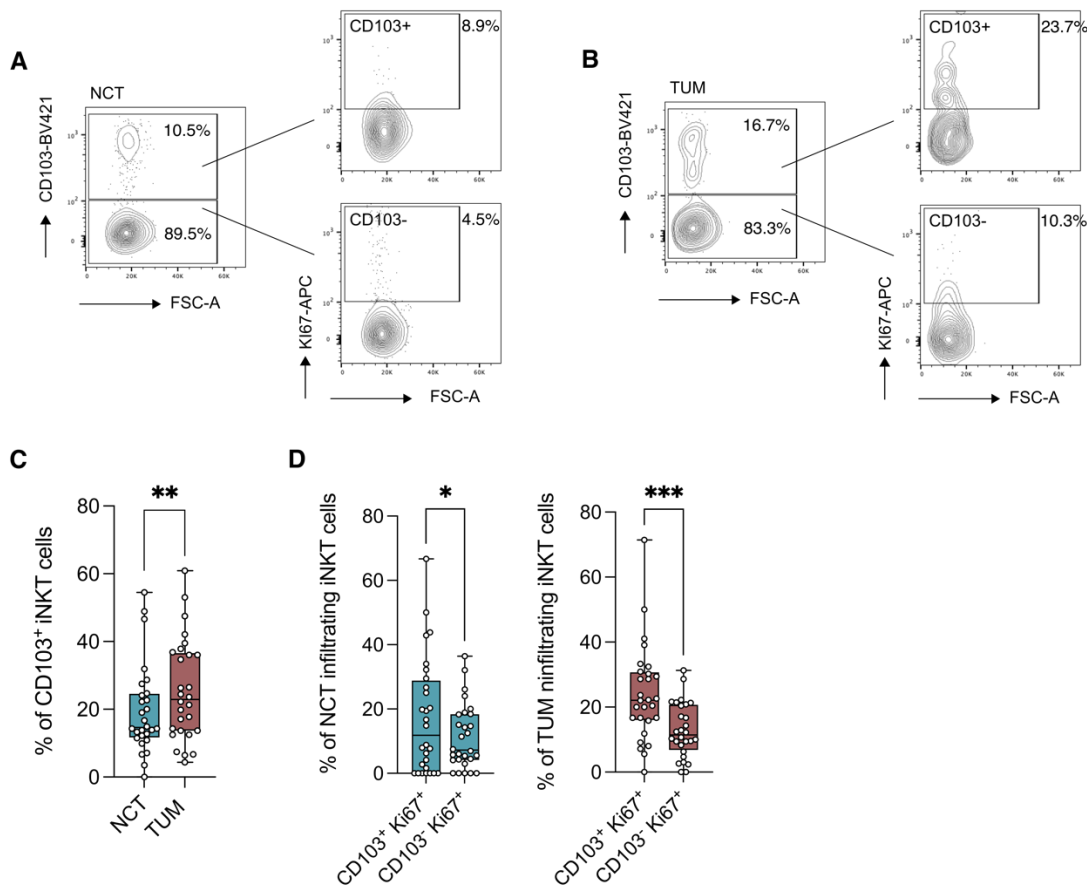
Figure 3.6: *iNKT cells express markers of tissue retention in NCT and TUM.* *(**A-B**) Representative plots of CD103$^+$, CD103$^+$Ki67$^+$ and CD103$^-$Ki67$^+$ iNKT cells in NCT (**A**) and TUM (**B**). (**C**) Frequency of CD103$^+$ iNKT cells in NCT and TUM (n = 28). (**D**) Frequency of CD103$^+$Ki67$^+$ and CD103$^-$Ki67$^+$ iNKT cells in NCT (left panel) and TUM (right panel) (n = 28). P < 0.05 (*), P < 0.01(**), P < 0.001(***), Wilcoxon matched-pairs signed rank test.*

In conclusion, the phenotypical analyses of intestinal iNKT cells showed that they are tissue resident cells able to produce a vast array of cytokines (IFNγ, TNFα, IL4, IL13, GM-CSF, IL17, IL22 and IL10). However when infiltrating CRC lesions iNKT cells are skewed toward an exhausted Th17-like phenotype characterized by the production of both GM-CSF and IL17, the expression of inhibitory molecules and a proliferative behavior in mucosal resident cells (Figure 3.4, Figure 3.5, Figure 3.6).

3.1.3 Tumor-infiltrating iNKT cells reduced their cytotoxic potential

iNKT cells are known to be able of releasing classical T-helper associated cytokines and also cytotoxic molecules, such as granzymes and perforin. We have recently shown that iNKT cells released granzyme B and perforin *in vitro,* killing CRC cell lines and patients derived tumor cells[151] . Thus, we investigated *ex vivo* iNKT cells production of granzymes and perforin and their expression of death ligands. The analysis of our CRC patients' cohort confirmed that intestinal iNKT cells produce granzyme A (GrzA), granzyme B (GrzB) and perforin (Figure 3.7A), albeit their production did not differ between NCT and TUM infiltrating iNKT cells (Figure 3.7A). The expression of Fas ligand (FasL), but not of tumor necrosis factor-related apoptosis inducing ligand (TRAIL) was decreased in tumor infiltrating iNKT cells (Figure 3.7B). These data show that tumor-infiltrating iNKT cells decrease their expression of death ligands, possibly affecting their cytotoxic functions.
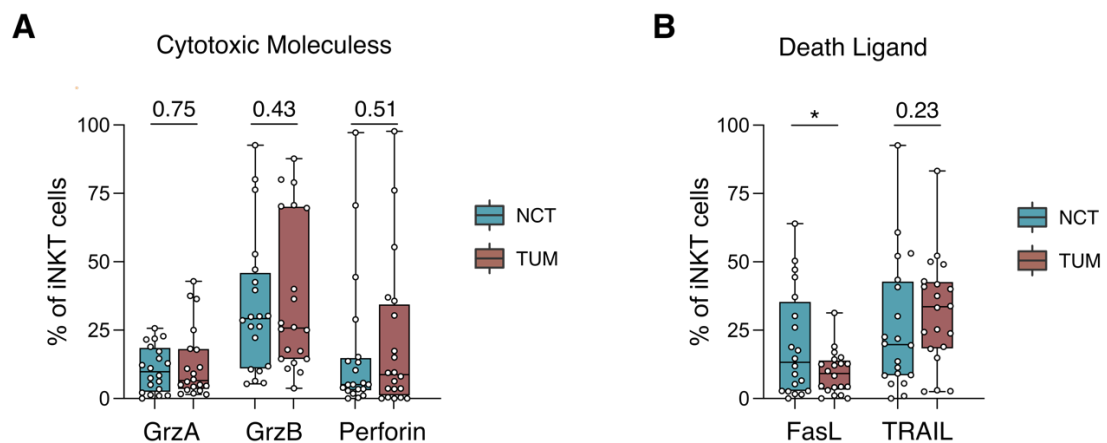
Figure 3.7: *iNKT cells do not alter their expression of cytotoxic granules and death ligands in CRC.* *(**A-B**) Frequency of GrzA$^+$, GrzB$^+$, Perforin$^+$ (**A**), FasL$^+$ and TRAIL$^+$ (**B**) iNKT cells in NCT and TUM (n = 20), with representative plots. P < 0.05 (*), Wilcoxon matched-pairs signed rank test.*

3.1.4 iNKT cells have a unique phenotype among tumor - infiltrating conventional and unconventional lymphocytes

We showed that iNKT cells have a Th17-like phenotype in CRC lesions (Figure 3.4). Previous works reported that Th17-associated cytokines are produced also by conventional, unconventional T cells and innate lymphoid cells (ILCs) in the context of CRC [4]. Thus, we investigated if differences existed among these cells in terms of tissue infiltration and Th17 cytokines expression. We first assessed the frequency of tumor-infiltrating conventional ($CD3^+Tet^-$) T-helper ($CD4^+$) and cytotoxic ($CD8^+$) T cells, mucosal-associated invariant T cells (MAIT), $\gamma\delta$ T cells and ILCs (Figure 3.8A-B). Gating strategies for conventional and unconventional T cells are shown in Figure 2.4. We observed a decreased infiltration of $CD4^+$ Th cells in TUM whereas no difference in the abundance of cytotoxic T cells was detected (Figure 3.8A). $\gamma\delta$ T cells significantly infiltrated TUM while MAIT and ILCs were present at similar abundances in NCT and TUM (Figure 3.8B).
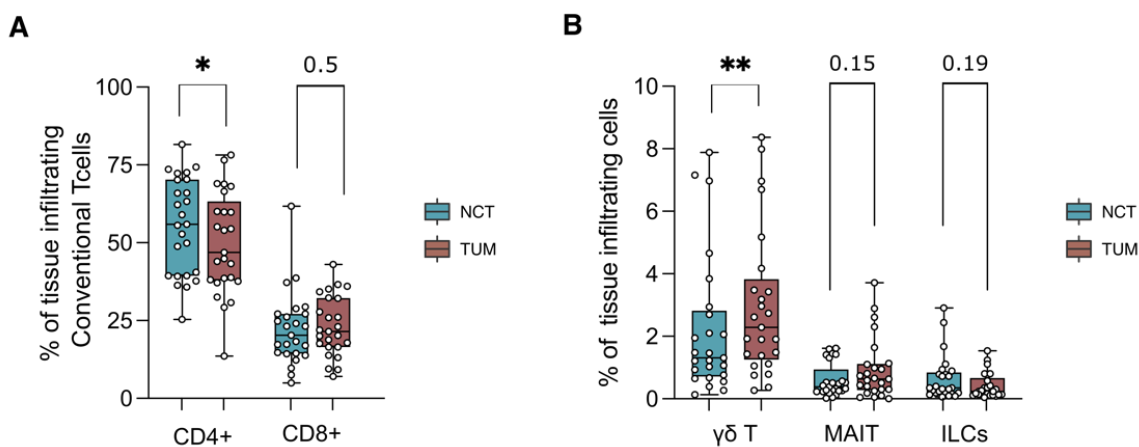
***Figure 3.8**: Conventional and unconventional T cells and ILCs infiltrate NCT and TUM tissues. (A-B) Frequency of conventional $CD4^+$, $CD8^+$ (A) and unconventional $\gamma\delta$ T cells, MAIT and ILCs (B) in NCT and TUM. (n = 25). P < 0.05 (*), P < 0.01(**), Wilcoxon matched-pairs signed rank test.*

We observed an increased production of IL17 by TUM-infiltrating CD4$^+$ Th, γδ T and MAIT cells, but not by cytotoxic CD8$^+$ T cells and ILCs (Figure 3.9A). GM-CSF secretion was similar in TUM and NCT for both conventional and unconventional lymphoid cells, except for TUM-infiltrating γδ T who showed a decreased GM-CSF production (Figure 3.9B-C). Most importantly, iNKT cells were the highest producers of IL17 and GM-CSF compared to conventional, unconventional T cells and ILCs in CRC lesions, suggesting preferential functions for tumor-infiltrating iNKT cells (Figure 3.9D).
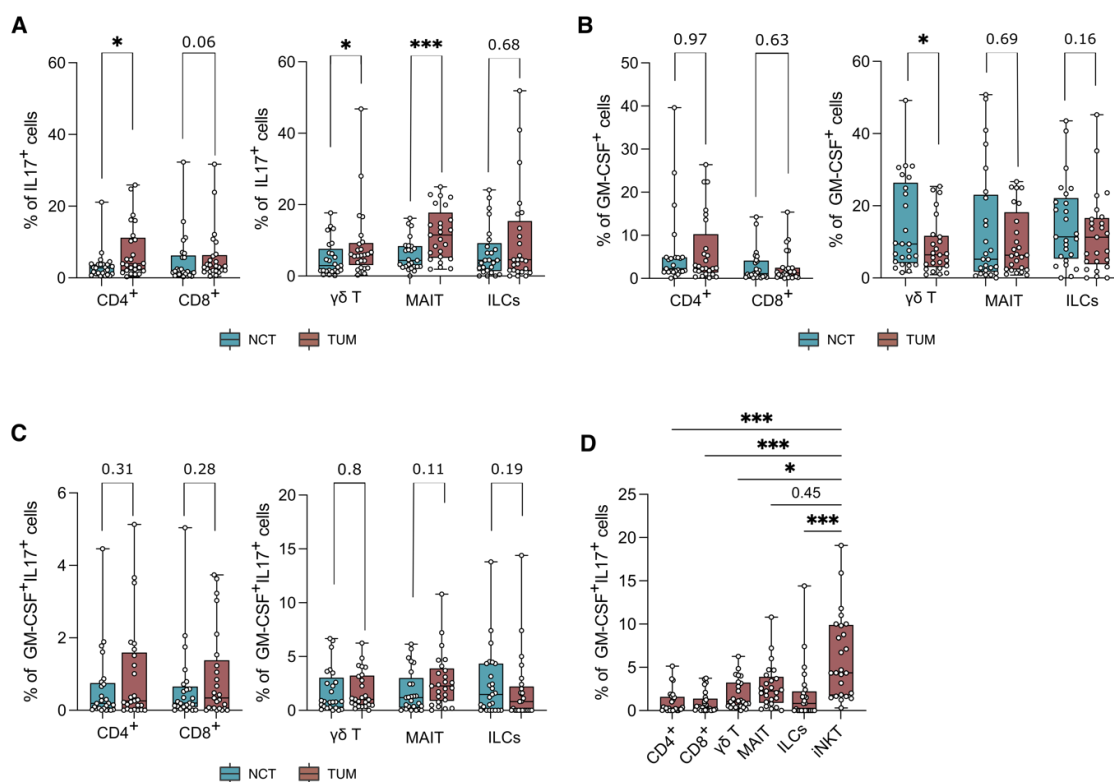
Figure 3.9: iNKT cells are unique in the expression of GM-CSF$^+$Il17$^+$ among conventional, unconventional T cells and ILCs. (**A-B-C**) Frequency of IL17$^+$ (**A**), GM-CSF$^+$ (**B**) and IL17$^+$GM-CSF$^+$ (**C**) conventional CD4$^+$, CD8$^+$ and unconventional γδ T cells, MAIT and ILCs in NCT and TUM. (n = 25). (**D**) Frequency of GM-CSF$^+$IL17$^+$ conventional CD4$^+$, CD8$^+$, unconventional γδ T cells, MAIT, ILCs and iNKT cells in TUM. $P < 0.05$ (*), $P < 0.01$(**), $P < 0.001$(***), Wilcoxon matched-pairs signed rank test.

3.1.5 Tumor associated neutrophils significantly infiltrate CRC lesions and express a mature, aged phenotype

It is well known that CRC lesions are characterized by the infiltration of lymphoid cells, but also of myeloid and B cells. Thus, we analyzed the tumor infiltration of B cells ($CD45^+CD19^+$), neutrophils ($CD45^+CD66b^+CD15^+$), monocytes ($CD45^+CD68^+CD11c^+$), macrophages ($CD45^+CD69^+CD11c^-$) and DCs ($CD45^+CD68^-CD11c^+$) in our CRC cohort (Figure 3.10A-C). No differences were observed for B cells and monocytes (Figure 3.10A), while neutrophils and macrophages significantly infiltrated tumor lesions compared to the paired-healthy site (Figure 3.10B-C). On the contrary, DCs were more abundant in NCT tissues (Figure 3.10C).
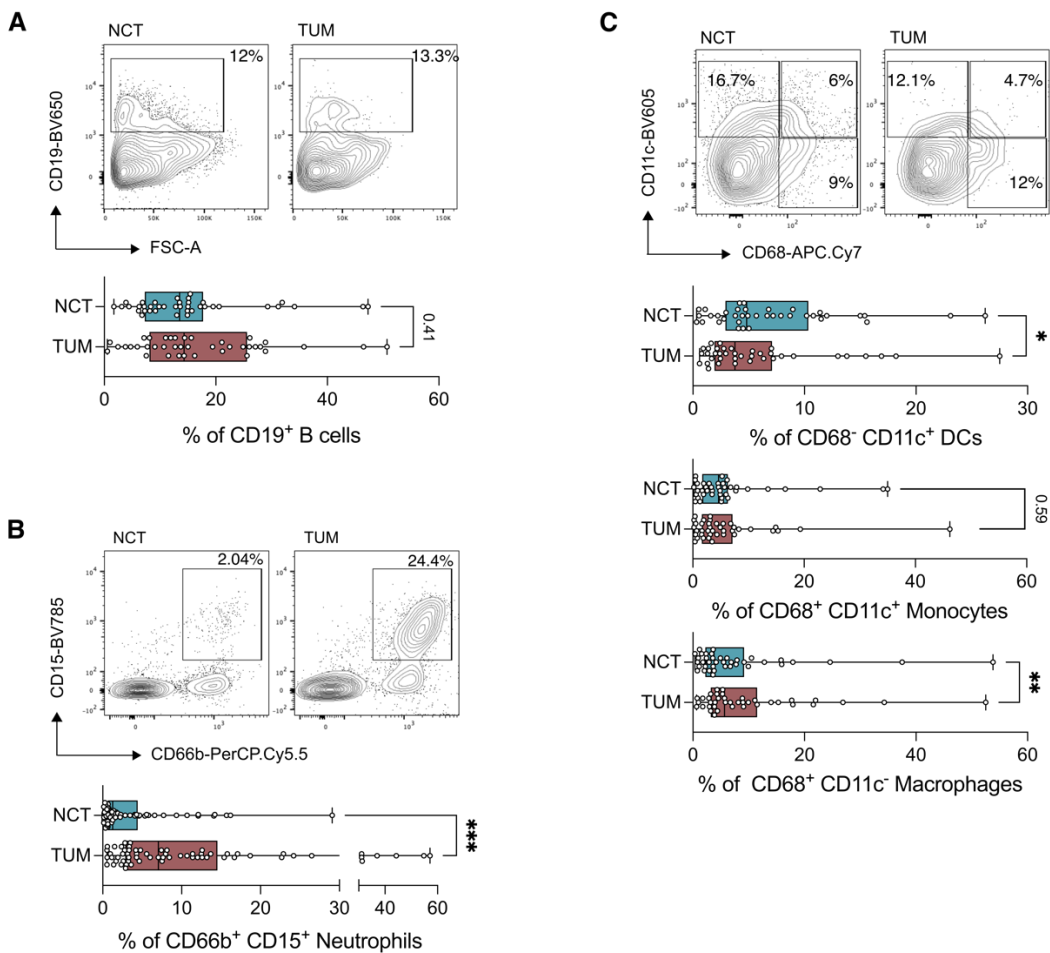
__Figure 3.10:__ Neutrophils infiltrate CRC lesions. (A-B-C) Frequency of B cells (A), neutrophils (B), dendritic cells, monocytes and macrophages (C), with representative plots (n = 75). P < 0.05 (*), P < 0.01(**), P < 0.001(***), Wilcoxon matched-pairs signed rank test.

Neutrophils are a heterogenous cell population that can acquire different phenotypical and functional roles in CRC [64]. In our CRC cohort, tumor associated neutrophils (TAN) downregulated the expression of the antigen presenting molecules MHC-II and CD1d (Figure 3.11A-B) while no differences were observed for the immune regulatory molecule PD-L1 (Figure 3.11C). TANs showed an aged ($CXCR4^+CD62L^{low}$), mature phenotype ($CD33^{mid}CD10^+CD16^+$) (Figure 3.11D-F), which can be endowed with both anti-tumorigenic and pro-tumorigenic functionalities *in vivo* [68]. Aged neutrophils infiltrating tumors overexpressed the PD-L1 molecule (Figure 3.11E), supporting their pro-tumorigenic role.
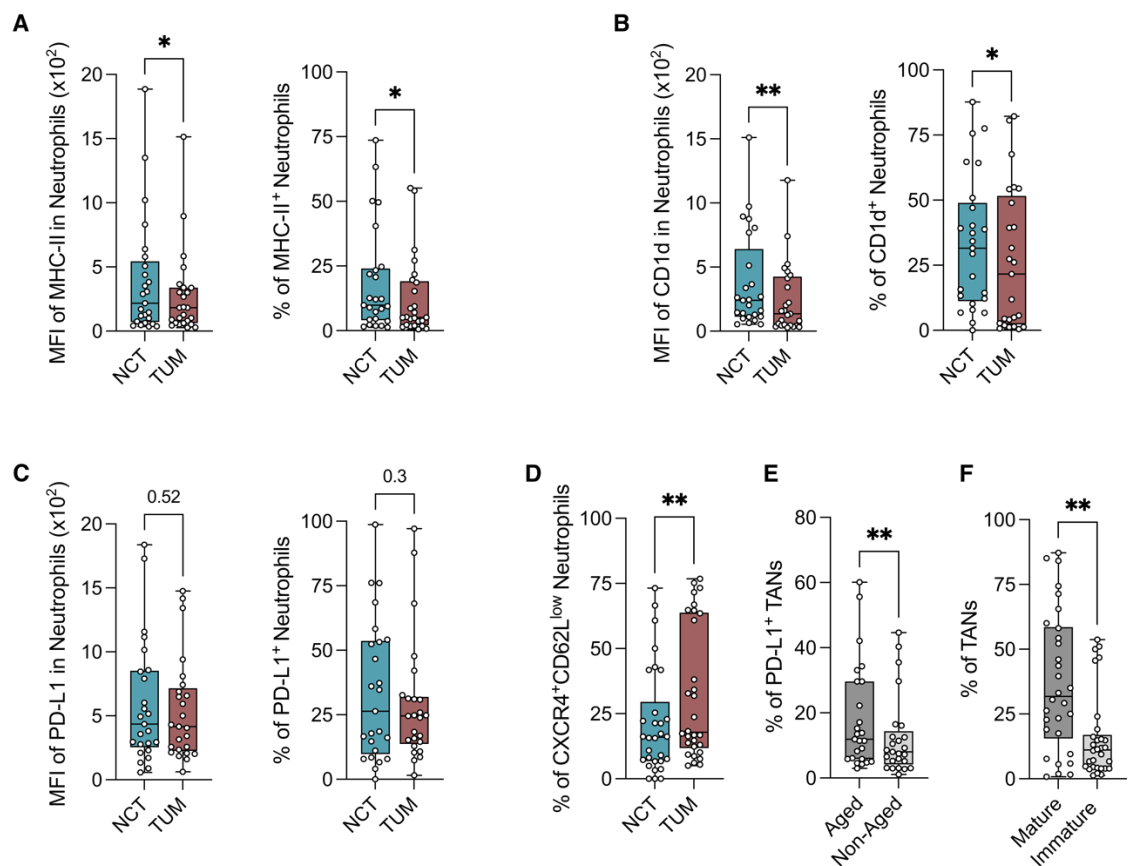
Figure 3.11: *Tumor associated neutrophils downregulate antigen-presenting molecules and acquire a mature, aged phenotype. (A-B-C) MFI and frequency of MHC-II (A), CD1d (B) and PD-L1 (C) in neutrophils infiltrating NCT and TUM (n = 25). (D) Frequency of aged neutrophils ($CXCR4^+CD62L^{low}$) in NCT and TUM (n = 25). (E) Frequency of mature ($CD33^{mid}CD10^+CD16^+$) and immature ($CD33^{mid}CD10^-CD16^+$) neutrophils in NCT and TUM (n = 25). P < 0.05 (*), P < 0.01(**), Wilcoxon matched-pairs signed rank test.*

3.1.6 iNKT cells precede neutrophils infiltration in tumors and their phenotype correlates with neutrophil's abundance

GM-CSF and IL17 are central cytokines in neutrophils biology [85]. Given their production by CRC-infiltrating iNKT cells and the predictive value of neutrophils, we hypothesized a potential crosstalk between iNKT cells and neutrophils in the context of CRC. We stratified patients according to disease staging (TNM stage) and observed that CRC lesions were significantly infiltrated by iNKT cells at early stages of the disease (Stage 0/I) while neutrophils infiltrated late CRC stages (Stage II/III) (Figure 3.12A-B). Although iNKT cells and neutrophils showed no associations, the IL17$^+$GM-CSF$^+$ iNKT cell population positively correlated with neutrophils abundance, suggesting a close interaction between the tumor-infiltrating population of iNKT cells and neutrophils (Figure 3.12C-D).
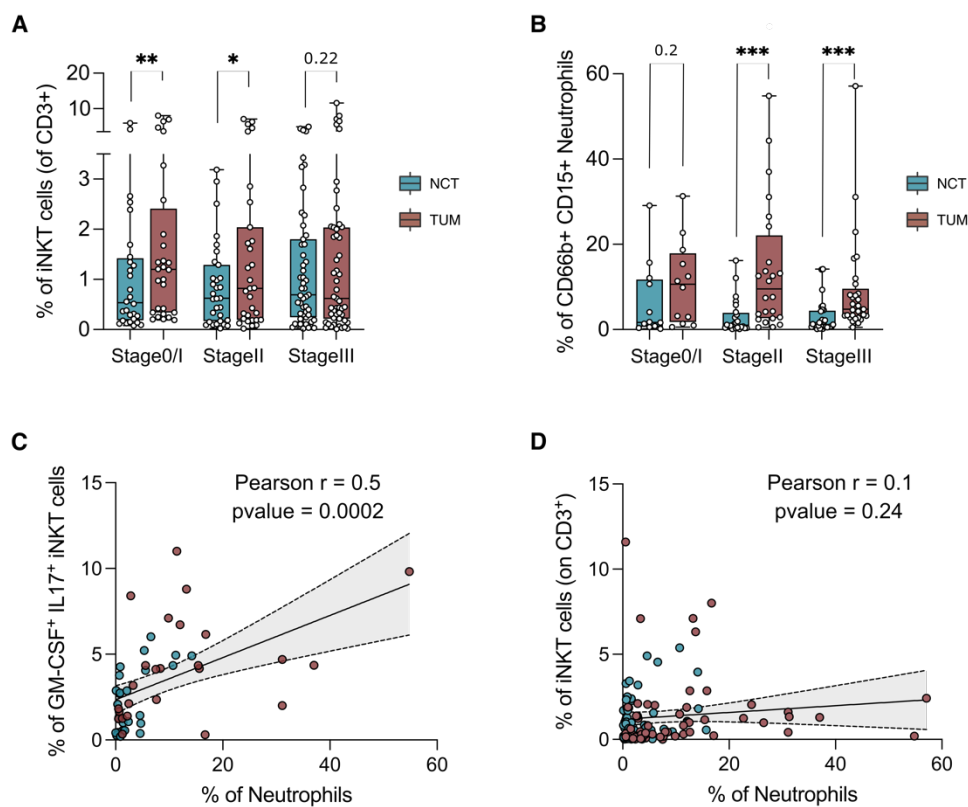
Figure 3.12: *iNKT cells precede neutrophils infiltration in CRC lesions.* ***(A-B)*** *Frequency of iNKT cells (A) and neutrophils (B) infiltrating NCT and TUM over TNM CRC stages (n = 115 for iNKT cells and n = 75 for neutrophils). (C) Correlation of IL17$^+$GM-CSF$^+$iNKT and neutrophils infiltrating NCT and TUM (n = 25). (D) Correlation of iNKT and neutrophils infiltrating NCT and TUM (n = 75). P < 0.05 (*), P < 0.01(**), P < 0.001(***), Wilcoxon matched-pairs signed rank test, Two-tailed Spearman test for correlation analysis.*

3.1.7 Professional APCs upregulate CD1d, the iNKT-restricted antigen presenting molecule in tumors

To further characterize the functional interactions of iNKT cells within the tumor microenvironment, we evaluated if professional APCs and epithelial cells altered the expression of antigen presenting molecules in tumor tissues. DCs, monocytes and macrophages upregulated the CD1d antigen presenting molecule, both in terms of MFI and percentage in TUM tissues, whereas B cells did not change their expression of CD1d (Figure 3.13A-B). TUM-infiltrating DCs and monocytes expressed also higher levels of the MHC-II presenting molecule (Figure 3.13C-D), suggesting a general increased in the process of antigenic presentation in tumors. Macrophages, on the other hand, upregulated only the expression of CD1d (Figure 3.13A-D), supporting the hypothesis that they can boost early activation of iNKT cells [158]. Since it has been shown that epithelial cells can directly interact with iNKT cells and influence their activation status, we examined CD1d expression on epithelial $CD45^-EpCAM^+$ cells and found it was not upregulated by tumor cells, however the expression of MHC-II was slightly increased (p-value = 0.06) (Figure 3.13A-D).
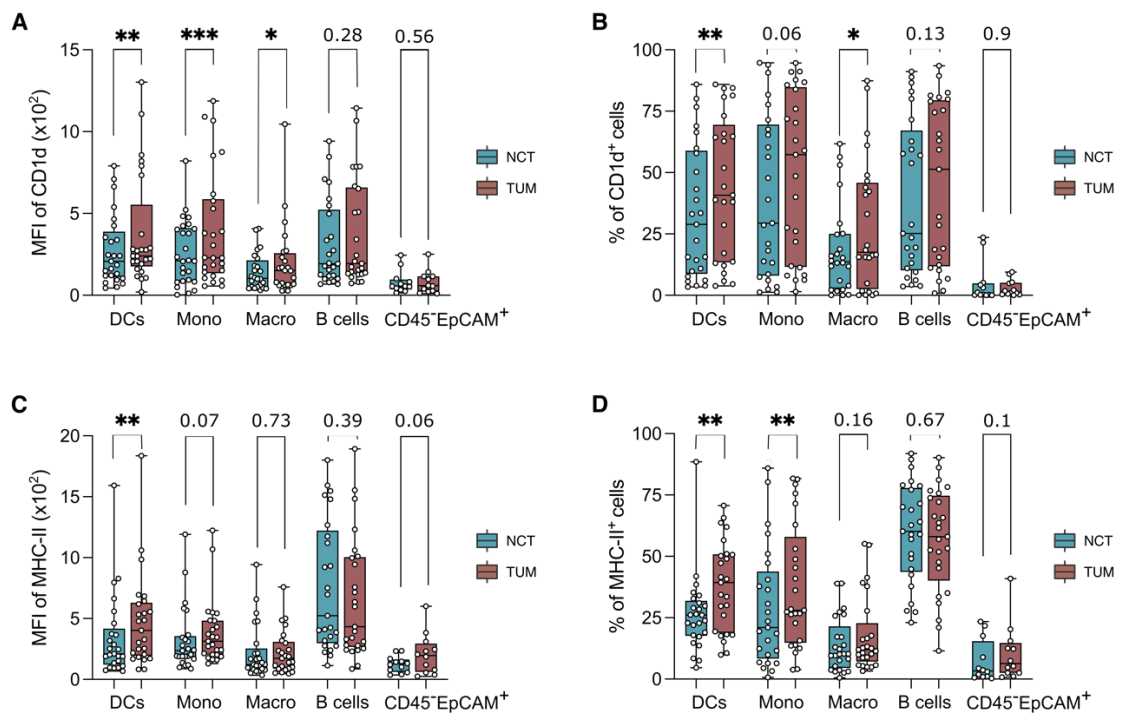
Figure 3.13: *APCs upregulate antigen presenting molecules in CRC lesions. **(A-B)** MFI **(A)** and frequency **(B)** of CD1d in DCs, monocytes (Mono), macrophages (Macro), B cells and $CD45^-EpCAM^+$ infiltrating NCT and TUM (n = 25, n = 12 for $CD45^-EpCAM^+$). **(C-D)** MFI **(C)** and frequency **(D)** of*

Finally, as iNKT cells do express cytotoxic molecules (Figure 3.7) and are able to kill tumor epithelial cells *in vitro* [151], we checked for the expression of death receptors on freshly isolated epithelial cells. However, no death receptors (FasR, TRAILR1 and TRAILR2) were upregulated. Only a mild upregulation (p-value = 0.06) of TRAILR1 in terms of MFI was detected on tumor CD45⁻EpCAM⁺ cells (Figure 3.14A-B).
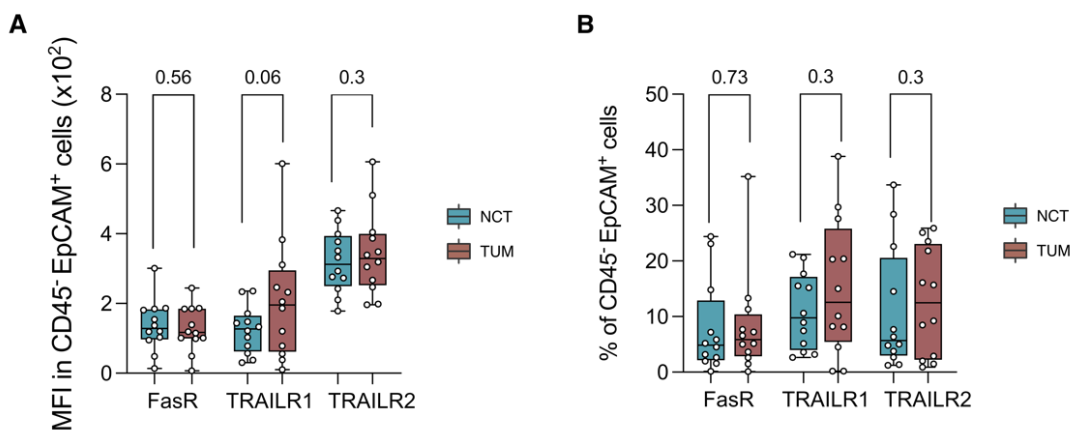
Figure 3.14: *Tumor epithelial cells do not change their expression of death receptors. (**A-B**) MFI (**A**) and frequency (**B**) of Fas receptors (FasR), TRAIL receptors 1 and 2 in CD45⁻ EpCAM⁺ cells of NCT and TUM (n = 12). Wilcoxon matched-pairs signed rank test.*

3.2 Dissecting the TME beyond its immune infiltrate

The tumor microenvironment (TME) is composed of cellular components (*i.e.* stromal cells, fibroblasts and immune cells), non-cellular one's (*i.e.* extracellular matrix components, pH and vasculature structures) and of the tumor-associated microbiota [26], [27]. We hypothesized that the TME can support or induce the tumor-associated phenotype of iNKT cells.

To test this hypothesis, we focused on two main parts of the TME: I) The characterization of NCT and TUM tissue from a genetic and proteomic point of view. II) The taxonomic definition of NCT and TUM associated mucosal bacteria species.

3.2.1 Tumor tissues are discriminated by a Th17 gene signature and support neutrophils and iNKT cells recruitment

To analyze the TME composition we assessed the gene expression profiles of NCT and TUM by qPCR and their protein composition by tissue-ELISA. Based on gene expression, NCT and TUM samples clustered apart (Figure 3.15A). TUM tissues were characterized by the upregulation of Th17 associated genes (*IL23, IL22, IL17* and *CCL20*), and neutrophils and iNKT cells recruiting chemokines (*IL8* and *CXCL16*) (Figure 3.15B), while NCT showed increased expression of genes belonging to the TGFß pathway (*TGFß, ACVRL1*), and to Th1 and Th2 responses (*TBX21* and *GATA3*) (Figure 3.15B). Correlation analysis of genes expression data identified two positively correlated clusters, mainly representative of genes upregulated in TUM or NCT (Figure 3.15C), suggesting that the TME is collectively shaped toward a Th17 response.
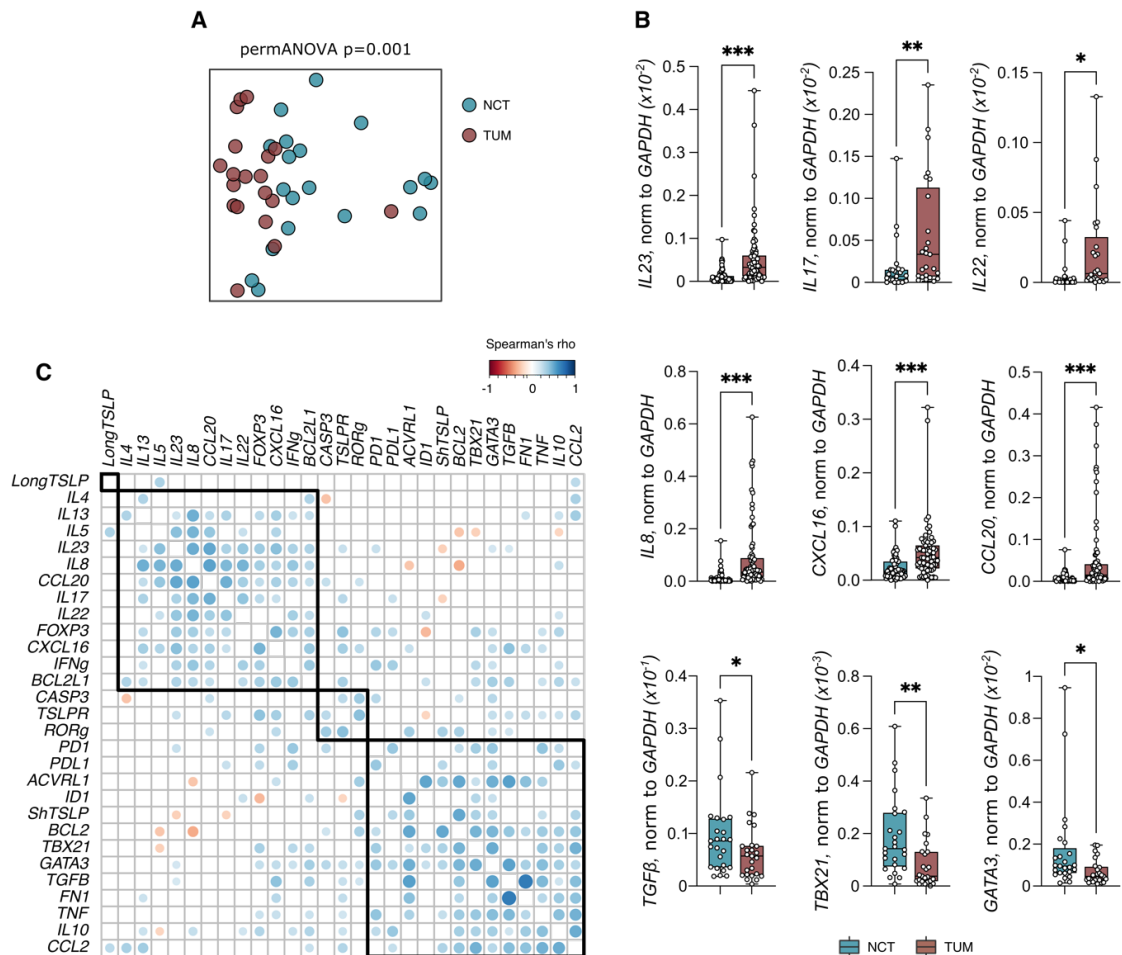
***Figure 3.15:** Gene expression discriminate colonic non tumor tissues from CRC lesions. (**A**) PCoA of gene expression profiles in NCT and TUM as measured by PermANOVA (n = 20). (**B**) Expression of IL23, IL17, IL22, IL8, CXCL16, CCL20, TGFß, TBET and GATA3 in NCT and TUM tissues (n = 75*

Given the importance of IL8 and CXCL16 in recruiting neutrophils and iNKT cells, we checked for their protein expression and found they were both increased in TUM samples (Figure 3.16).
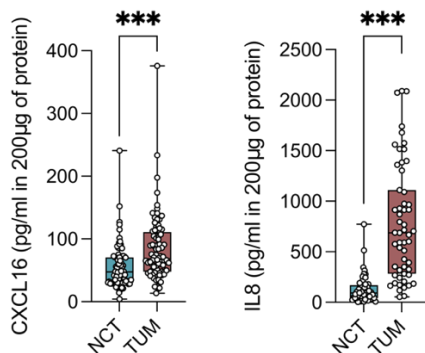
Figure 3.16*: iNKT cells and neutrophils recruiting chemokines are more abundant in tumor tissues. Protein quantification of CXCL16 and IL8 in NCT and TUM tissues (n = 100 for CXCL16, n = 75 for IL8). P < 0.001(***), Wilcoxon matched-pairs signed rank test.*

3.2.2 CRC-associated microbiota is enriched in oncogenic pathobionts

The gut microbiota is an important player of the TME, especially in CRC [31]. iNKT cells rapidly respond to bacterial antigens, showing different cytokines responses [9], [166], [168]. We analyzed the bacterial mucosal composition of either NCT or TUM tissues. Although no differences were observed in the microbial community structure (Figure 3.17A-B), TUM was enriched in oncogenic bacteria such as *Fusobacterium,* whereas NCT is enriched in *Porphyromonas* and *Bacteroides* (Figure 3.17C-D).
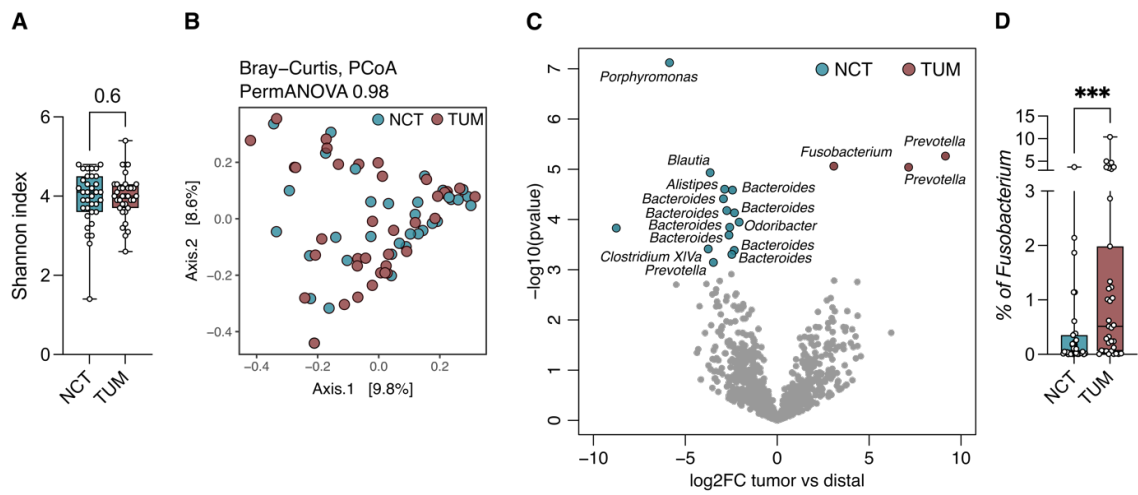
Figure 3.17: *Mucosal composition of tumor tissues is enriched in Fusobacterium. (**A**)Alpha-diversity measured by Shannon entropy index. (**B**) PCoA for beta-diversity of NCT or TUM mucosal microbiota measured by Bray-Curtis distance. (**C**) Volcano plot representing the significantly enriched bacterial taxa (FDR P < 0.05) in the mucosal microbiota of NCT and TUM. Names of the significantly enriched amplicon sequence variants [ASVs] reported are classified to the genus level. (**D**)Abundance of Fusobacterium in mucosal microbiota of NCT and TUM tissues. (n = 35), P < 0.001 (***), Wilcoxon matched-pairs signed rank test.*

3.3 Priming of iNKT cells with *Fusobacterium nucleatum*

Fusobacterium nucleatum (Fn) is a well-known bacterium widely studied for its direct and indirect oncogenic functions [31]. Given the capability of iNKT cells to quickly respond to bacterial stimuli and the importance of *Fusobacterium nucleatum* in CRC pathophysiology, we investigated whether *Fn* could induce specific functional changes in iNKT cells. We determined the effects of *Fusobacterium nucleatum* on iNKT cells with the experimental settings described in Figure 3.18. *Fn*-primed iNKT cells were tested for: I) *In vitro* cytotoxicity to CRC cell lines, II) transcriptomic variations by RNA-sequencing, III) Proteomic changes by flow cytometry.
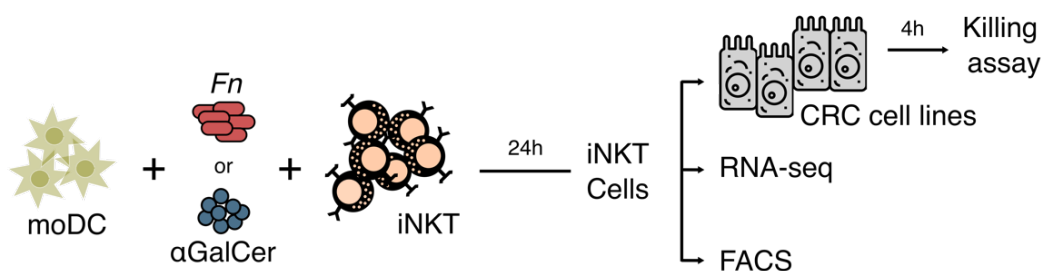
Figure 3.18:*In vitro experimental design for iNKT cells priming.*

3.3.1 *Fusobacterium nucleatum* does not influence the killing activity of iNKT cells

To address the effect of *Fusobacterium nucleatum* on iNKT cells cytotoxic potential (Figure 3.19A) we primed iNKT cells with *Fn* and then assessed their killing activity towards CRC cells lines, as performed in [151]. We observed that *Fn*-primed iNKT cells do not change their killing activity compared to the negative control (NS) (Figure 3.19B), suggesting that *Fn* does not influence iNKT cell cytotoxic potential. In accordance with literature, iNKT priming with αGalCer boosted their killing capabilities (Figure 3.19B), suggesting that lines used in the experiments maintained their cytotoxic activities.
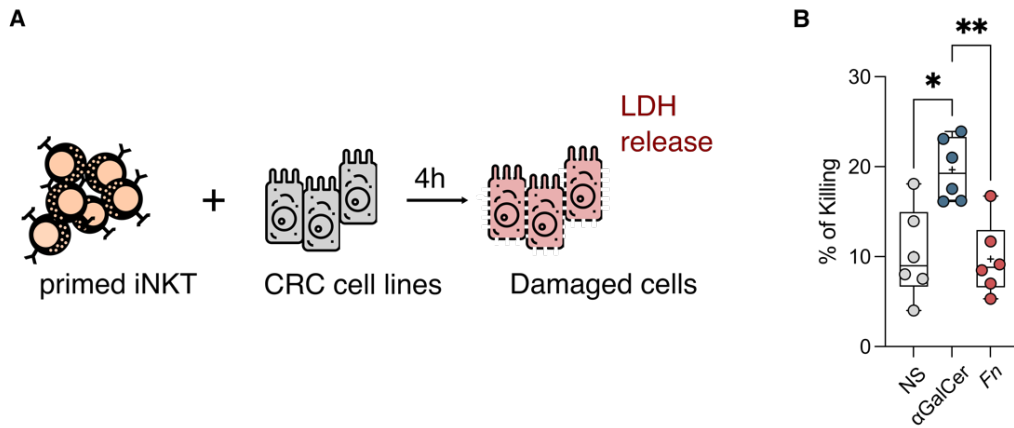
Figure* 3.19: Fusobacterium nucleatum do not affect the cytotoxic potential of iNKT cells. (A)*
*Experimental design of iNKT cells' cytotoxicity assay. (**B**) Percentage of killing of epithelial cells by*
Fn- or αGalCer-primed iNKT cells. Results are representative of three (n = 3) independent
experiments. P < 0.01(**), Wilcoxon matched-pairs signed rank test.

3.3.2 *Fusobacterium nucleatum* promotes the expression of neutrophil recruiting genes on iNKT cells

To evaluate the effects of *Fn* on iNKT cells, we performed RNA-seq of *Fn*-, αGalCer-, or unstimulated (NS) iNKT cells. By analyzing the genes differentially expressed in *Fn*-primed iNKT cells we observed they upregulate chemokine recruiting genes (*CXCL8, CCL20, CCL22* and *CCL4L2*), whereas they downregulate genes associated with cytotoxicity (*PFN1, GLNY and GZMA*) and Th1 activation (*CD2* and *IL7R*) (Figure 3.20A). By comparing the genes differentially expressed between *Fn*-primed and αGalCer-primed iNKT cells, we noticed an upregulation of chemokine recruiting genes (*CXCL2, CXCL8, CXCL3, CCL3L1, CCL20, CCL22* and *CCL4L2*) on *Fn*-primed iNKT cells, whereas αGalCer induced the upregulation of genes associated with Th1-like (*IFNG, TBX21* and *LTB*) and cytotoxic responses (*GRZA, GRZB, GRZH, GNLY* and *NKG7*) (Figure 3.20B). *Fn*-primed iNKT cells, on the other hand, upregulated the expression of chemokine recruiting genes and were characterized by a neutrophil chemotaxis gene signature (Figure 3.20B-C).
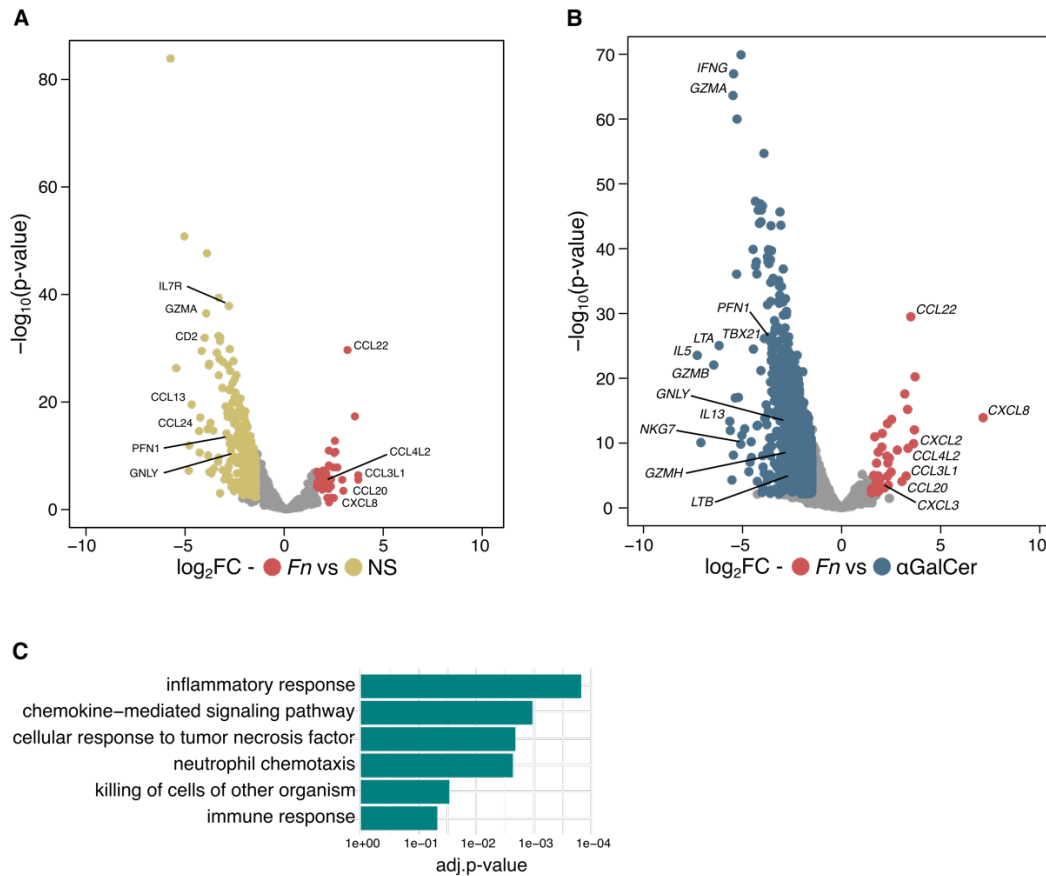
Figure 3.20: *Fusobacterium nucleatum upregulates genes of neutrophil chemotaxis in iNKT cells.* ***(A-B)*** *Volcano plot of differentially expressed genes in Fn-primed iNKT cells vs NS (A) and Fn- vs αGalCer-primed iNKT cells (B); for each gene (dots) the differential expression (log2fold-change [log2FC]) and the statistical significance (log10p-value) is shown (FDR-corrected P = 0.05 and log2FC > |1.5|).* ***(C)*** *Gene Ontology of differentially expressed genes in Fn-primed iNKT cells analyzed in B (Bonferroni-corrected P < 0.05 and log2FC > 1).*

Although we did not detect upregulation of IL17 and GM-CSF by *Fn*-primed iNKT cells on a transcriptomic level (Figure 3.20), we observed an increased abundance of IL17^{+} and GM-CSF^{+} iNKT cells by flow cytometry, upon *Fn* stimulation compared to the negative control (Figure 3.21A-B). As expected αGalCer-primed iNKT cells upregulated the expression of IFNγ (Figure 3.21C).
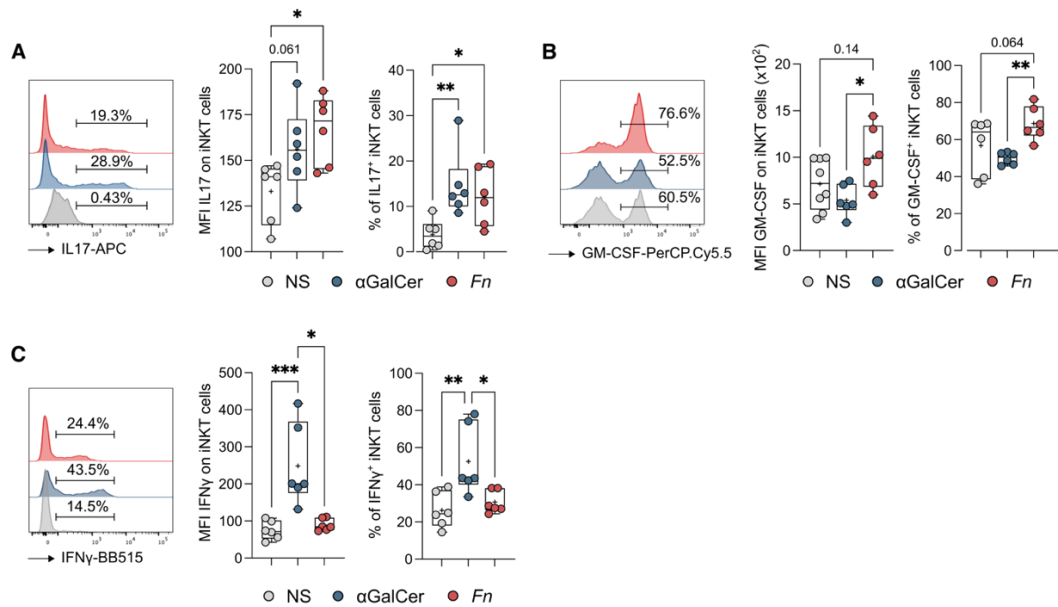
Figure 3.21: *Fusobacterium nucleatum induces overexpression of GM-CSF and IL17 on iNKT cells.*
*(**A-B-C**) Representative histograms (left panels), MFI (middle panels) and frequency (right panels) of*
*IL17+ (**A**), GM-CSF+ (**B**) and IFNγ+ (**C**) iNKT cells unstimulated (NS), αGalCer- or Fn-primed;*
Results are representative of three (n = 3) independent experiments. P < 0.05 (*), P < 0.01 (**),
P < 0.001(***); Kruskal-Wallis test followed by uncorrected Dunn's test.

To validate the production of the key chemokines and cytokines investigated (*i.e.* IL17, GM-CSF and IL8) by *Fn*-primed iNKT cells, we performed ELISA assays of iNKT cells culture supernatants. We observed a significant higher release of IL8 (encoded by *CXCL8*), GM-CSF and IL17 in the supernatant of *Fn*-primed iNKT cells compared to the negative control (

Figure **3.22**A-C). In agreement with RNAseq, FACS data and with previous literature we observed higher levels of IFNγ in the supernatant of αGalCer-primed iNKT cells (

Figure **3.22**D). Altogether these findings suggest that *Fn* stimulates the production of Th17 associated cytokines (IL17, GM-CSF and IL8) on iNKT cells.
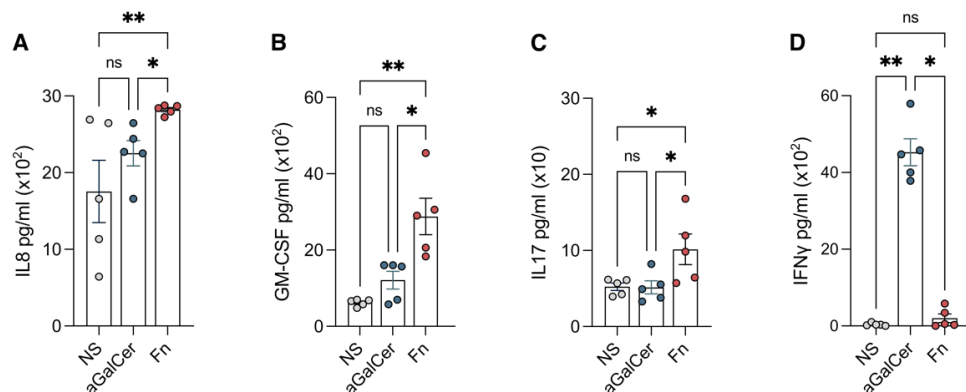
Figure 3.22: Fusobacterium nucleatum stimulates production of IL8, GM-CSF and IL17 in iNKT cells. (A-B-C-D) Quantification of IL8 (**A**), GM-CSF (**B**), IL17 (**C**) and IFNγ (**D**) produced by Fn-, αGalCer-or NS primed iNKT cells. Results are representative of three (n = 3) independent experiments. P < 0.05 (*), P < 0.01 (**), Kruskal-Wallis test followed by uncorrected Dunn's test.

3.4 Functional cross-talk between *Fn*-primed iNKT cells and neutrophils

Since IL17⁺GM-CSF⁺ iNKT cells and neutrophils abundances correlated in human CRC (Figure 3.12) and *Fn*-primed iNKT cells were characterized by a neutrophil chemotactic gene signature (Figure 3.20), we aimed at dissecting the interplay between these two cellular populations *in vitro*. We evaluated I) vitality, II) migration and III) immunosuppressive capacities of neutrophils upon stimulation with the culture supernatants or directly with *Fn*- and αGalCer-primed iNKT cells (Figure 3.23).
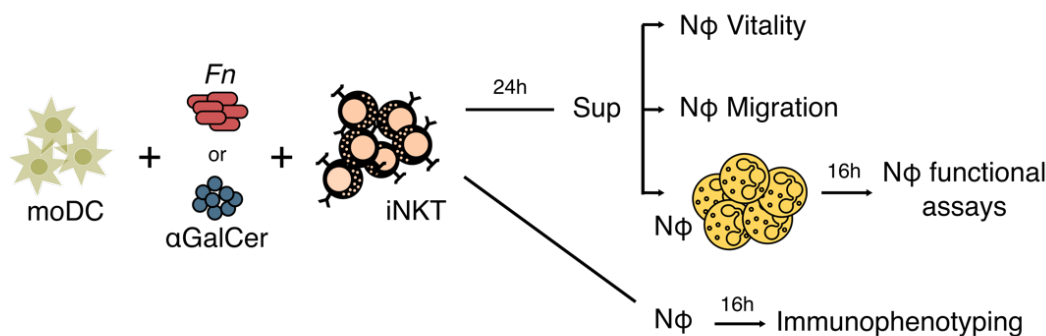
Figure 3.23: Experimental design for in vitro assessment of iNKT cells effect on neutrophils.

3.4.1 Activation of iNKT cells sustain neutrophil survival and *Fn* promotes iNKT-mediated neutrophil chemotaxis

Activation of iNKT cells with *Fn* led to the production of Th17 cytokines (Figure 3.21), which can be involved in the immune regulation of neutrophils. We observed that supernatants of activated iNKT cells *(i.e. Fn* and αGalCer activation) were sufficient to sustain neutrophil survival over 60% after 16 h of culture (Figure 3.24A-B).
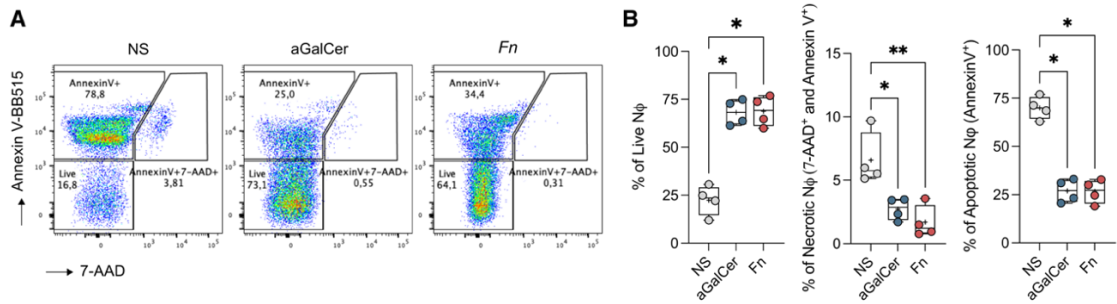
Figure 3.24: *Supernatants of activated iNKT cells support neutrophils survival. (**A**) Representative plots of the Annexin V and 7-AAD staining of neutrophils cultured with supernatants from NS, αGalCer- or Fn-primed iNKT cells. (**B**) Percentages of live (Annexin V- 7-AAD-), necrotic (Annexin V+ 7-AAD+) and apoptotic (Annexin V+ 7-AAD-) neutrophils upon culture from primed iNKT cells. Results are representative of three (n = 3) independent experiments. P < 0.05 (*), P < 0.01 (**); Kruskal-Wallis test followed by uncorrected Dunn's test.*

However, the supernatant of *Fn*-primed iNKT cells induced also neutrophil migration *in vitro* (Figure 3.25A-B). The recruitment of neutrophils was hampered by the addition of Reparixin, an allosteric inhibitor for IL8 receptors (p-value = 0.06) (Figure 3.25B), suggesting that IL8 is the main chemokine involved in the iNKT-mediated recruitment of neutrophils.
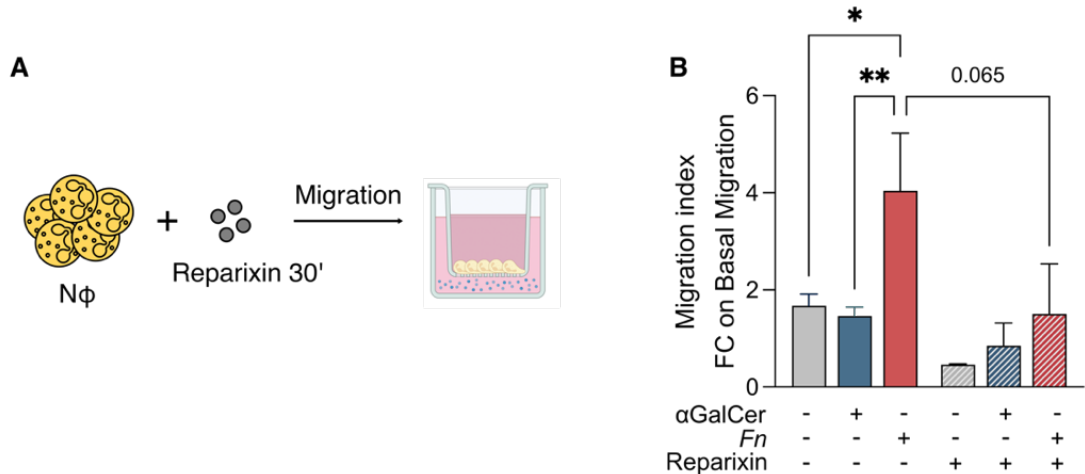
Figure 3.25: *Supernatant of Fn-primed iNKT cells recruit neutrophils. (**A**) Experimental design of neutrophils migration in vitro. (**B**) Fold-change of neutrophils migration index on basal migration, upon exposure to unstimulated (gray bar), αGalCer (blue bars) or Fn-primed (red bars) iNKT cell supernatants in the absence (full bars) or presence (pattern fill bars) of reparixin (20 μM). Results are representative of three (n = 3) independent experiments. P < 0.05 (*), P < 0.01 (**); Kruskal-Wallis test followed by uncorrected Dunn's test.*

3.4.2 *Fn*-primed iNKT cells promote neutrophils-T cells suppression and reduce their ROS production

We have demonstrated that activated iNKT cells support neutrophils vitality (Figure 3.24) and *Fusobacterium nucleatum* promotes iNKT cells recruitment of neutrophils through IL8 (Figure 3.25). Nonetheless, activated iNKT cells can also affect neutrophils immune responses. Neutrophils cultured with *Fn*-primed iNKT supernatant significantly increased their T cell suppression activity *in vitro*, by hampering the proliferation of activated naïve CD4$^+$ T cells (Figure 3.26A-B).
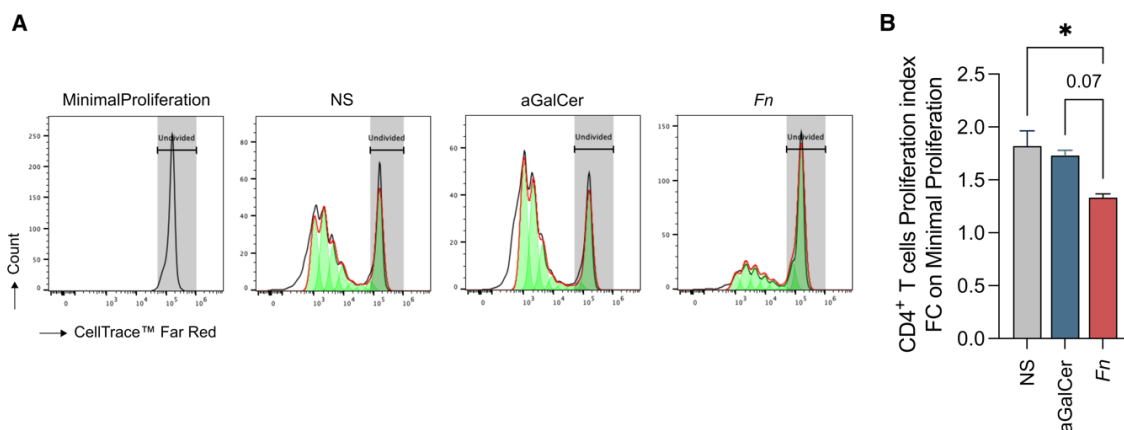
Figure 3.26: *Neutrophils cultured with supernatant of Fn-primed iNKT cells suppress näive CD4$^+$ T cells proliferation.* ***(A-B)*** *Fold-change of näive CD4$^+$T cells proliferation index, on basal proliferation, co-cultured with neutrophils and cell free supernatants from unstimulated (NS), αGalCer- or Fn-primed iNKT cells* ***(B)*** *with representative plots* ***(A)***. *Results are representative of three (n = 3) independent experiments. P < 0.05 (*); Kruskal-Wallis test followed by uncorrected Dunn's test.*

Suppression of activated T cells by neutrophils is already described in literature and can be driven by various mechanisms, among which the release of immunosuppressive molecules, of arginase enzyme and nitric oxides. Neutrophils cultured with the supernatant from either *Fn*- or αGalCer-primed iNKT cells upregulated the immunosuppressive marker PD-L1 (Figure 3.27A). However, only neutrophils cultured with the supernatant of *Fn*-primed iNKT cells decreased their respiratory burst activity (Figure 3.27B), which has been demonstrated to support basal T cell proliferation.
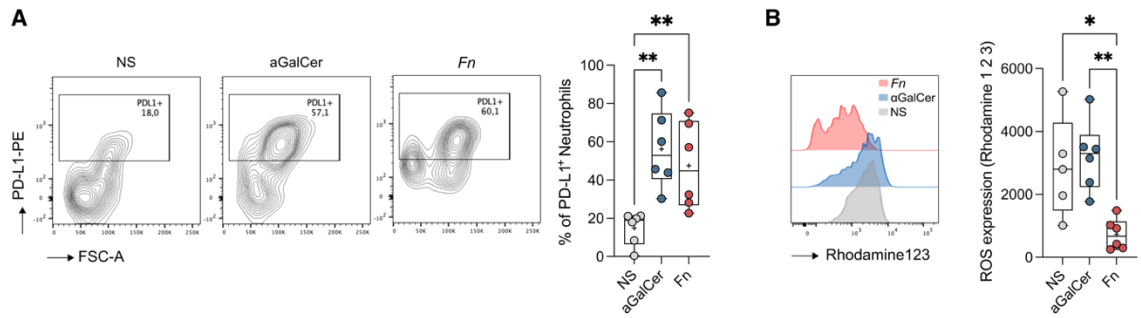
Figure 3.27: *Primed-iNKT cells upregulate PD-L1 on neutrophils and their respiratory burst capacity.* (*A*) *Frequency of PD-L1$^+$ neutrophils exposed to the culture supernatants of NS, αGalCer- or Fn-primed iNKT cells.* (*B*) *Respiratory burst quantification of neutrophils exposed to the supernatants of NS, αGalCer- or Fn-primed iNKT cells. P < 0.05 (*), P < 0.01 (**); Kruskal-Wallis test followed by uncorrected Dunn's test. Data are representative of three independent experiments.*

3.5 iNKT cells functions in murine models of CRC

To functionally elucidate the interplay between tumor-infiltrating iNKT cells and neutrophils in CRC development, we used the spontaneous $APC^{Min/+}$ model of intestinal cancer, three different inducible murine models of CRC (*i.e.* inflammation driven CRC and MC38 subcutaneous and intracecal implantation) and iNKT deficient animals ($CD1d^{-/-}$, $Traj18^{-/-}$).

3.5.1 The spontaneous $APC^{Min/+}$ murine model of CRC is not suitable as disease organism for our study

Analyzing the immune infiltrate of tumor lesions in the $APC^{Min/+}$ model of spontaneous intestinal cancer, we observed that iNKT cells were present at similar abundances in NCT and TUM (Figure 3.28A). TUM-infiltrating iNKT cells increased their expression of PD-1 and decreased the one of GM-CSF and IL17 (Figure 3.28B-C). In accordance with our hypothesis, neutrophils infiltration was decreased in tumor lesions (Figure 3.28D). Tumor-infiltrating neutrophils also expressed lower percentages of the immunosuppressive molecule PD-L1 (Figure 3.29E). These data suggest that, although the connection between GM-CSF$^+$IL17$^+$ iNKT cells and neutrophils is present as absence of both populations was observed, the $APC^{Min/+}$ model is not a suitable tool for our study.
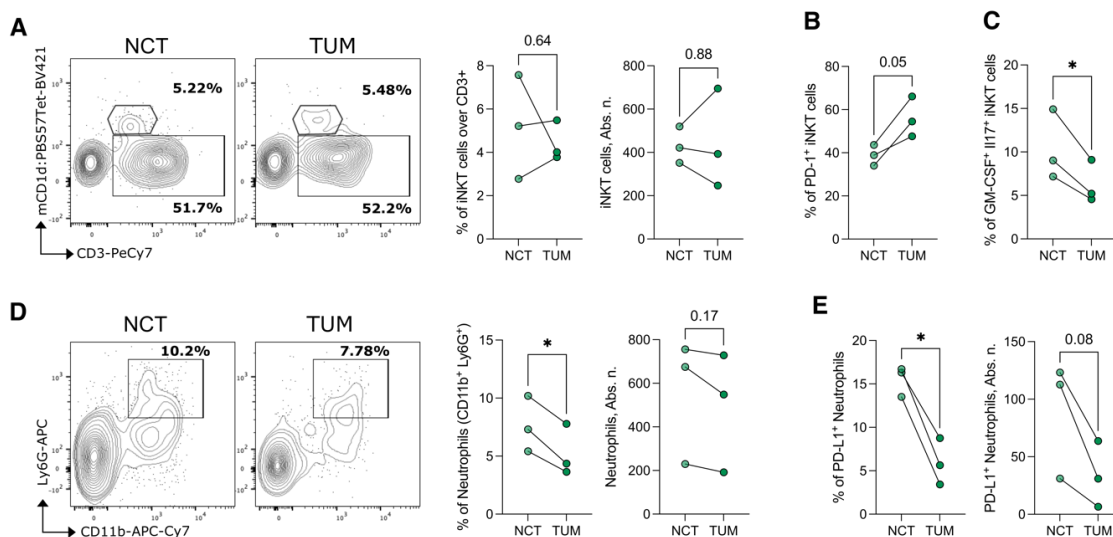
Figure 3.28: *$APC^{Min/+}$ lesions are not infiltrated by GM-CSF$^+$IL17$^+$ iNKT cells and neutrophils. **(A)** Frequency and absolute numbers of iNKT cells infiltrating NCT and TUM in $APC^{Min/+}$ mice, with representative plots. **(B-C)** Frequency of PD-1$^+$ **(B)** and GM-CSF$^+$IL17$^+$ **(C)** iNKT cells infiltrating*

*NCT and TUM in APC^{Min/+} mice. (**D**) Frequency and absolute numbers of neutrophils infiltrating NCT and TUM in APC^{Min/+} mice, with representative plots. (**E**) Frequency and absolute numbers of PD-L1^+ neutrophils infiltrating NCT and TUM in APC^{Min/+} mice. $P < 0.05$ (*); Mann-Whitney test; Wilcoxon matched-pairs signed rank test for NCT versus TUM. Data are representative of at least three independent experiments.*

3.5.2 The inflammation-driven CRC model at early-stage reproduces human findings

We evaluated the dynamic of the inflammation-driven AOM/DSS model of CRC in terms of tumor formation, development and cells infiltration. In wild-type, C57BL/6, mice we observed that tumor infiltrating iNKT cells reach their peak abundance at day 21-28 (Figure 3.29A), while neutrophils kinetic started 7 days later, reaching maximum tumor infiltration at day 42 (T1; Figure 3.29A). Tumor infiltration of both cell populations tended to decrease at day 70 (T2, Figure 3.29A). Clinical endoscopic scores of tumors [194] at T1 and T2 showed tumors are formed at T1 but have a lower severity degree (Figure 3.29B). Indeed, the number of tumors did not change over time but their size increased (Figure 3.29C-D).
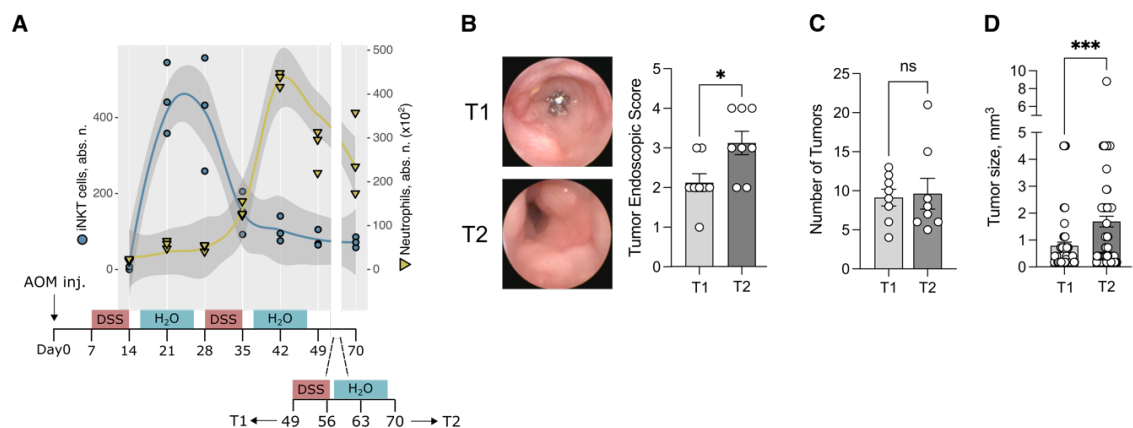
Figure 3.29: *__Establishment of early-stage AOM/DSS murine model of CRC.__ (**A**) Experimental AOM/DSS CRC model (bottom panel) and kinetic of iNKT cells (yellow triangles) and neutrophils (blue circles) infiltration in tumors. (**B**) Tumor endoscopic scores at T1 and T2, with representatives' pictures. (**C-D**) Number of tumors (**C**) and tumor sizes (**D**) at T1 and T2. $P < 0.05$ (*), $P < 0.001$ (***); Unpaired t-test. Data are representative of at least three independent experiments.*

Characterizing the immune infiltrate at early- (T1) and late- (T2) stages, we observed that iNKT cells infiltrated tumor lesions both at T1 and T2 (Figure 3.30A-C). However, the abundance of PD-1+ and GM-CSF+IL17+ increased in TUM, only at T1 and not at T2 (Figure 3.30B-D). IFNγ+ iNKT cells decreased in TUM at T1, while they increased at T2 (Figure 3.30B-D). Neutrophils as well infiltrated TUM lesions and had an immunosuppressive phenotype, expressing PD-L1, both at T1 and T2 (Figure 3.30E-H). These results show that at early-stage the AOM/DSS model reproduced the immunological picture that we have observed in human CRC, becoming a valuable tool to study the functional interaction between iNKT cells and neutrophils *in vivo*.
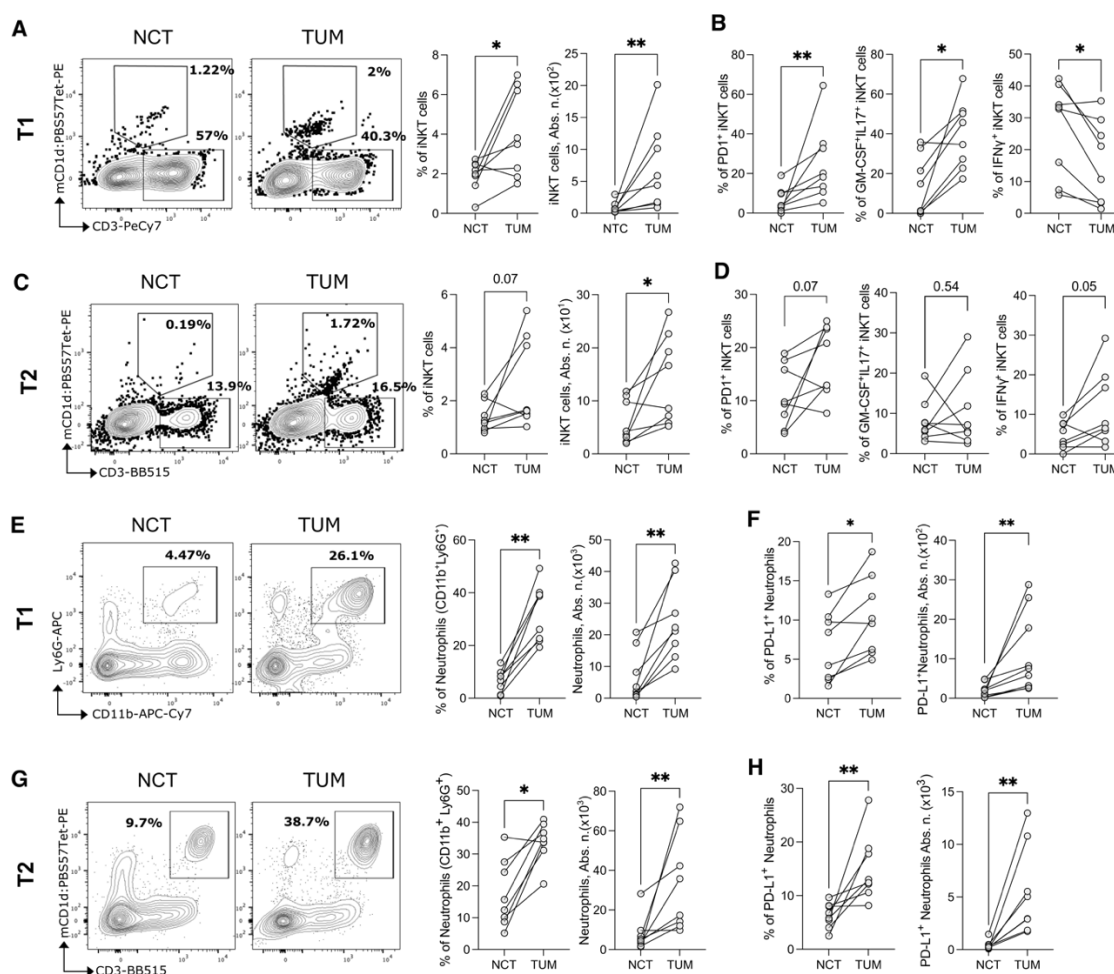
Figure 3.30: iNKT cells and neutrophils in the AOM/DSS model at T1 mirror their human CRC-infiltrating phenotype. (A-C) Frequency and absolute numbers of iNKT cells infiltrating NCT and TUM in AOM/DSS-treated mice at T1 (A) and T2 (C), with representative plots. (B-D) Frequency of PD-1+, GM-CSF+IL17+ and IFNγ+ iNKT cells infiltrating NCT and TUM at T1 (B), and T2 (D). (E-G) Frequency and absolute numbers of neutrophils infiltrating NCT and TUM at T1 (E) and T2 (G), with representative plots. (F-H) Frequency and absolute numbers of PD-L1+ neutrophils infiltrating NCT and TUM at T1 (F) and T2 (H). P < 0.05 (*), P < 0.01 (**); Mann-Whitney test; Wilcoxon matched-pairs signed rank test for NCT versus TUM. Data are representative of at least three independent experiments.

3.5.3 iNKT deficiency slows tumor formation and reduces TANs recruitment

To study the involvement of iNKT cells in tumor formation we applied the AOM/DSS protocol to two different strains of iNKT deficient animals, the *CD1d*^{-/-} which lacks type I and II NKT cells and CD1d expression on APCs and the *Traj18*^{-/-} which lacks only type I NKT cells. Both showed lower tumor degrees compared to wild-type, C57BL/6 animals, as measured by endoscopic score, number and volume of tumors formed (Figure 3.31A-C).
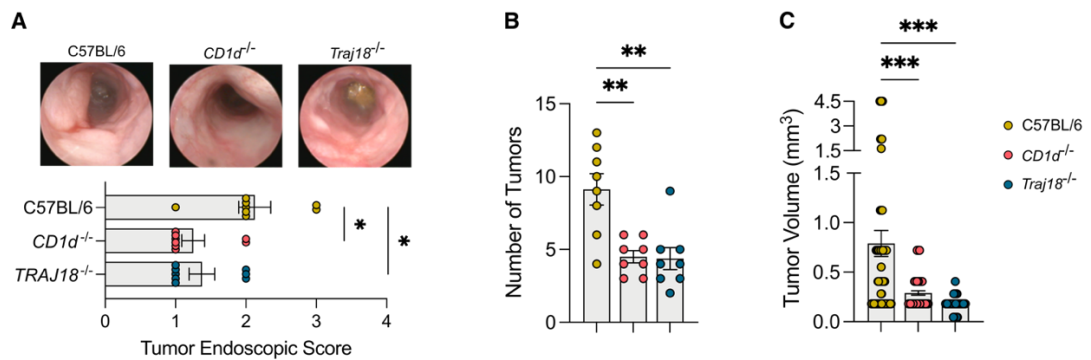
Figure 3.31: *CD1d*^{-/-} *and Traj18*^{-/-} *are less susceptible to tumor formation than C57BL/6. (**A**) Tumor endoscopic scores (bottom panel) in AOM/DSS treated C57BL/6 (yellow circle), CD1d*^{-/-} *(red circle) and Traj18*^{-/-} *(blue circle) with representative endoscopic pictures (top panel). (**B-C**) Numbers (**B**) and size (**C**) of tumors in AOM/DSS treated C57BL/6 (yellow circle), CD1d*^{-/-} *(red circle) and Traj18*^{-/-} *(blue circle). P < 0.05 (*), P < 0.01 (**), P < 0.001 (***); Kruskal-Wallis test followed by uncorrected Dunn's test. Data are representative of at least three independent experiments.*

By analyzing the immune infiltrate of C57BL/6, *CD1d*^{-/-} and *Traj18*^{-/-} we found that iNKT deficient animals had lower abundance of TANs (Figure 3.32A). TANs abundance positively correlated with the number of tumors formed in C57BL/6 ($r = 0.79$, p-value = 0.001), while a negative correlation was observed for *CD1d*^{-/-} ($r = -0.42$ p-value = 0.28) and *Traj18*^{-/-} ($r = -0.74$, p-value = 0.03) (Figure 3.32B). Based on these observations we hypothesized iNKT cells may skew neutrophils toward a pro-tumorigenic phenotype *in vivo*.
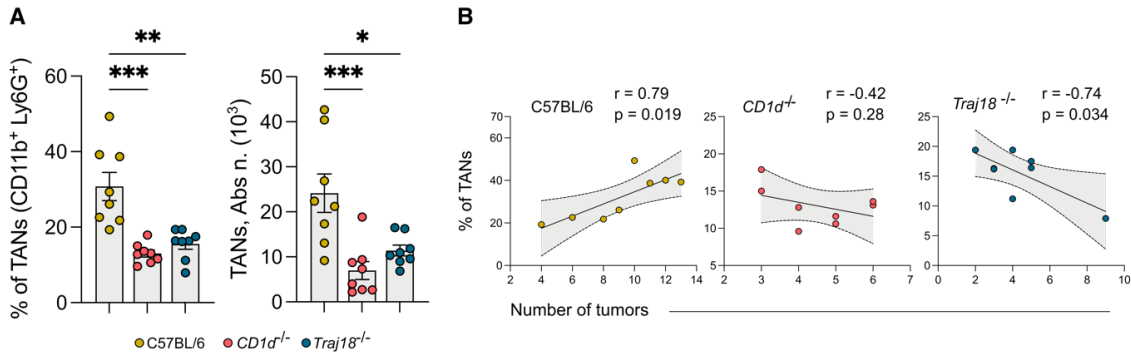
Figure 3.32: *CD1d$^{-/-}$ and Traj18$^{-/-}$ tumors are less infiltrated by neutrophils than C57BL/6. (A) Frequency (left panels) and absolute numbers (right panels) of TANs in C57BL/6 (yellow circle), Cd1d$^{-/-}$ (red circle) and Traj18$^{-/-}$ (blue circle) animals. (B) Correlation analysis of TANs frequency and number of tumors in C57BL/6, CD1d$^{-/-}$ and Traj18$^{-/-}$ animals. P < 0.05 (*), P < 0.01 (**), P < 0.001 (***); Kruskal-Wallis test followed by uncorrected Dunn's test. Data are representative of at least three independent experiments.*

3.5.4 iNKT cells promote TANs immunosuppressive phenotype *in vivo*

To elucidate the phenotype of neutrophils in presence/absence of iNKT cells, we sorted NCT and TUM infiltrating neutrophils from untreated and AOM/DSS treated C57BL/6 and *Traj18$^{-/-}$* mice. We observed that TANs in *Traj18$^{-/-}$* were enriched in genes involved in the mitogen-activated protein kinases (MAPK) signaling pathway (*Map3k14, Map14, Map12*), hypoxia (*Hif1a*) and neutrophil extracellular traps formation (NETs; *Hmgb1, Hmgb2, Ceacam1, Mmp15, Mmp21*) (Figure 3.33A, C). On the other hand, C57BL/6 TANs upregulated gene associated with immune suppression (*Il10*, *S100a8*), inflammation and cell recruitment (*Ccl3, Cxcl2, Cxcr5, Nfkbie, Nfkbiz, Socs3, Atf4, Ptsg2, Pla2g7*) (Figure 3.33A, C). Performing pathway enrichment analysis, C57BL/6 TANs were associated with the inflammatory TNF signaling pathway (Figure 3.33B).

To understand whether the differential transcriptional activity of C57BL/6 and *Traj18$^{-/-}$* TANs was related to functionally different populations of polymorphonuclear myeloid-derived suppressor cells (PMN-MDSCs), we analyzed a publicly available scRNA-seq dataset of PMN-MDSC form tumor-bearing mice [209]. The t-sne overlay analysis revealed that C57BL/6 TANs were enriched for genes expressed in a cluster of 'activated' PMN-MDSC signature (PMN3) (Figure 3.33D) while *Traj18$^{-/-}$* TANs upregulated the expression of genes associated with a population of 'classical' PMN-MDSC (PMN2)

(Figure 3.33E), reflecting different pathways of neutrophils activation in the presence or absence of iNKT cells.
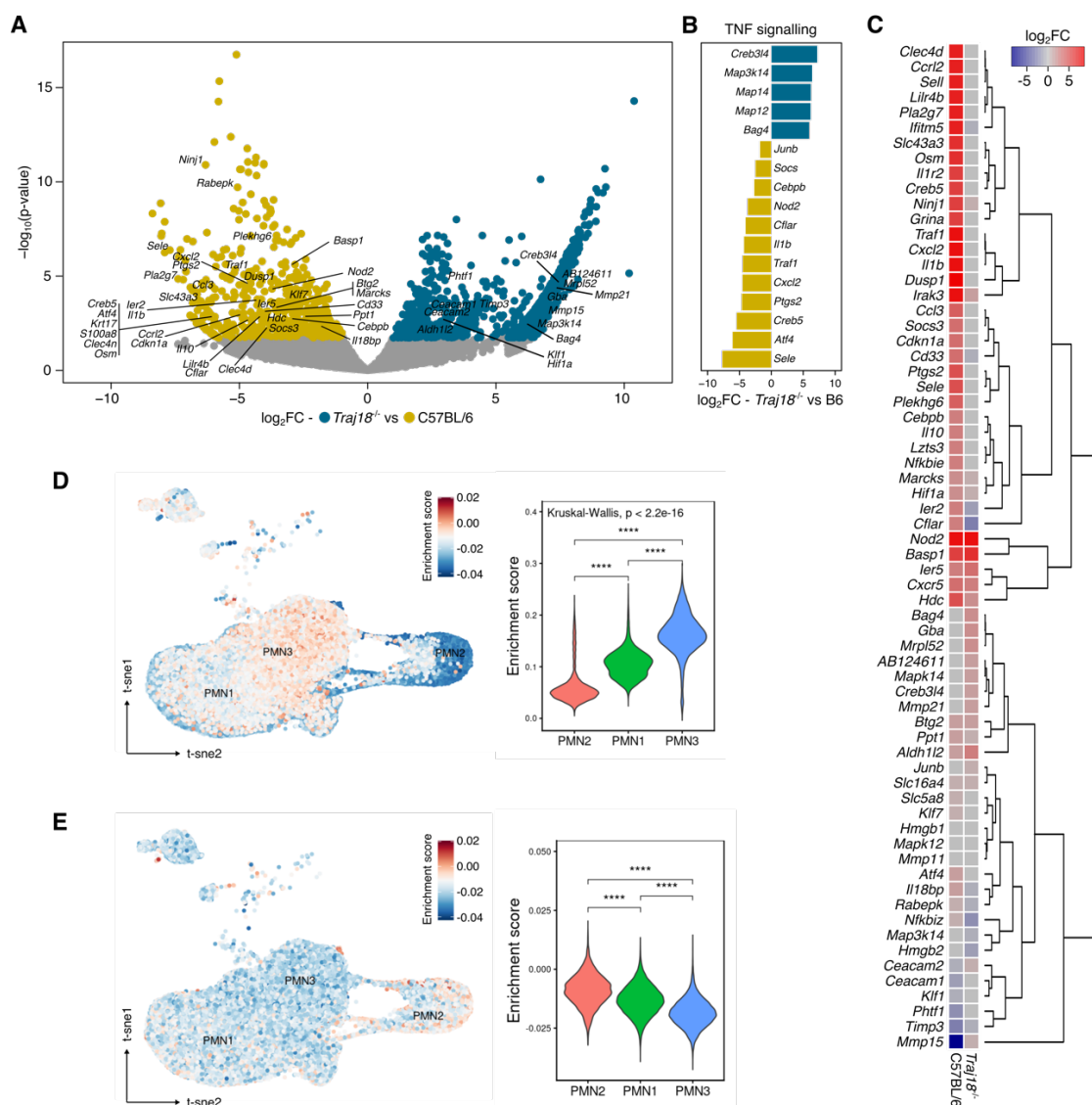
Figure 3.33: *Tumor infiltrating neutrophils in C57BL/6 and Traj18^{-/-} differentially express pro-tumorigenic-like gene signatures. (**A**) Volcano plot representing the DEGs of TANs in C57BL/6 and Traj18^{-/-} animals; for each gene (dots) the differential expression (log2fold-change [log2FC]) and the statistical significance (log10p-value) is shown (FDR-corrected P = 0.05 and log2FC > |1.5|). (**B**) DEGs enriched in the KEGG TNF signaling pathway (Bonferroni-corrected p < 0.05 and log2FC > |1|). (**C**) Heatmap and hierarchical clustering of MDSC-related DEGs (FDR-corrected p-value < 0.05 and log2FC > |1|) in tumor infiltrating neutrophils vs healthy colon infiltrating neutrophils from C57BL/6 and Traj18^{-/-} animals. (**D**) C57BL/6 and (**E**) Traj18^{-/-} TANs gene expression signatures (genes with an FDR-corrected p-value < 0.1 and log2FC ≥ |1|) and relative expression values of the single cell PMN-MDSC data set from Veglia et al., 2021. P < 0.0001 (****); Kruskal-Wallis test followed by uncorrected Dunn's test. Data are representative of three independent experiments.*

A phenotypical characterization of C57BL/6, *CD1d*^{-/-} and *Traj18*^{-/-} TANs showed an elevated expression of Ly6G on *CD1d*^{-/-} and *Traj18*^{-/-} TANs (Figure 3.34A-B). CD11b$^+$Ly6G^{High} TANs (Figure 3.34A-B) had higher ROS production and decreased expression of the immunosuppressive marker PD-L1 compared to CD11b$^+$Ly6G^{Low} (Figure 3.34C-D).

Taken together these data highlight that TANs have an immunosuppressive phenotype in murine tumors, sustained by the presence of iNKT cells.
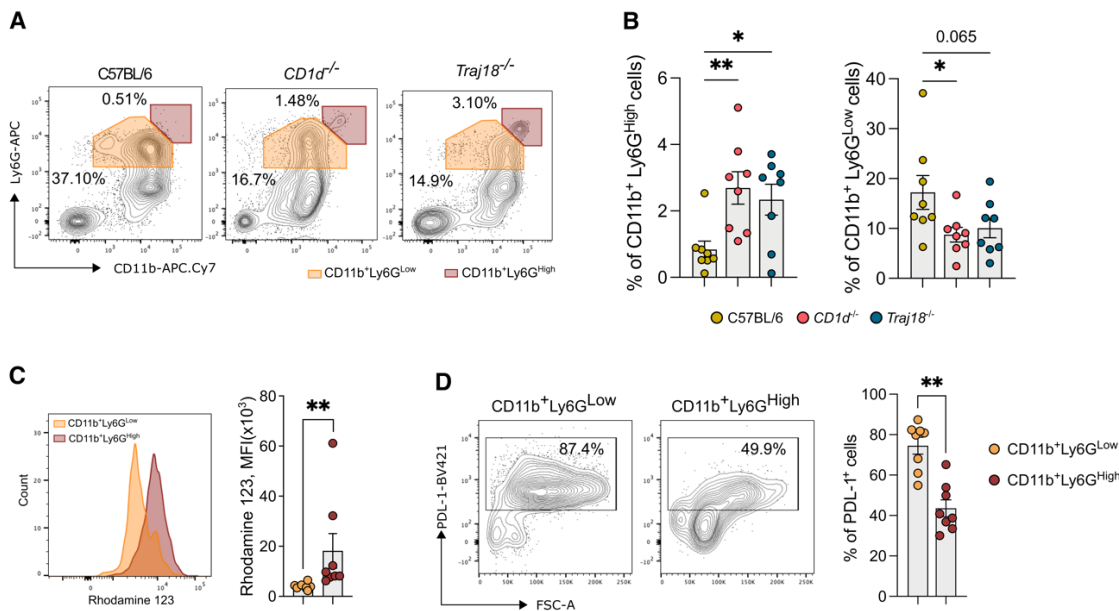
Figure 3.34:*Tumor infiltrating neutrophils in iNKT deficient mice are less immunosuppressive. (**A-B**) Frequency of CD11b$^+$, Ly6G^{High} and Ly6G^{Low} TANs in C57BL/6, CD1d$^{-/-}$ and Traj18$^{-/-}$ animals (**B**), with representative plots (**A**). (**C-D**) Respiratory burst quantification (**C**) and frequency of PD-L1$^+$ (**D**) in CD11b$^+$, Ly6G^{High} and Ly6G^{Low} TANs in Traj18$^{-/-}$ mice. Data points from two pooled independent experiments representative of at least three. P < 0.05 (*), P < 0.01 (**), P < 0.001(***); Kruskal-Wallis and Mann-Whitney tests.*

3.6 Syngeneic MC38 murine models of CRC

To study whether the role of iNKT cells in modulating TANs recruitment and phenotype as well as CRC development is confined to inflammation-driven CRC, we investigated two syngeneic MC38 models. We used: I) a canonical protocol implanting MC38 cell subcutaneously, with the advantage to have a robust, fast (15 days) CRC model that enabled us to study the role of immune system. II) an alternative protocol implanting MC38-Luciferase cells orthotopically in the cecum, with the advantage to have a more physiologic tumor microenvironment comprising also of intestinal microbiota.

3.6.1 iNKT cells support tumor growth, but treatment with αGalCer enables tumor control

In the syngeneic, subcutaneous MC38 model, we observed that $Traj18^{-/-}$ had a delayed tumor growth compared to C57BL/6 mice (Figure 3.35A-C). In agreement with our previous findings, C57BL/6 mice were significantly more infiltrated by TANs compared to $Traj18^{-/-}$ mice (Figure 3.35D).
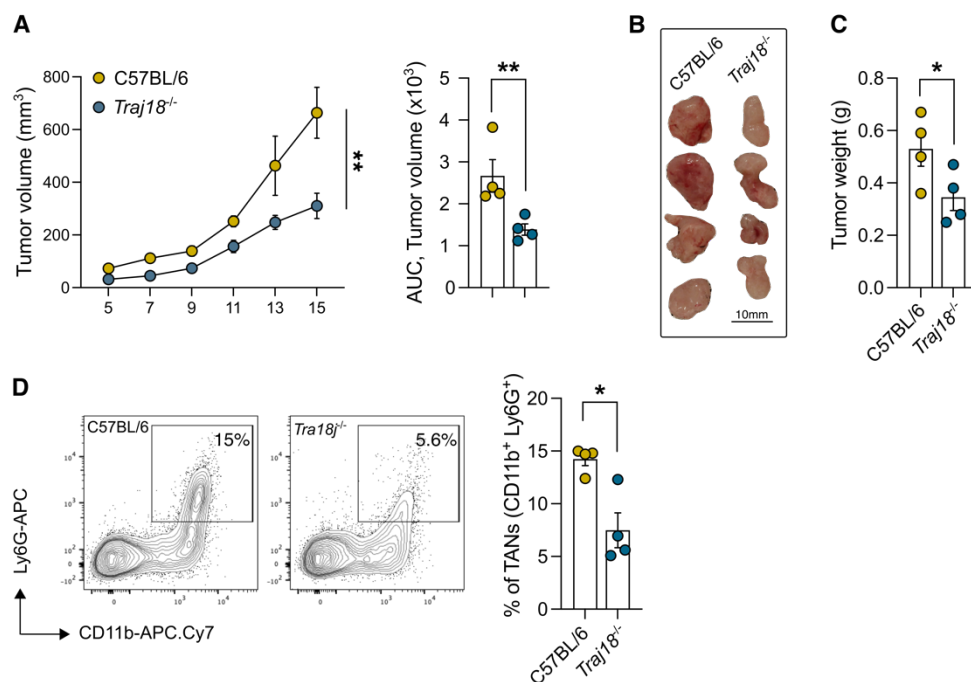
Figure 3.35: *$Traj18^{-/-}$ mice have a delayed tumor growth compared to C57BL/6 in the MC38 CRC model. (**A**) MC38 tumor growth in C57BL/6 and $Traj18^{-/-}$ animals, with their relative area under the curve (AUC). (**B-C**) Representative pictures (**B**) and weight of tumors (**C**) in C57BL/6 and $Traj18^{-/-}$ mice. (**D**) Frequency of TANs in C57BL/6 and $Traj18^{-/-}$ mice, with representative plots. Data are representative of one of three independent experiments. $P < 0.05$ (*), $P < 0.01$ (**). Mann-Whitney test.*

Modulating the iNKT cells functionalities with αGalCer, we observed that tumor growth was significantly hampered in C57BL/6 animals (Figure 3.36A-C) and tumor-infiltrating iNKT cells acquired an anti-tumorigenic phenotype associated with the overexpression of IFNγ (Figure 3.36D). This finding is in line with the notion that αGalCer polarizes iNKT cells towards Th1-like cytokines [140], as we also observed in our *in vitro* experiments (Figure 3.21), rather than towards Th17-like ones (Figure 3.36F).
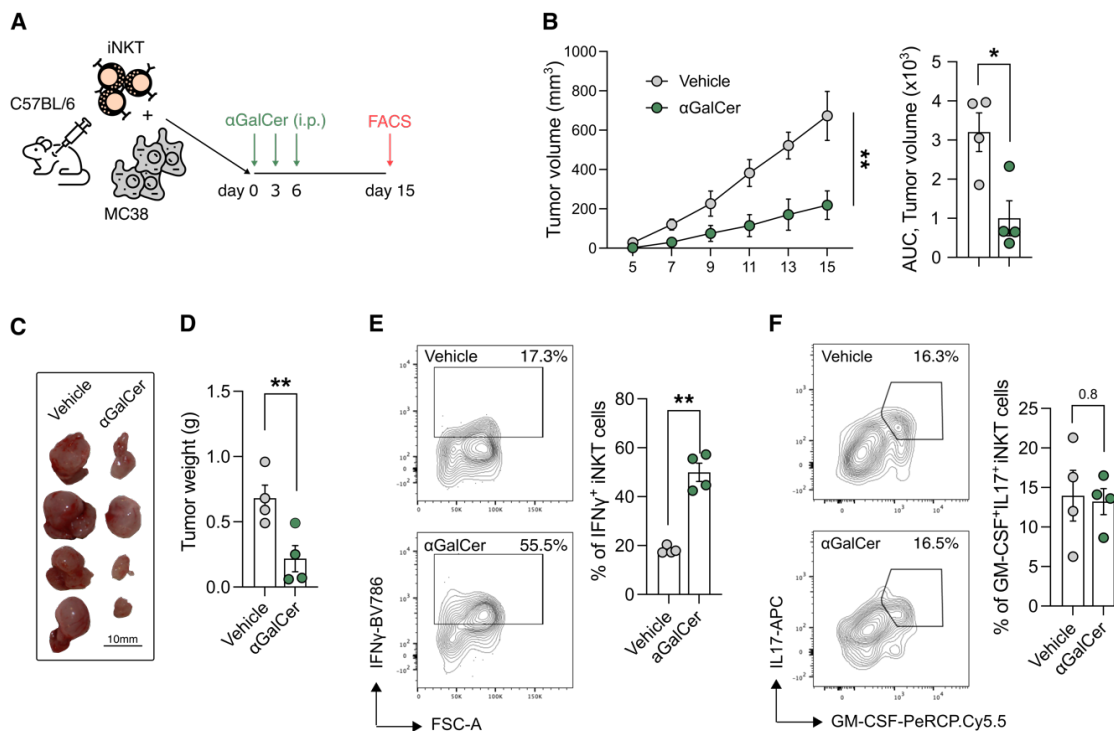
Figure 3.36: *αGalCer treatment control tumor growth in the syngeneic MC38 subcutaneous model. (A) Schematic representation of the experimental design. (B) Tumor growth in C57BL/6 treated with αGalCer or with vehicle, with their relative AUC. (C-D) Representative pictures (C) and weight of tumors (D) in C57BL/6 treated with αGalCer or with vehicle. (E-F) Frequency of tumor infiltrating IFNγ⁺ (E) and GM-CSF⁺IL17⁺ (F) iNKT cells in αGalCer or vehicle treated C57BL/6 animals, with representative plots. Data are representative of one of three independent experiments. P < 0.05 (*), P < 0.01 (**). Mann-Whitney test.*

We further validated the previous results by reconstituting *Traj18⁻/⁻ mice* with iNKT cells. Indeed, *Traj18⁻/⁻* mice reconstituted with iNKT cells showed a higher tumor growth than control *Traj18⁻/⁻* mice and promoted TANs recruitment (Figure 3.37A-D). Treatment with αGalCer controlled tumor growth confirming that iNKT cells could be re-activated to become anti-tumorigenic (Figure 3.37A-D).
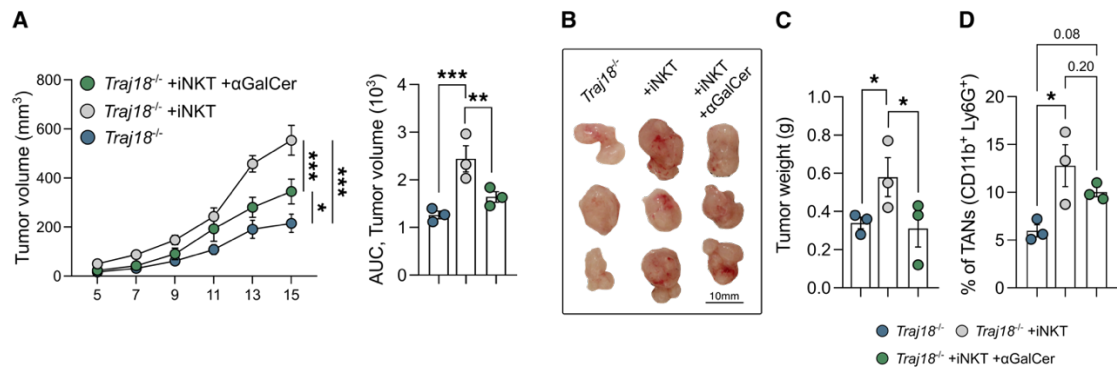
Figure 3.37*: iNKT reconstitution of Traj18$^{-/-}$ support tumor growth. (**A**) Tumor growth and AUC of Traj18$^{-/-}$ (blue circle), Traj18$^{-/-}$ re-constituted with splenic iNKT cells (grey circle) and Traj18$^{-/-}$ re-constituted with iNKT cells and treated with αGalCer. (**B-C**) Representative photos (**B**) and weight of tumors (**C**) in Traj18$^{-/-}$ and Traj18$^{-/-}$ re-constituted with iNKT cells and treated with αGalCer or with vehicle. (**D**) Frequency of TANs in Traj18$^{-/-}$ and Traj18$^{-/-}$ re-constituted with iNKT cells and treated with αGalCer or with vehicle. Data are representative of one of three independent experiments. P < 0.05 (*), P < 0.01 (**), P < 0.001 (***). Mann-Whitney test.*

3.6.2 Orthotopically implanted MC38 tumors are infiltrated mainly by iNKT17 cells

To have a physiologic CRC mouse model that takes into account also the role of the intestinal microbiota in shaping the TME, we adopted an orthotopic CRC model of MC38 intracecal (I.c.) implantation. Due to the intrinsic variability of the technique only 80% of mice developed tumors after surgery (Figure 3.38A). Tumor-infiltrating iNKT cells showed a Th17and Th1-like phenotype in orthotopically injected mice, expressing primarily TNFα, GM-CSF and IL17 compared to other Th1 and Th2 cytokines (Figure 3.38B), while splenic iNKT cells expressed mainly Th1-associated cytokines (Figure 3.38B). Comparing the phenotype of iNKT cells infiltrating I.c. or subcutaneous (S.c.) tumors we observed that iNKT cells increased the expression of CD69 and decreased the one of PD-1 in I.c. tumors (Figure 3.38C). iNKT cells infiltrating I.c. tumors overexpressed the cytokine IL17, while they did not change the expression of GM-CSF or IFNγ compared to iNKT cells infiltrating S.c. tumors (Figure 3.38D). These findings sustain the relevance of the gut microbiota in shaping the Th17-like phenotype of iNKT cells. In accordance with previous results treatment with αGalCer improved mice survival (Figure 3.38E), reduced tumor size (Figure 3.38F) and induced the expression of IFNγ on iNKT cells (Figure 3.38G).
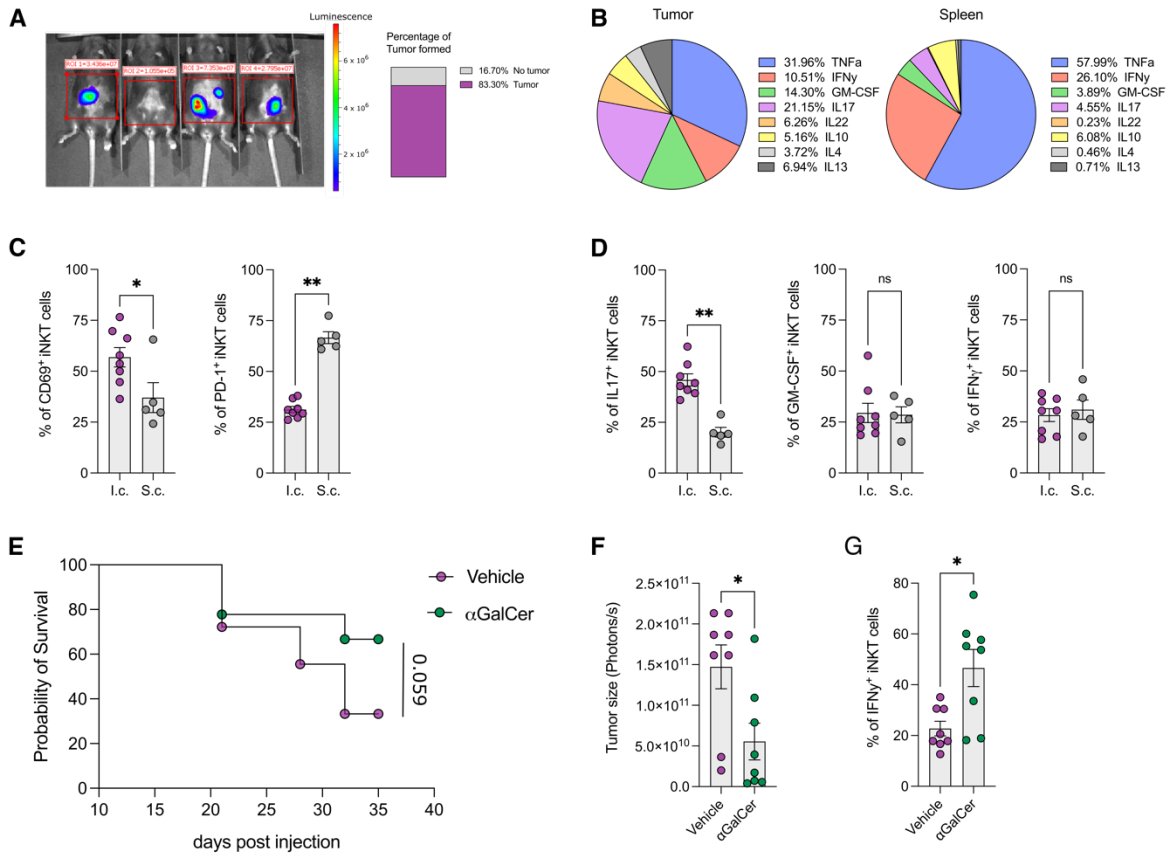
Figure 3.38: *Intracecal tumors are infiltrated by activated iNKT cells producing IL17. (**A**) Percentage of tumor formation (purple) in intracecal MC38-Luc implantation, with IVIS representative image. (**B**) Percentage of TNFα, IFNγ, GM-CSF, IL17, IL22, IL10, IL4, IL13-producing iNKT cells in tumor (left panel) or spleen (right panel) in C57BL/6 mice. (**C-D**) Percentage of CD69⁺, PD-1⁺ (**C**), IL17⁺, GM-CSF⁺ and IFNγ⁺ (**D**) iNKT cells in intracecal (I.c.) or subcutaneous (S.c.) tumors in C57BL/6 mice. (**E**) Survival probability of C57BL/6 mice with intracecal tumors treated with vehicle (purple dots) or αGalCer (green dots). (**F**) Tumor size at the day of sacrifice calculated by Photons/s in intracecal tumor mice upon treatment with vehicle (purple dots) or αGalCer (green dots). (**G**) Frequency of IFNγ⁺ iNKT cells in intracecal tumor mice treated with vehicle (purple dots) or αGalCer (green dots). P < 0.05 (*), P < 0.01 (**). Mann-Whitney test, Log-rank (Mantel-Cox) test for survival curve comparison.*

3.7 CRC associated murine microbiota induces upregulation of GM-CSF and IL17 in murine iNKT cells

We have demonstrated the importance of CRC-associated microbiota in shaping iNKT phenotype *in vitro* (Chapter3.3, 3.4) and *in vivo* (Chapter3.6.2). However, we wondered whether the CRC-associated microbiota effect was strain dependent. We found no significant differences in the microbial community structure of C57BL/6 and iNKT

deficient (*CD1d$^{-/-}$*) mice at steady state (Figure 3.39A-B). On the other hand, the induction of tumorigenesis by AOM/DSS treatment promoted significant alterations in the microbial community structure and the enrichment of different tumor-associated bacteria in C57BL/6 and iNKT deficient mice (Figure 3.39C-D). Nevertheless, priming of freshly isolated splenic iNKT cells with the tumor-associated microbiota from C57BL/6, *CD1d$^{-/-}$* and *Traj18$^{-/-}$* mice always induced upregulation of GM-CSF and IL17, independently of the mouse strain (Figure 3.39E) suggesting that a dysbiotic, CRC-associated microbiota is sufficient to induce an iNKT pro-tumorigenic phenotype irrespective of defined microbial composition.
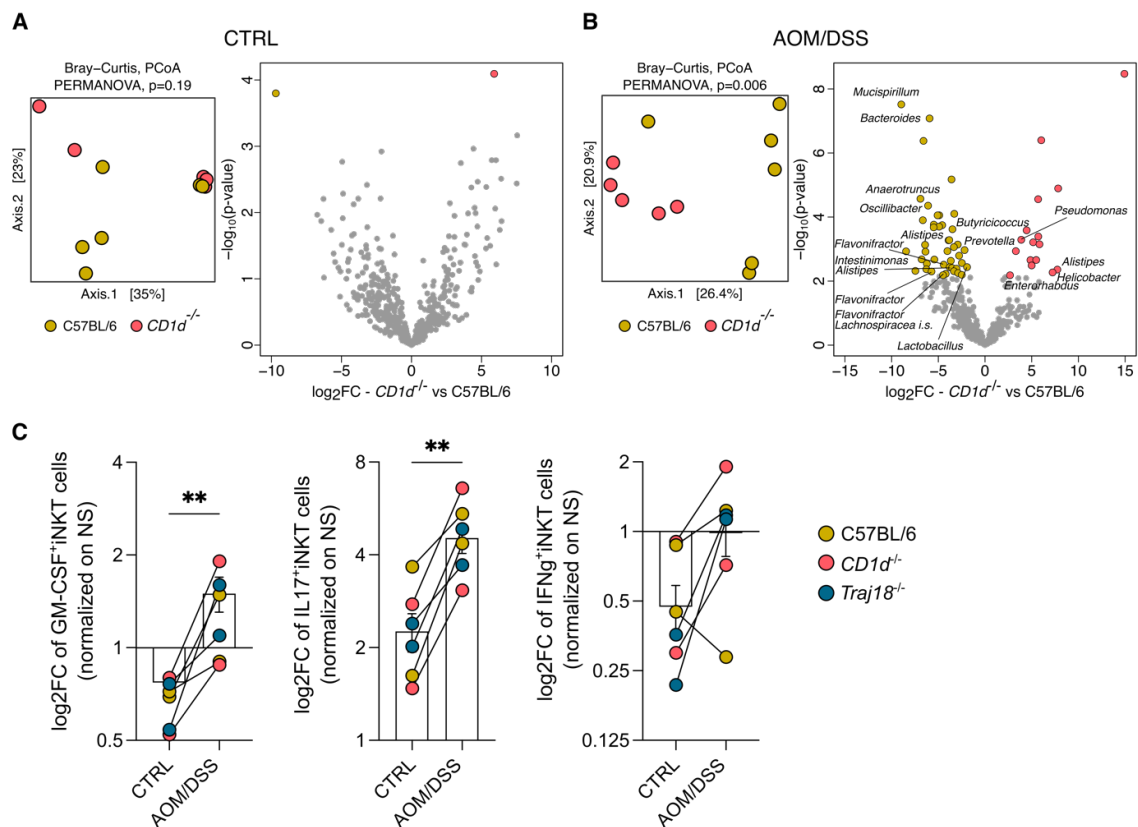
Figure 3.39: *Murine CRC associated microbiota induce expression of GM-CSF and IL17 in iNKT cells.* **(A-B)** *PCoA of microbiota beta-diversity measured by Bray-Curtis distance (left panels) and volcano plots (right panels) of the significantly enriched bacterial taxa (FDR P <0.05) in untreated, controls (CTRL)* **(A)** *and AOM/DSS treated* **(B)** *C57BL/6 and CD1d$^{-/-}$ mice. Significantly enriched ASVs classified to the genus level are shown.* **(C)** *Frequency of GM-CSF$^+$, IL17$^+$ and IFNγ$^+$ iNKT cells primed with BMDCs and heat-killed gut microbiota of CTRL or AOM/DSS treated C57BL/6, CD1d$^{-/-}$ and Traj18$^{-/-}$ animals. Data shown from three independent experiments are expressed as log2fold-change (log2FC) normalized to BMDCs endogenous stimulation. P < 0.01 (**). Mann-Whitney test.*

3.8 Survival analyses of human CRC patients reveal iNKT cells as negative prognostic factor

To clinically translate our findings and contextualize their significance in CRC patients, we performed Kaplan-Meier and multivariate survival analysis in two different CRC cohorts with iNKT cell infiltration as discriminator factor.

3.8.1 iNKT cells are a negative prognostic factors, reverting the beneficial role of neutrophils in the internal CRC cohort

Stratifying patients as iNKT^High and iNKT^Low, based on the optimal cut-off for iNKT cell distribution in tumor lesions, we observed that iNKT infiltration was a negative prognostic factor for relapse-free survival at 4 years (Figure 3.40A). On the contrary, neutrophils infiltration, was a positive prognostic factor in our internal human CRC (Figure 3.40B), as already observed in other studies [69]–[71] TANs clinical relevance was affected by iNKT cells infiltration. Indeed, stratifying neutrophils^High patients according to the infiltration of iNKT cells revealed that patients with neutrophils^High iNKT^High infiltration have a reduced survival curve compared to neutrophils^High iNKT^Low patients (Figure 3.40C).
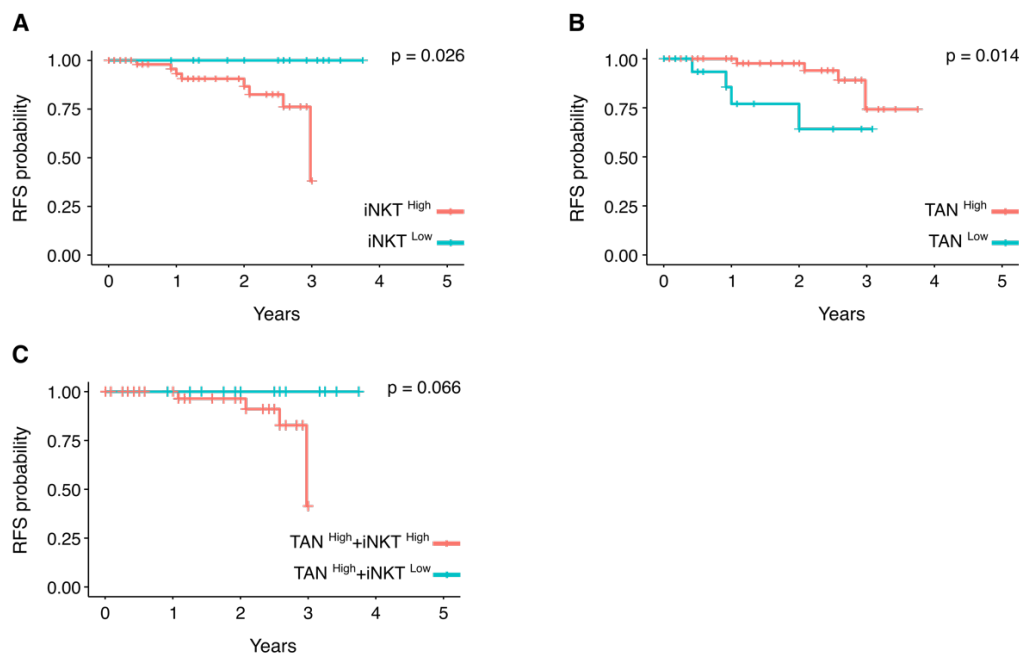
Figure 3.40: *Relapse-free survival of the internal CRC cohort reveals iNKT infiltration as negative prognostic factor.* ***(A-B-C)*** *Kaplan-Meier relapse free survival (RFS) curves of the internal CRC*

*patient's cohort stratifying for iNKT infiltration (**A**) or neutrophils infiltration (**B**), in the whole population (**A-B**) or inside the population of TAN^High patients (**C**).*

To assess whether confounders factors affect the prognostic significance of iNKT cells we performed multivariate Cox regression analysis on the internal CRC cohort. Infiltration of iNKT result as negative prognostic factor with hazard ratio (HR) equal to 1.87 (Figure 3.41) and it is not affected by age, gender, MMR status, size of primary tumor (T), involvement of regional lymph nodes (N), tumor grading (G) and tumor location (Figure 3.41).
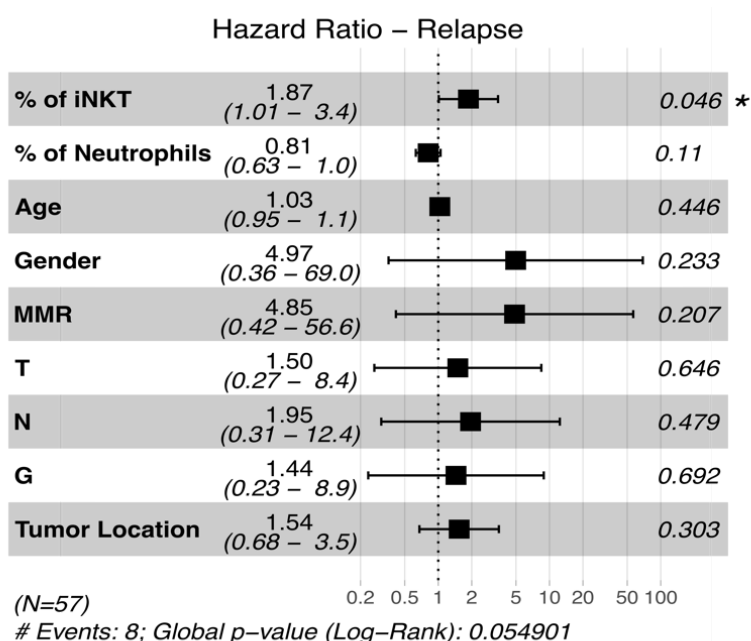
Figure 3.41: iNKT cells infiltration is an independent negative prognostic factor for the relapse of CRC patients. Multivariate analysis of CRC patients' relapse calculated by Log-Rank test and taking in consideration infiltration of iNKT cells, of neutrophils, age, gender, MMR status, size of primary tumor (T), involvement of regional lymph nodes (N), tumor grading (G) and tumor location.

3.8.2 Overall survival analysis of the COAD-TCGA validate the negative prognostic value of iNKT cells

To confirm the observations made on the internal CRC cohort we used as validating cohort the COAD dataset of TCGA. Upon exclusion of metastatic stage IV patients, we conducted overall survival analysis (10 years) stratifying patients for the expression of *CEACAM8*. *CEACAM8* encodes for CD66b, the marker commonly used to identify neutrophils. In agreement with previous observations (Figure 3.42B), high expression of *CEACAM8* was a favorable prognostic factor (Figure 3.42A), while its combination with *ZBTB16* reversed the prognosis (Figure 3.42B) *ZBTB16* encodes for PLZF, the master regulator of iNKT cell development. Altogether these results show that iNKT cells have a negative prognostic value in CRC and suggest to reconsider neutrophils infiltration as a positive prognostic factor *per se*.
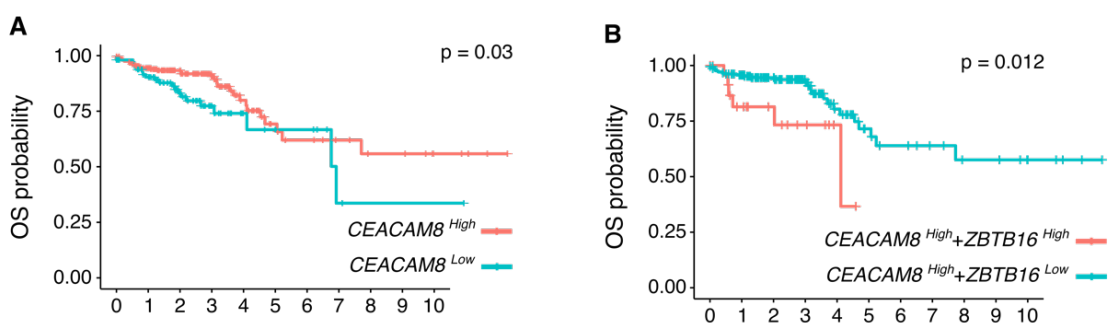
Figure 3.42*: ZBTB16 expression capsize the positive prognostic value of CEACAM8 expression in TCGA dataset of CRC. (**A**) Kaplan-Meier overall survival (OS) curves of the adenocarcinoma dataset of TCGA stratifying for CEACAM8 expression. (**B**) Kaplan-Meier OS curves of the adenocarcinoma dataset of TCGA stratifying for ZBTB16 expression inside the population of CEACAM8^High expressing patients.*

4 Discussion

iNKT cells are involved in the maintenance of intestinal homeostasis [7], [8], in the clearance of pathogens [10] and in immune surveillance against different tumor malignancies [15].

In mice, iNKT cells were shown to have opposite roles in tumor immunology, promoting development of intestinal polyps in the $APC^{Min/+}$ strain [139], but restraining tumor formation in transgenic models of pancreatic cancer [131], [134]. In human, accurate identification, lack of large samples availability and low cell abundance are major challenges for iNKT cell studies. Before the advent of αGalCer-loaded tetramers, iNKT cells were identified using a combination of NK markers such as CD161 or CD56 and the T cell specific marker CD3 [104]. With this approach it is likely to detect several unconventional T cells such as type II NKT, MAIT or γδ T cells, in addition to iNKT cells. Here, by using αGalCer-loaded tetramers and supervised [9] and unsupervised analytical approaches [196], [212] we showed that iNKT cells infiltrate the intestinal lamina propria of human CRC patients, with higher abundance in the tumor lesions compared to the adjacent normal tissues (Section3.1.2). We further validated these observations by analyzing publicly available dataset of single cell RNA-sequencing of CRC immune infiltrate (Section3.1.2). Additionally, we observed that tumor samples were enriched with the iNKT cells chemoattractant molecule CXCL16, at a genetic and protein level (Section3.2.1), suggesting that iNKT cells are actively recruited into the tumor.

Distinct subsets of iNKT cells can be distinguished based on their functionalities, cytokines release and tissue localization [8], [89]. We have previously described that intestinal iNKT cells promote tissue homeostasis producing the immunoregulatory cytokine IL10 [9], [168]. However, iNKT cells can also produce cytotoxic and pro-inflammatory cytokines such as IFNγ, TNFα and IL17 in physiological and pathological contexts [166]. In CRC lesions, we showed that tumor-infiltrating iNKT cells acquire a Th17-like phenotype with the co-expression of IL17 and GM-CSF and the upregulation of exhaustion markers (Section3.1.2). This phenotype is characteristic of tumor-infiltrating iNKT cells and it is unique among other unconventional T cells (*i.e.* γδ T cells and ILCs) (Section3.1.4). Previous studies proposed a relevant role for γδ T cells and ILCs in the production of either IL17 or GM-CSF in CRC [4]; however, none of the

previous studies analyzed the release of the aforementioned cytokines by iNKT cells in the same patients, as we did. IL17 and GM-CSF have emerged as new players in CRC progression [4], through direct and indirect mechanisms. GM-CSF sustains tumor formation in AOM/DSS treated animals promoting VEGF release, angiogenesis and adenoma formation [213]. IL17 supports tumor formation and its deficiency or pharmacological blockade reduces tumor load in the $APC^{Min/+}$ mouse model [56]. Accordingly, we observed the upregulation of Th17-associated genes in the tumor lesions (*i.e. IL23*, *IL17* and *IL22*) of our study cohort (Section3.2.1).

GM-CSF and IL17 are known mediators of myeloid cells recruitment and activation in chronic inflammatory disorders and at tumor sites [4], [85]. In CRC, IL17 promotes the recruitment of neutrophils [214]. In gastric cancer, tumor derived GM-CSF recruits neutrophils and promotes their immunosuppressive behaviors [66]. Consistently, we found that CRC lesions were characterized by an increased infiltration of neutrophils (Section3.1.5) whose abundance positively correlated with GM-CSF$^+$IL17$^+$ iNKT cells (Section3.1.6). TANs are highly heterogenous cells with a wide potential in dictating cancer development [64], [72]. In our CRC cohort, we identified distinct functional subsets of neutrophils, expressing the immunosuppressive molecule PD-L1, the antigen presenting molecules MHC-II and CD1d, as well as marker of aging and maturation (*i.e.* CXCR4, CD62L, CD33, CD10 and CD16) (Section3.1.5). Aged neutrophils (CXCR4$^+$CD62L^{Low}) significantly infiltrate tumor lesions, suggesting a shift in their inflammatory properties. It has been shown that the CXCL12/CXCR4 axis is important for the establishment and maintenance of neutrophils niches in lung tissues, where they can exert inflammatory and angiogenic functions [215]. The transcriptional signatures of lung and gut neutrophils were highly similar, differing from that of neutrophils of hematopoietic origin (bone marrow, spleen and blood) [215]. This observation suggests that, similarly to lung neutrophils, also intestinal neutrophils could be retained at tissue sites through the CXCL12-CXCR4 axis. Moreover, aged neutrophils have increased immunosuppressive properties toward cytotoxic CD8$^+$ T cells *in vitro* through the release of Arginase-1 and the upregulation of PD-L1 [216], observations that we have also reported in our cohort. TANs showed also a mature (CD33^{mid}CD10$^+$CD16$^+$) phenotype (Section3.1.6) which can be associated with T cell immunosuppressive properties. We then hypothesized that neutrophils immunosuppressive properties and functionalities could be due to the activity of tumor, GM-CSF$^+$IL17$^+$ iNKT cells. Accordingly, we showed that upon stimulation with tumor-like iNKT cells neutrophils enhanced their T-

cell immunosuppressive properties by restricting näive CD4+ T cell proliferation (Section3.4).

iNKT cells are rapidly, effectively and differentially activated by endogenous and microbial signals, being phenotypically skewed by changes in the gut microbiota composition [10], [113], [116], [158]. Indeed, intestinal dysbiosis imprints iNKT cells toward an inflammatory phenotype whereas normobiosis promotes their IL10-mediated regulatory functions [9], [166], [168].

CRC patients have a dysbiotic microbiota which participate to the carcinogenic process [31]. CRC-associated microbiota can induce genotoxicity of tumor cells and can affect the activation and exhaustion statuses of immune cells [31]. The analysis of the mucosa-associated microbiota of our CRC patient cohort identified *Fusobacterium* as significantly enriched within tumor lesions (Section3.2.2). *Fusobacterium nucleatum (F. nucleatum)* is a known oncogenic bacterium, associated with mucosal adherence, tumor genotoxicity and immune suppression [175]–[178]. *F. nucleatum* promotes tumor cell proliferation activating the Wnt/β-catenin pathway through the binding of the FadA virulence factor [173], [176]. Additionally, *F. nucleatum* promotes carcinogenesis by suppressing anti-tumor immune responses and supporting tumor cell immune evasion [171], [174]. For instance, the virulence factor Fap2 on *F. nucleatum* binds the co-inhibitory molecule TIGIT on NK and T cells, hampering their cytotoxic properties [178]. We observed the upregulation of TIGIT on tumor-infiltrating iNKT cells (Section3.1.7), thus we hypothesize that Fap2 interaction with TIGIT could induce iNKT cell anergy. Moreover, *F. nucleatum* exacerbates inflammation and promotes inflammation-driven CRC by upregulating the expression of IL17 (both IL17A and IL17F) in CD4+ T cells [176]. Consistently we demonstrated that *F. nucleatum* induces the expression of Th17 cytokines, (*i.e.* IL17 and GM-CSF) on iNKT cells without affecting their killing capability (Section3.3.1). Moreover, stimulation with *F. nucleatum,* imprinted a neutrophil-chemotactic gene signature on iNKT cells, which upregulated the expression of *CXCL8,* the gene encoding for the specific neutrophil-recruiting chemokine IL8 (Section3.3.2). We have deeply investigated the effect of *F. nucleatum* on iNKT cells phenotype and we observed that it promotes the expression and production of Th17 associated cytokines, however, we cannot exclude that other bacteria may have the same effects on iNKT cells. Indeed, dysbiotic gut microbiota of IBD patients stimulates the production of pro-inflammatory cytokines (*i.e.* IFNγ and IL17) on iNKT cells [166], suggesting that several bacteria are able to boost their Th17 phenotype. However, in our

set we have used only *F. nucleatum* as representative of CRC-associated pathobionts as it allows to avoid the higher degree of complexity which would be introduced by the usage of undefined bacterial communities. Additionally, we have recently obtained selected mutant of *F. nucleatum* that will be used in future projects for the mechanistic dissection of the *F. nucleatum*-iNKT crosstalk. For the seek of this project, *F. nucleatum*-primed iNKT cells were used as representative of tumor-like iNKT cells and thus as a tool to study their effect on other members of the TME.

In this context we observed that *F. nucleatum*-primed iNKT cells promoted neutrophils migration, activation, and T cell immunosuppression (Section3.4). Neutrophils migration was mediated by iNKT cells production of IL8, since the blockade of its signaling pathway via the CXCR1/2 allosteric inhibitor Reparixin, reduced neutrophil migration index. Finally, iNKT cells conditioned by *F. nucleatum* promoted the immunosuppressive phenotype of neutrophils as measured by PD-L1 expression and of ROS production. Neutrophils respiratory burst activity and ROS production has been initially associated only with T cell damage, inhibition and apoptosis [217], however it is now emerging that respiratory burst byproducts have a role as signaling messengers in proliferative cellular pathways [218]. High ROS levels induce oxidative stress that compromises T cell proliferation and activation [217], whereas mild ROS levels are needed for proper T cell expansion, activation and effector functions [218]. We observed that neutrophils cultured with αGalCer-primed iNKT cells released equivalent amount of ROS compared to neutrophils cultured with unstimulated iNKT cells. However, neutrophils cultured with *F. nucleatum*-primed iNKT cells released significant lower amount of ROS compared to unstimulated and αGalCer-primed iNKT cells and suppressed T cell proliferation (Section3.4.2). We hypothesized that unstimulated neutrophils and the one cultured with αGalCer-primed iNKT cells released a mild quantity of ROS needed for T cell proliferation, whereas neutrophils cultured with *F. nucleatum*-primed iNKT cells released suboptimal, insufficient amount of ROS, thus limiting T cell proliferation.

Different examples of direct interactions between iNKT cells and neutrophils have been described in inflammation and in tumor pathologies [162]–[164]. In inflammation, neutrophils regulate iNKT cell extravasation to the pulmonary interstitium [164] and license them to regulate self-reactive B cells in the spleen [163]. In melanoma, iNKT cells crosstalk with neutrophils skews neutrophil production of cytokines from regulatory (IL10) to pro-inflammatory (IL12) [162].

Here, we dissected the crosstalk between iNKT cells and neutrophils in three different murine models of CRC. At first, we investigated the genetically-driven $APC^{Min/+}$ model of CRC, but we did not observe upregulation of either tumor GM-CSF$^+$IL17$^+$ iNKT cells or neutrophils compared to healthy lamina propria (Section3.5.1). The $APC^{Min/+}$ murine model expresses genetic alterations of sporadic human CRC; however, $APC^{Min/+}$ mice develop multiple polyps residing in the small intestine rather than tumor lesions in the colon [21]. Induction of colonic tumors upon AOM-treatment in the $APC^{Min/+}$ strain showed infiltration of neutrophilic granulocytes in the colonic lesions compared to the one present in the small intestine [21]. Nonetheless, our findings are in accordance with previous studies from the laboratory of Dr. Susanna Cardell, that detected similar infiltration of iNKT17 in intestinal polyps and in healthy lamina propria of $APC^{Min/+}$ [139]. Consistently with our hypothesis, Dr. Susanna Cardell observed a decreased infiltration of neutrophils in polyps of iNKT deficient $APC^{Min/+}$ mice compared to iNKT proficient $APC^{Min/+}$ [139]. In the inflammation-driven AOM/DSS murine model of CRC we observed that tumor-infiltrating iNKT cells have the same pro-inflammatory phenotype observed in patients (Section3.5.2) and that TANs infiltration is dependent on iNKT cells. In wild-type animals, iNKT cells infiltration in tumors preceded the one of neutrophils and we hypothesized a similar situation happening in patients, since iNKT cells and neutrophils infiltration followed the TNM staging in our cohort.

Lack of iNKT cells *in vivo* reduced TANs infiltration and limited tumor growth (Section3.5.3). TANs abundance positively correlates with tumor burden in wild-type mice but not in iNKT deficient ones, suggesting iNKT cells could influence tumor properties of neutrophils. Indeed, iNKT cells did not only affect TANs abundance but profoundly altered their gene expression profile. *Traj18$^{-/-}$* TANs expressed a classical PMN-MDSCs gene signature opposed to wild-type TANs that showed an "activated" PMN-MDSC signature (Section3.5.4). PMN-MDSC are pathologically activated PMNs characterized by immunosuppressive properties and pro-tumorigenic activities [209]. We observed that, wild-type TANs expressed inflammation-related, immune regulatory and effector genes (*i.e. Ccl3, Cxcl2, Socs3, Atf4, Il10, S100a8* and *Junb*) which are typical of functional PMN-MDSC, while *Traj18$^{-/-}$* TANs were associated to more classical PMN-MDSC which are hypothesized to generate in different environments [209]. The diversity of TANs in wild-type and iNKT deficient animals was observed also by flow cytometry analysis, since we detected different populations of neutrophils according to Ly6G and PD-L1 expression (Section3.5.4).

We further dissected the iNKT-neutrophil axis in two additional murine model of CRC. We assessed the relevance of iNKT cells for tumor progression in an inflammation-independent model of CRC, using the syngeneic MC38 CRC model (Section3.6). Indeed, subcutaneous implantation of MC38 cells in wild-type animals led to higher tumor growth and TANs infiltration compared to subcutaneous implantation in iNKT-deficient *Traj18*$^{-/-}$ mice (Section3.6.1), supporting the role for iNKT cells in driving tumorigenesis, independently of inflammation.

Since we addressed the role of the CRC-associated pathobiont *F.nucleatum* in shaping the tumor phenotype of iNKT cells *in vitro*, we aimed to assess the influence of the CRC-associated microbiota also *in vivo*. We adopted an orthotopic model of intracecal MC38 implantation that was previously used to describe gut microbiota manipulation of T cell trafficking into CRC [219]. We observed that iNKT cells infiltrating intracecal tumor expressed a marked Th17-phenotype compared to splenic iNKT cells and to iNKT cells infiltrating subcutaneous tumor (Section3.6.2), suggesting that the gut microbiota play a relevant role in shaping the iNKT cell phenotype.

Contrasting findings are reported in literature concerning the ability of iNKT cells to shape and to be shaped by the gut microbiota are reported in literature [220], [221]. We observed there was a significant β-diversity in the microbiota composition of AOM/DSS treated iNKT proficient and deficient mice. Thus, we tested the effect of the microbiota of AOM/DSS treated *CD1d*$^{-/-}$, *Traj18*$^{-/-}$ and wild-type mice on iNKT cells and observed that CRC-associated microbiota induced GM-CSF and IL17 and reduced IFNγ expression, independently of the strain of origin (Section3.7).

We have shown that the absence of iNKT cells is associated with worsening of the disease in several murine models of CRC (Section3.5). In human, a previous study proposed beneficial, prognostic roles for iNKT cells in CRC [12]. However, in that report iNKT cells were identified by immunohistochemistry with a TCR-Vα24 antibody, which is an approach with low sensitivity and specificity for the detection of iNKT cells. Conversely, more recent works identified iNKT cells as inducer of intestinal polyposis in mice [139] and circulating NKT-like cells as negative prognostic factor in human CRC [154]. We demonstrated that in our CRC cohort infiltration of iNKT cells is an independent negative prognostic factor for patients' survival, which is not affected by age, gender, MMR status, size of primary tumor (T), involvement of regional lymph nodes (N), tumor grading (G) and tumor location (Section3.8.1). Neutrophils infiltration is instead considered a positive prognostic factor in human CRC [69]–[71]. Nevertheless, our *in vitro* and *in vivo*

experiments showed that neutrophils have pro-tumorigenic functions but dependent on iNKT cell activity.

Survival analysis of our study cohort showed that TANs infiltration correlates with positive prognosis. However, in patients with high TANs infiltration we observed that the survival probability was significantly decreased with iNKT cells infiltration (Section3.8.1). We validated these observations using an external cohort, the COAD-TCGA dataset, and proved that high *CEACAM8* expression, the gene encoding for the neutrophil marker CD66b, is a positive prognostic factor in CRC, whereas its combination with the expression of *ZBTB16*, the gene encoding for the iNKT master regulator PLZF, is associated with unfavorable prognosis (Section3.8.2). Although we are aware that gene expression is not directly proportional to protein translation and that PLZF is expressed also by other unconventional T cells, this is the first evidence validating in two independent cohorts that iNKT cells can be associated with negative prognosis in CRC through their effect on TANs. To overcome these limitations, we tried to perform transcriptome deconvolution of TCGA data and to estimate tumor infiltrating iNKT and neutrophil percentages using available tools such as CIBERSORT [222], [223], however the accuracy of these analysis depend on predefined cell signatures, cell profiles and of technical biases [222]–[225]. To the best of our knowledge there is not yet a defined gene signature for iNKT cells identification, thus limiting the possibility to apply deconvolution tools to single-cell or bulk-RNA sequencing data.

Although we have shown that iNKT cells have a pro-tumorigenic role in CRC, their anti-tumor activities associated with their release of IFNγ, their production of lytic granules and their expression of death ligands have been described in many experimental and preclinical studies [11], [14], [15], [151]. The vast majority of these studies have been performed *in vivo* upon αGalCer activation and functional skewing of iNKT cells [11]. Indeed, *in vivo* administration of αGalCer promotes iNKT cells cytotoxicity in different pathological setting. αGalCer-loaded B cells were killed by iNKT cells through Fas/FasL interaction [155]. Interestingly, we observed that tumor-infiltrating iNKT cells reduced FasL expression in our CRC cohort (Section3.1.3), while tumor cells did not showed a concomitant change of Fas expression (Section3.1.7). Nonetheless, the major mechanism of iNKT cell-mediated tumor protection is the potent release of anti-tumor cytokines, such as IFNγ [11]. However, stimulation of iNKT cells with the analog, β-mannosylceramide (β-ManCer) was shown to protect mice from lung metastasis in an IFNγ independent manner [226]. The treatment reduced tumor growth by inducing iNKT

cell production of TNFα, nitric oxide synthase (NOS) and by preventing their anergy [226]. Nevertheless, it is widely accepted that TNFα in the context of CRC is a pro-tumorigenic cytokine, rather than an anti-tumorigenic one [4], while IFNγ has clear anti-tumorigenic properties [75]–[77]. We observed that both human and murine iNKT cells decreased the expression of IFNγ in CRC lesions (Section3.1.2), diminishing their anti-tumorigenic potential. However, we could re-activate iNKT cells *in vivo* by treating tumor bearing mice with αGalCer. Treatment induced potent upregulation of IFNγ, in two independent model of CRC, by tumor infiltrating iNKT cells and led to control of tumor growth (Section3.6).

iNKT cells are currently under study for their use in cancer immunotherapy [155], [185] and treatment with αGalCer or vaccination with αGalCer-loaded DCs showed positive results in preclinical models of melanoma, pancreatic and intestinal cancers [185]. However, αGalCer treatment gave only suboptimal responses in clinical trials since it induces long-lasting anergy on iNKT cells [186]. Thus, novel approaches to exploit iNKT cell properties, such as TCR-engineered iNKT cells, CAR-iNKT cells and targeted microbiota stimulation to avoid iNKT cells anergy are now emerging [183].

5 Conclusions and Perspectives

Collectively, our study reveals opposites, pro-tumorigenic and anti-tumorigenic roles for iNKT cells in colon cancer. For the first time we examined the phenotype of tumor-infiltrating iNKT cells in human CRC, validating it in different murine CRC models, and identified a functional axis with tumor associated neutrophils, that can influence the evolution of the disease. We elucidated cellular and molecular mechanisms by which iNKT cells and TANs affect CRC developmental trajectory and suggest the involvement of the tumor microenvironment, specifically the gut microbiota, in shaping iNKT cell phenotype.

We observed that tumor-infiltrating iNKT cells have a pro-tumorigenic cytokines profile, characterized by the expression of GM-CSF and IL17, while they maintained cytotoxic properties in the adjacent non-tumor mucosa. Tumor-like iNKT cells can be generated *in vitro* upon stimulation with the CRC-associated pathobiont *Fusobacterium nucleatum* and induced neutrophils recruitment, survival and immunosuppression. *In vivo* treatment with the iNKT ligand αGalCer restored the cytotoxic capabilities of iNKT cells and induced iNKT cell mediated tumor control.

Based on the results obtained in this work we propose the following working model (Figure 5.1) describing the anti-tumorigenic and the pro-tumorigenic functional roles of iNKT cells in CRC immunity:

I)   During CRC progression, iNKT cells infiltrate the tumor and lose their cytotoxic capabilities. iNKT cells are shaped by the tumor mucosal microbiota, specifically by *Fusobacterium nucleatum,* to express GM-CSF, IL17 and IL8. These cytokines induce TANs recruitment and functional skewing toward an immunosuppressive phenotype, causing tumor immune evasion and leading to enhanced tumor growth.

II)   Upon stimulation with αGalCer, iNKT cells upregulate a cytotoxic gene signature and express IFNγ showing direct anti-tumorigenic properties. Concomitantly, TANs express tumor degrading molecules and inflammatory molecules., ultimately limiting tumor development
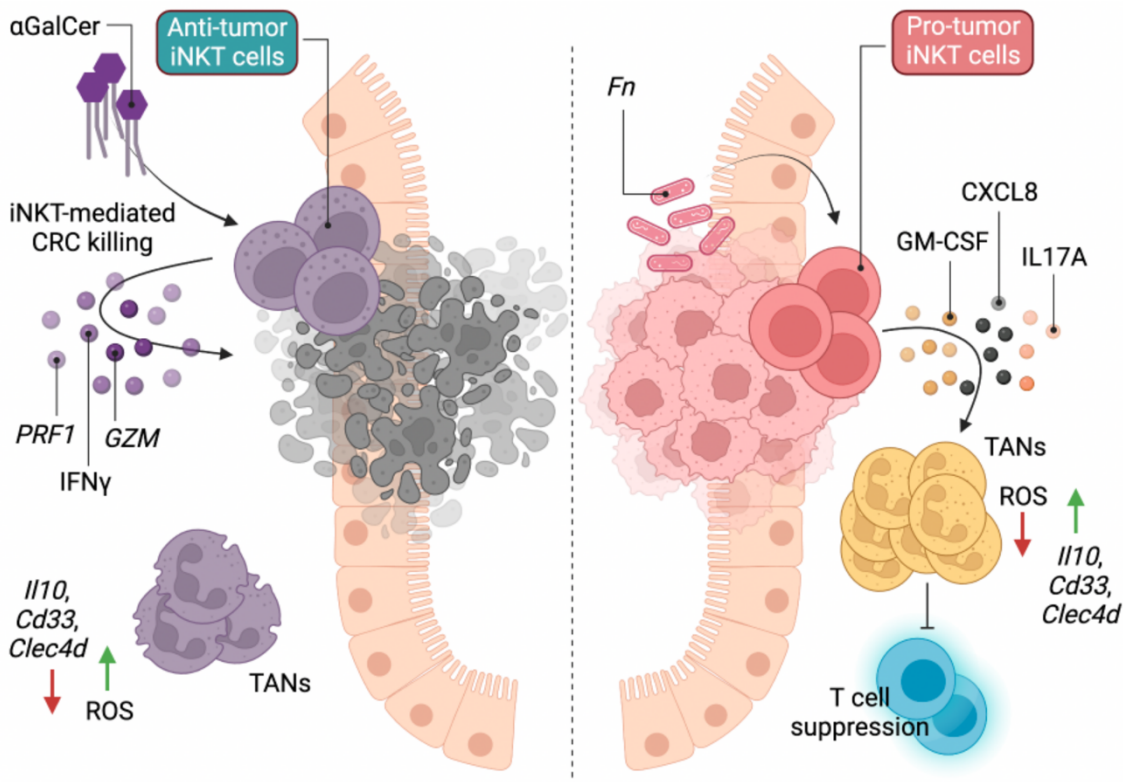
Figure 5.1: *Schematic model of iNKT cells mediated pro and antitumor immunity in CRC. αGalCer restores the cytotoxic properties of iNKT cells leading to tumor control (left side), while the CRC-associated pathobiont Fusobacterium nucleatum (Fn) induces expression of GM-CSF, CXCL8 and IL17 on iNKT cells, which in turn recruit TANs and induce their T-cell immunosuppressive functions. This figure was created with BioRender.com.*

In this study we highlighted how tumor-associated microbiota can skew pro-tumorigenic properties of iNKT cells, ultimately affecting tumor growth. Given the pleiotropic responses of iNKT cells to different microbiota composition [9], [166], we propose that manipulation of the microbiota can be exploited to design novel cellular therapies in CRC. Indeed, it is already known that the abundance of some commensal bacterial species correlates with good response to immunotherapies in melanoma patients [181]. *Bifidobacterium longum, Collinsella aerofaciens, and Enterococcus faecium* are associated to favorable responses to anti-PD-1 therapy [227], [228], whereas the antitumor effect of CTLA-4 blockade is dependent on distinct *Bacteroides* species [229]. Although these bacterial strains and more generally patients' microbiota composition influence the outcome of immunotherapies, their direct effect on specialized subsets of T cells, such as iNKT cells, has never been tested. Thus, future experiments dissecting the inhibition/stimulation of iNKT cells with patients' derived microbiota could be used to understand mechanisms by which the microbiota blunt cytotoxic immune responses. This

will lead to the formulation of microbiota-dependent new line of interventions to correct patients' immune abnormalities.

Additionally, iNKT cells are promising candidates for cellular immunotherapies, mainly due to their low toxicity and their low risk of alloreaction [155]. CAR-iNKT and TCR-engineered iNKT cells showed promising results in the treatment of both, liquid and solid tumors *in vivo* [193]. TCR-engineered iNKT cells migrate well into solid tumors [193], which is a major limitation for this type of therapy, suggesting that iNKT cells could be harnessed for successful adoptive cell therapy. TCR-engineered iNKT cells are able to target directly cancer cells, mainly due to the engineered TCR, but they are also capable of targeting suppressive myeloid cells [155], [193]. Accordingly, we have identified a functional axis between iNKT cells and tumor associated neutrophils, in colon cancer. However, we found that tumor iNKT cells induce immunosuppressive properties on tumor associated neutrophils, promoting immune evasion and carcinogenesis. The functional behaviors of tumor iNKT cells can be driven by the tumor associated microbiota, thus we suggest that microbiota composition should be taken in account in the formulation of novel adoptive cell therapies with iNKT cells. Investigating possible microbial ligands and bacteria derived antigens will certainly push this research field forward, and it will help in designing rationale iNKT cell therapies.

Bibliography

[1]   L. Rahib, M. R. Wehner, L. M. Matrisian, and K. T. Nead, 'Estimated Projection of US Cancer Incidence and Death to 2040', *JAMA Netw Open*, vol. 4, no. 4, pp. 1–14, 2021, doi: 10.1001/jamanetworkopen.2021.4708.

[2]   F. R. Greten and S. I. Grivennikov, 'Inflammation and Cancer: Triggers, Mechanisms, and Consequences', *Immunity*, vol. 51, pp. 27–41, 2019.

[3]   M. Schmitt and F. R. Greten, 'The inflammatory pathogenesis of colorectal cancer', *Nat Rev Immunol*, vol. 21, no. 10, pp. 653–667, 2021, doi: 10.1038/s41577-021-00534-x.

[4]   N. R. West, S. Mccuaig, F. Franchini, and F. Powrie, 'Emerging cytokine networks in colorectal cancer', *Nat Rev Immunol*, vol. 15, no. 10, pp. 615–629, 2015, doi: 10.1038/nri3896.

[5]   R. Okumura and K. Takeda, 'Maintenance of gut homeostasis by the mucosal immune system', *Proc Jpn Acad Ser B Phys Biol Sci*, vol. 92, no. 9, pp. 423–435, 2016, doi: 10.2183/pjab.92.423.

[6]   J. Chen, E. Pitmon, and K. Wang, 'Microbiome, inflammation and colorectal cancer', *Semin Immunol*, vol. 32, no. October, pp. 43–53, 2017, doi: 10.1016/j.smim.2017.09.006.

[7]   A. Bendelac, P. B. Savage, and L. Teyton, 'The Biology of NKT Cells', *Annu Rev Immunol*, vol. 25, no. 1, pp. 297–336, 2007, doi: 10.1146/annurev.immunol.25.022106.141711.

[8]   C. M. Crosby and M. Kronenberg, 'Tissue-specific functions of invariant natural killer T cells', *Nat Rev Immunol*, vol. 18, no. 9, pp. 559–574, 2018, doi: 10.1038/s41577-018-0034-2.

[9]   C. Burrello *et al.*, 'IL10 secretion endows intestinal human iNKT cells with regulatory functions towards pathogenic T lymphocytes in Crohn's disease patients', *J Crohns Colitis*, vol. 16, pp. 1–14, 2022, doi: 10.1093/ecco-jcc/jjab232.235.

[10]   S. Vogt and J. Mattner, 'NKT Cells Contribute to the Control of Microbial Infections', *Front Cell Infect Microbiol*, vol. 11, no. September, pp. 1–12, 2021, doi: 10.3389/fcimb.2021.718350.

[11]   H. Zhang, J. Nguyen, M. Pham, and A. Smith, 'iNKT cell modulation of tumor microenvironment (TME) and antitumor immunity: the role of antitumorigenic and protumorigenic iNKT cells', *The Journal of Immunology*, vol. 204, no. 88.3, 2020.

[12]   T. Tachibana *et al.*, 'Increased intratumor Vα24-positive natural killer T cells: A prognostic factor for primary colorectal carcinomas', *Clinical Cancer Research*, vol. 11, no. 20, pp. 7322–7327, 2005, doi: 10.1158/1078-0432.CCR-05-0877.

[13]   Y. Wang, *Natural killer T (NKT) lymphocytes regulate intestinal tumor immunity*. 2017. [Online]. Available: https://gupea.ub.gu.se/bitstream/2077/52418/1/gupea_2077_52418_1.pdf

[14]   Y. Wang, S. K. Sedimbi, L. Löfbom, G. S. Besra, S. A. Porcelli, and S. L. Cardell, 'Promotion or suppression of murine intestinal polyp development by iNKT cell directed immunotherapy', *Front Immunol*, vol. 10, no. MAR, pp. 1–15, 2019, doi: 10.3389/fimmu.2019.00352.

[15]   M. Terabe and J. A. Berzofsky, 'Tissue-Specific Roles of NKT Cells in Tumor Immunity', *Front Immunol*, vol. 9, 2018, doi: 10.3389/fimmu.2018.01838.

[16]   R. Siegel, K. Miller, and A. Jemal, 'Cancer Statistics, 2019', *CA Cancer J Clin*, vol. 69, no. 1, pp. 7–34, 2019.

[17] Q. Hong *et al.*, 'Transcriptomic Analyses of the Adenoma-Carcinoma Sequence Identify Hallmarks Associated With the Onset of Colorectal Cancer', *Front Oncol*, vol. 11, no. August, pp. 1–18, 2021, doi: 10.3389/fonc.2021.704531.

[18] A. Walther, E. Johnstone, C. Swanton, R. Midgley, I. Tomlinson, and D. Kerr, 'Genetic prognostic and predictive markers in colorectal cancer', *Nat Rev Cancer*, vol. 9, no. 7, pp. 489–499, 2009, doi: 10.1038/nrc2645.

[19] S. H. Lin *et al.*, 'The somatic mutation landscape of premalignant colorectal adenoma', *Gut*, vol. 67, no. 7, pp. 1299–1305, 2018, doi: 10.1136/gutjnl-2016-313573.

[20] A. R. Moser, H. C. Pitot, and W. F. Dove, 'A dominant mutation that predisposes to multiple intestinal neoplasia in the mouse', *Science (1979)*, no. 4940, pp. 247–322, 1990.

[21] R. Jackstadt and O. J. Sansom, 'Mouse models of intestinal cancer', *Journal of Pathology*, vol. 238, no. 2, pp. 141–151, 2016, doi: 10.1002/path.4645.

[22] E. M. Stoffel and F. Kastrinos, 'Familial colorectal cancer, beyond lynch syndrome', *Clinical Gastroenterology and Hepatology*, vol. 12, no. 7, pp. 1059–1068, 2014, doi: 10.1016/j.cgh.2013.08.015.

[23] T. Ried *et al.*, 'The landscape of genomic copy number alterations in colorectal cancer and their consequences on gene expression levels and disease outcome', *Mol Aspects Med*, vol. 69, no. July, pp. 48–61, 2019, doi: 10.1016/j.mam.2019.07.007.

[24] G. della Chiara *et al.*, 'Epigenomic landscape of human colorectal cancer unveils an aberrant core of pan-cancer enhancers orchestrated by YAP/TAZ', *Nat Commun*, vol. 12, no. 1, 2021, doi: 10.1038/s41467-021-22544-y.

[25] Y. Chen, X. Zheng, and C. Wu, 'The Role of the Tumor Microenvironment and Treatment Strategies in Colorectal Cancer', *Front Immunol*, vol. 12, no. December, pp. 1–21, 2021, doi: 10.3389/fimmu.2021.792691.

[26] N. M. Anderson and C. M. Simon, 'The tumor microenvironment', *Current Biology, PRIMER*, vol. 30, no. 16, pp. 921–925, 2020.

[27] P. I. Franco Ribeiro, A. Rodrigues Perillo, L. Borges de Menezes, and M. Miguel Pacheco, 'Tumor microenvironment components: Allies of cancer progression', *Pathol Res Pract*, vol. 216, no. 1, 2020.

[28] S. Galland and I. Stamenkovic, 'Mesenchymal stromal cells in cancer: a review of their immunomodulatory functions and dual effects on tumor progression', *Journal of Pathology*, vol. 250, no. 5, pp. 555–572, 2020, doi: 10.1002/path.5357.

[29] J. Winkler, A. Abisoye-Ogunniyan, K. J. Metcalf, and Z. Werb, 'Concepts of extracellular matrix remodelling in tumour progression and metastasis', *Nat Commun*, vol. 11, no. 1, pp. 1–19, 2020, doi: 10.1038/s41467-020-18794-x.

[30] M. Damaghi, J. W. Wojtkowiak, and R. J. Gillies, 'pH sensing and regulation in cancer', *Front Physiol*, vol. 4 DEC, no. December, pp. 1–10, 2013, doi: 10.3389/fphys.2013.00370.

[31] W. S. Garrett, 'The gut microbiota and colon cancer', *Science (1979)*, vol. 364, no. 6446, pp. 1133–1135, 2019, doi: 10.1126/science.aaw2367.

[32] N. Cullin, C. Azevedo Antunes, R. Straussman, C. K. Stein-Thoeringer, and E. Elinav, 'Microbiome and cancer', *Cancer Cell*, vol. 39, no. 10, pp. 1317–1341, 2021, doi: 10.1016/j.ccell.2021.08.006.

[33] G. Bergers *et al.*, 'Matrix metalloproteinase-9 triggers the angiogenic switch during carcinogenesis', *Nat Cell Biol*, vol. 2, no. 10, pp. 737–744, 2000, doi: 10.1038/35036374.

[34] J. Yang *et al.*, 'Guidelines and definitions for research on epithelial–mesenchymal transition', *Nat Rev Mol Cell Biol*, vol. 21, no. 6, pp. 341–352, 2020, doi: 10.1038/s41580-020-0237-9.

[35] Z. Zhang *et al.*, 'Genomics and prognosis analysis of epithelial-mesenchymal transition in colorectal cancer patients', *BMC Cancer*, vol. 20, no. 1, pp. 1–12, 2020, doi: 10.1186/s12885-020-07615-5.

[36] D. M. Gilkes, G. L. Semenza, and D. Wirtz, 'Hypoxia and the extracellular matrix: Drivers of tumour metastasis', *Nat Rev Cancer*, vol. 14, no. 6, pp. 430–439, 2014, doi: 10.1038/nrc3726.

[37] R. T. Netea-Maier, J. W. A. Smit, and M. G. Netea, 'Metabolic changes in tumor cells and tumor-associated macrophages: A mutual relationship', *Cancer Lett*, vol. 413, pp. 102–109, 2018, doi: 10.1016/j.canlet.2017.10.037.

[38] X. Zhong *et al.*, 'Warburg effect in colorectal cancer: the emerging roles in tumor microenvironment and therapeutic implications', *J Hematol Oncol*, vol. 15, no. 1, pp. 1–29, 2022, doi: 10.1186/s13045-022-01358-5.

[39] C. Schiliro and B. L. Firestein, 'Mechanisms of metabolic reprogramming in cancer cells supporting enhanced growth and proliferation', *Cells*, vol. 10, no. 5, pp. 1–41, 2021, doi: 10.3390/cells10051056.

[40] C. J. Tape, 'The Heterocellular Emergence of Colorectal Cancer', *Trends Cancer*, vol. 3, no. 2, pp. 79–88, 2017.

[41] B. Zhong *et al.*, 'Colorectal cancer-associated fibroblasts promote metastasis by up-regulating LRG1 through stromal IL-6/STAT3 signaling', *Cell Death Dis*, vol. 13, no. 1, 2022, doi: 10.1038/s41419-021-04461-6.

[42] A. Calon *et al.*, 'Dependency of Colorectal Cancer on a TGF-β-Driven Program in Stromal Cells for Metastasis Initiation', *Cancer Cell*, vol. 22, no. 5, pp. 571–584, 2012, doi: 10.1016/j.ccr.2012.08.013.

[43] J. A. Joyce and D. T. Fearon, 'T cell exclusion, immune privilege, and the tumor microenvironment', *Cancer Immunology, Immunotherapy*, vol. 348, no. 6230, pp. 74–79, 2015.

[44] N. A. Leonard *et al.*, 'Stromal cells promote matrix deposition, remodelling and an immunosuppressive tumour microenvironment in a 3d model of colon cancer', *Cancers (Basel)*, vol. 13, no. 23, 2021, doi: 10.3390/cancers13235998.

[45] Ö. Canli *et al.*, 'Myeloid Cell-Derived Reactive Oxygen Species Induce Epithelial Mutagenesis', *Cancer Cell*, vol. 32, no. 6, pp. 869-883.e5, 2017, doi: 10.1016/j.ccell.2017.11.004.

[46] S. I. Grivennikov, 'Inflammation and colorectal cancer: colitis-associated neoplasia', *Semin Immunopathol*, vol. 35, no. 2, pp. 229–244, 2013, doi: 10.1007/s00281-012-0352-6.Inflammation.

[47] F. Colotta, P. Allavena, A. Sica, C. Garlanda, and A. Mantovani, 'Cancer-related inflammation, the seventh hallmark of cancer: links to genetic instability', *Carcinogenesis*, vol. 30, no. 7, pp. 1073–1081, 2009.

[48] R. Nowarski, N. Gagliani, S. Huber, and R. A. Flavell, 'Innate immune cells in inflammation and cancer', *Cancer Immunol Res*, vol. 1, no. 2, pp. 77–84, 2013, doi: 10.1158/2326-6066.CIR-13-0081.

[49] M. Schmitt *et al.*, 'Paneth Cells Respond to Inflammation and Contribute to Tissue Regeneration by Acquiring Stem-like Features through SCF/c-Kit Signaling', *Cell Rep*, vol. 24, no. 9, pp. 2312–2328, 2018.

[50] M. Ernst *et al.*, 'STAT3 and STAT1 mediate IL-11-dependent and inflammation-associated gastric tumorigenesis in gp130 receptor mutant mice', *Journal of Clinical Investigation*, vol. 118, no. 5, pp. 1727–1738, 2008, doi: 10.1172/JCI34944.

[51] T. L. Putoczki *et al.*, 'Interleukin-11 is the dominant Il-6 family cytokine during gastrointestinal tumorigenesis and can be targeted therapeutically', *Cancer Cell*, vol. 24, no. 2, pp. 257–271, 2013, doi: 10.1016/j.ccr.2013.06.017.

[52] J. Li *et al.*, 'Temporal DNA methylation pattern and targeted therapy in colitis-Associated cancer', *Carcinogenesis*, vol. 41, no. 2, pp. 235–244, 2020, doi: 10.1093/carcin/bgz199.

[53] E. Foran *et al.*, 'Upregulation of DNA methyltransferase - mediated gene silencing, anchorage-independent growth, and migration of colon cancer cells by interleukin-6', *Molecular Cancer Research*, vol. 8, no. 4, pp. 471–481, 2010, doi: 10.1158/1541-7786.MCR-09-0496.

[54] S. Tseng-Rogenski, Y. Hamaya, D. Y. Choi, and J. M. Carethers, 'Interleukin 6 Alters Localization of hMSH3, Leading to DNA Mismatch Repair Defects in Colorectal Cancer Cells', *Gastroenterology*, vol. 148, no. 3, pp. 579–589, 2015, doi: 10.1016/S0959-437X(00)00066-6.

[55] S. Wu *et al.*, 'A human colonic commensal promotes colon tumorigenesis via activation of T helper type 17 T cell responses', *Nat Med*, vol. 15, no. 9, pp. 1016–1022, 2009, doi: 10.1038/nm.2015.A.

[56] W. J. Chae, T. F. Gibson, D. Zelterman, L. Hao, O. Henegariu, and A. L. M. Bothwell, 'Ablation of IL-17A abrogates progression of spontaneous intestinal tumorigenesis', *Proc Natl Acad Sci U S A*, vol. 107, no. 12, pp. 5540–5544, 2010, doi: 10.1073/pnas.0912675107.

[57] R. Sugimura and Y. Chao, 'Deciphering Innate Immune Cell-Tumor Microenvironment Crosstalk at a Single-Cell Level', *Front Cell Dev Biol*, vol. 10, no. May, pp. 1–17, 2022, doi: 10.3389/fcell.2022.803947.

[58] M. della Chiesa *et al.*, 'NK Cell-Based Immunotherapy in Colorectal Cancer', pp. 1–20, 2022.

[59] G. Pietropaolo *et al.*, 'NK cell and ILC heterogeneity in colorectal cancer. New perspectives from high dimensional data', *Mol Aspects Med*, vol. 80, no. May, 2021, doi: 10.1016/j.mam.2021.100967.

[60] J. N. Kather and N. Halama, 'Harnessing the innate immune system and local immunological microenvironment to treat colorectal cancer', *Br J Cancer*, vol. 120, no. 9, pp. 871–882, 2019, doi: 10.1038/s41416-019-0441-6.

[61] A. Mantovani, P. Allavena, F. Marchesi, and C. Garlanda, 'Macrophages as tools and targets in cancer therapy', *Nat Rev Drug Discov*, vol. 21, no. 11, pp. 799–820, 2022, doi: 10.1038/s41573-022-00520-5.

[62] D. Gabrilovich *et al.*, 'The terminology issue for myeloid-derived suppressor cells', *Cancer Res*, vol. 67, no. 1, pp. 425–426, 2007, [Online]. Available: https://www.ncbi.nlm.nih.gov/pmc/articles/PMC3624763/pdf/nihms412728.pdf

[63] F. Veglia, E. Sanseviero, and D. I. Gabrilovich, 'Myeloid-derived suppressor cells in the era of increasing myeloid cell diversity', *Nat Rev Immunol*, vol. 21, no. 8, pp. 485–498, 2021, doi: 10.1038/s41577-020-00490-y.

[64] C. C. Hedrick and I. Malanchi, 'Neutrophils in cancer: heterogeneous and multifaceted', *Nat Rev Immunol*, vol. 22, no. 3, pp. 173–187, 2022, doi: 10.1038/s41577-021-00571-6.

[65] S. K. Wculek, V. L. Bridgeman, F. Peakman, and I. Malanchi, 'Early Neutrophil Responses to Chemical Carcinogenesis Shape Long-Term Lung Cancer Susceptibility', *iScience*, vol. 23, no. 7, p. 101277, 2020, doi: 10.1016/j.isci.2020.101277.

[66] T. T. Wang *et al.*, 'Tumour-activated neutrophils in gastric cancer foster immune suppression and disease progression through GM-CSF-PD-L1 pathway', *Gut*, vol. 66, no. 11, pp. 1900–1911, 2017, doi: 10.1136/gutjnl-2016-313075.

[67] Á. Teijeira *et al.*, 'CXCR1 and CXCR2 Chemokine Receptor Agonists Produced by Tumors Induce Neutrophil Extracellular Traps that Interfere with Immune Cytotoxicity', *Immunity*, vol. 52, no. 5, pp. 856-871.e8, 2020, doi: 10.1016/j.immuni.2020.03.001.

[68] M. Siwicki and M. J. Pittet, 'Versatile neutrophil functions in cancer', *Semin Immunol*, vol. 57, no. August, p. 101538, 2021, doi: 10.1016/j.smim.2021.101538.

[69] V. Governa *et al.*, 'The interplay between neutrophils and CD8+ T cells improves survival in human colorectal cancer', *Clinical Cancer Research*, vol. 23, no. 14, pp. 3847–3858, 2017, doi: 10.1158/1078-0432.CCR-16-2047.

[70] R. Mizuno, K. Kawada, Y. Itatani, R. Ogawa, Y. Kiyasu, and Y. Sakai, 'The role of tumor-associated neutrophils in colorectal cancer', *Int J Mol Sci*, vol. 20, no. 3, pp. 1–14, 2019, doi: 10.3390/ijms20030529.

[71] M. R. Galdiero *et al.*, 'Occurrence and significance of tumor-associated neutrophils in patients with colorectal', *Int J Cancer*, 2016.

[72] S. Jaillon, A. Ponzetta, D. di Mitri, A. Santoni, R. Bonecchi, and A. Mantovani, 'Neutrophil diversity and plasticity in tumour progression and therapy', *Nat Rev Cancer*, no. 20, pp. 485–503, 2020.

[73] M. Tosolini *et al.*, 'Clinical impact of different classes of infiltrating T cytotoxic and helper cells (Th1, Th2, Treg, Th17) in patients with colorectal cancer', *Cancer Res*, vol. 71, no. 4, pp. 1263–1271, 2011, doi: 10.1158/0008-5472.CAN-10-2907.

[74] H. Raskov, A. Orhan, J. P. Christensen, and I. Gögenur, 'Cytotoxic CD8+ T cells in cancer and cancer immunotherapy', *Br J Cancer*, vol. 124, no. 2, pp. 359–367, 2021, doi: 10.1038/s41416-020-01048-4.

[75] A. M. Gocher, C. J. Workman, and D. A. A. Vignali, 'Interferon-γ: teammate or opponent in the tumour microenvironment?', *Nat Rev Immunol*, vol. 22, no. 3, pp. 158–172, 2022, doi: 10.1038/s41577-021-00566-3.

[76] K. P. Kotredes and A. M. Gamero, 'Interferons as inducers of apoptosis in malignant cells', *Journal of Interferon and Cytokine Research*, vol. 33, no. 4, pp. 162–170, 2013, doi: 10.1089/jir.2012.0110.

[77] P. Bhat, G. Leggatt, N. Waterhouse, and I. H. Frazer, 'Interferon-γ derived from cytotoxic lymphocytes directly enhances their motility and cytotoxicity', *Cell Death Dis*, vol. 8, no. 6, pp. 1–11, 2017, doi: 10.1038/CDDIS.2017.67.

[78] E. Müller *et al.*, 'Toll-like receptor ligands and interferon-γ synergize for induction of antitumor M1 macrophages', *Front Immunol*, vol. 8, no. OCT, 2017, doi: 10.3389/fimmu.2017.01383.

[79] S. Paul, S. Chhatar, A. Mishra, and G. Lal, 'Natural killer T cell activation increases iNOS+CD206- M1 macrophage and controls the growth of solid tumor', *J Immunother Cancer*, vol. 7, no. 1, pp. 1–13, 2019, doi: 10.1186/s40425-019-0697-7.

[80] G. Plitas and A. Y. Rudensky, 'Regulatory T Cells in Cancer', *Annu Rev Cancer Biol*, vol. 4, pp. 459–477, 2020, doi: 10.1146/annurev-cancerbio-030419-033428.

[81] R. J. P. Bonnal *et al.*, 'Clonally expanded EOMES+ Tr1-like cells in primary and metastatic tumors are associated with disease progression', *Nat Immunol*, vol. 22, no. 6, pp. 735–745, 2021, doi: 10.1038/s41590-021-00930-4.

[82] M. de Simone *et al.*, 'Transcriptional Landscape of Human Tissue Lymphocytes Unveils Uniqueness of Tumor-Infiltrating T Regulatory Cells', *Immunity*, vol. 45, no. 5, pp. 1135–1147, 2016, doi: 10.1016/j.immuni.2016.10.021.

[83] P. Gruarin *et al.*, 'Eomesodermin controls a unique differentiation program in human IL-10 and IFN-γ coproducing regulatory T cells', *Eur J Immunol*, vol. 49, no. 1, pp. 96–111, 2019, doi: 10.1002/eji.201847722.

[84] K. Gronke *et al.*, 'Interleukin-22 protects intestinal stem cells against genotoxic stress', *Nature*, vol. 566, no. 7743, pp. 249–253, 2019, doi: 10.1038/s41586-019-0899-7.

[85] L. I. Ruffolo *et al.*, 'GM-CSF drives myelopoiesis, recruitment and polarisation of tumour-associated macrophages in cholangiocarcinoma and systemic blockade

facilitates antitumour immunity', *Gut*, vol. 71, no. 7, pp. 1386–1398, 2022, doi: 10.1136/gutjnl-2021-324109.

[86] G. LeBlanc, F. K. Kreissl, J. Melamed, A. L. Sobel, and M. G. Constantinides, 'The role of unconventional T cells in maintaining tissue homeostasis', *Semin Immunol*, vol. 61–64, no. July, p. 101656, 2022, doi: 10.1016/j.smim.2022.101656.

[87] D. I. Godfrey, A. P. Uldrich, J. Mccluskey, J. Rossjohn, and D. B. Moody, 'The burgeoning family of unconventional T cells', *Nat Immunol*, vol. 16, no. 11, pp. 1114–1124, 2015, doi: 10.1038/ni.3298.1114.

[88] M. G. Constantinides and Y. Belkaid, 'Early-life imprinting of unconventional T cells and tissue homeostasis', *Science (1979)*, vol. 374, no. 6573, 2021, doi: 10.1126/science.abf0095.

[89] T. Baranek, C. de Amat Herbozo, T. Mallevaey, and C. Paget, 'Deconstructing iNKT cell development at single-cell resolution', *Trends Immunol*, vol. 43, no. 7, pp. 503–512, 2022, doi: 10.1016/j.it.2022.04.012.

[90] Q. Lin, M. Kuypers, D. J. Philpott, and T. Mallevaey, 'The dialogue between unconventional T cells and the microbiota', *Mucosal Immunol*, vol. 13, no. 6, pp. 867–876, 2020, doi: 10.1038/s41385-020-0326-2.

[91] D. I. Godfrey, J. le Nours, D. M. Andrews, A. P. Uldrich, and J. Rossjohn, 'Unconventional T Cell Targets for Cancer Immunotherapy', *Immunity*, vol. 48, no. 3, pp. 453–473, 2018, doi: 10.1016/j.immuni.2018.03.009.

[92] M. Shiroishi *et al.*, 'Human inhibitory receptors Ig-like transcript 2 (ILT2) and ILT4 compete with CD8 for MHC class I binding and bind preferentially to HLA-G', *Proc Natl Acad Sci U S A*, vol. 100, no. 15, pp. 8856–8861, 2003, doi: 10.1073/pnas.1431057100.

[93] M. Swets *et al.*, 'HLA-G and classical HLA class I expression in primary colorectal cancer and associated liver metastases', *Hum Immunol*, vol. 77, no. 9, pp. 773–779, 2016, doi: 10.1016/j.humimm.2016.03.001.

[94] S. M. M. Haeryfar, C. R. Shaler, and P. T. Rudak, 'Mucosa-associated invariant T cells in malignancies: a faithful friend or formidable foe?', *Cancer Immunology, Immunotherapy*, vol. 67, no. 12, pp. 1885–1896, 2018, doi: 10.1007/s00262-018-2132-1.

[95] C. R. Shaler *et al.*, 'Mucosa-associated invariant T cells infiltrate hepatic metastases in patients with colorectal carcinoma but are rendered dysfunctional within and adjacent to tumor microenvironment', *Cancer Immunology, Immunotherapy*, vol. 66, no. 12, pp. 1563–1575, 2017, doi: 10.1007/s00262-017-2050-7.

[96] E. J. Won *et al.*, 'Clinical relevance of circulating mucosal-associated invariant T cell levels and their anti-cancer activity in patients with mucosal-associated cancer', *Oncotarget*, vol. 7, no. 46, pp. 76274–76290, 2016, doi: 10.18632/oncotarget.11187.

[97] H. Andrlová *et al.*, 'MAIT and Vδ2 unconventional T cells are supported by a diverse intestinal microbiome and correlate with favorable patient outcome after allogeneic HCT', *Sci Transl Med*, vol. 14, no. 646, pp. 1–16, 2022, doi: 10.1126/scitranslmed.abj2829.

[98] J. H. Park and H. K. Lee, 'Function of γδ T cells in tumor immunology and their application to cancer therapy', *Exp Mol Med*, vol. 53, no. 3, pp. 318–327, 2021, doi: 10.1038/s12276-021-00576-0.

[99] A. Cordova *et al.*, 'Characterization of Human γδ T Lymphocytes Infiltrating Primary Malignant Melanomas', *PLoS One*, vol. 7, no. 11, pp. 1–9, 2012, doi: 10.1371/journal.pone.0049878.

[100] D. Pawlik-Gwozdecka, M. Zieliński, J. Sakowska, E. Adamkiewicz-Drozyńska, P. Trzonkowski, and M. Niedźwiecki, 'CD8+ γδ T cells correlate with favorable

prognostic factors in childhood acute lymphoblastic leukemia', *Archives of Medical Science*, vol. 17, no. 2, pp. 561–563, 2021, doi: 10.5114/aoms/132316.

[101] S. Nguyen *et al.*, 'Vδ2 T cells are associated with favorable clinical outcomes in patients with bladder cancer and their tumor reactivity can be boosted by BCG and zoledronate treatments', *J Immunother Cancer*, vol. 10, no. 8, pp. 1–10, 2022, doi: 10.1136/jitc-2022-004880.

[102] L. Rong, K. Li, R. Li, H. M. Liu, R. Sun, and X. Y. Liu, 'Analysis of tumor-infiltrating gamma delta T cells in rectal cancer', *World J Gastroenterol*, vol. 22, no. 13, pp. 3573–3580, 2016, doi: 10.3748/wjg.v22.i13.3573.

[103] B. S. Reis *et al.*, 'TCR-Vgd usage distinguishes protumor from antitumor intestinal gd T cell subsets', *Science (1979)*, vol. 377, no. 6603, pp. 276–284, 2022, doi: 10.1126/science.abj8695.

[104] O. Lantz and A. Bendelac, 'An invariant T cell receptor α Chain is used by a unique subset of major histocompatibility complex class I-specific CD4+ and CD4-8- T cells in mice and humans', *Journal of Experimental Medicine*, vol. 180, no. 3, pp. 1077–1106, 1994, doi: 10.1084/jem.180.3.1097.

[105] L. van Kaer, 'α-galactosylceramide therapy for autoimmune diseases: Prospects and obstacles', *Nat Rev Immunol*, vol. 5, no. 1, pp. 31–42, 2005, doi: 10.1038/nri1531.

[106] D. C. Barral and M. B. Brenner, 'CD1 antigen presentation: How it works', *Nat Rev Immunol*, vol. 7, no. 12, pp. 929–941, 2007, doi: 10.1038/nri2191.

[107] J. L. Matsuda *et al.*, 'Tracking the response of natural killer T cells to a glycolipid antigen using CD1d tetramers', *Journal of Experimental Medicine*, vol. 192, no. 5, pp. 741–753, 2000, doi: 10.1084/jem.192.5.741.

[108] I. Fuss *et al.*, 'IL-13Rα2-Bearing, Type II NKT Cells Reactive to Sulfatide SelfAntigen Populate the Mucosa of Ulcerative Colitis', *Gut*, vol. 63, no. 11, pp. 1728–1736, 2014, doi: 10.1136/gutjnl-2013-305671.IL-13R.

[109] V. Sriram, W. Du, J. Gervay-Hague, and R. R. Brutkiewicz, 'Cell wall glycosphingolipids of Sphingomonas paucimobilis are CD1d-specific ligands for NKT cells', *Eur J Immunol*, vol. 35, no. 6, pp. 1692–1701, 2005, doi: 10.1002/eji.200526157.

[110] L. C. Wieland Brown *et al.*, 'Production of α-Galactosylceramide by a Prominent Member of the Human Gut Microbiota', *PLoS Biol*, vol. 11, no. 7, 2013, doi: 10.1371/journal.pbio.1001610.

[111] Y. Kinjo *et al.*, 'Invariant natural killer T cells recognize glycolipids from pathogenic Gram-positive bacteria', *Nat Immunol*, vol. 12, no. 10, pp. 966–974, 2011, doi: 10.1038/ni.2096.

[112] Y. Kinjo *et al.*, 'Natural killer T cells recognize diacylglycerol antigens from pathogenic bacteria', *Nat Immunol*, vol. 7, no. 9, pp. 978–986, 2006, doi: 10.1038/ni1380.

[113] J. Mattner *et al.*, 'Exogenous and endogenous glycolipid antigens activate NKT cells during microbial infections', *Nature*, vol. 434, no. 7032, pp. 525–529, 2005, doi: 10.1038/nature03408.

[114] F. Facciotti *et al.*, 'Peroxisome-derived lipids are self antigens that stimulate invariant natural killer T cells in the thymus', *Nat Immunol*, vol. 13, no. 5, pp. 474–480, 2012, doi: 10.1038/ni.2245.

[115] M. Bedard *et al.*, 'Sterile activation of invariant natural killer T cells by ER-stressed antigen-presenting cells', *Proc Natl Acad Sci U S A*, vol. 116, no. 47, pp. 23671–23681, 2019, doi: 10.1073/pnas.1910097116.

[116] P. J. Brennan, M. Brigl, and M. B. Brenner, 'Invariant natural killer T cells: An innate activation scheme linked to diverse effector functions', *Nat Rev Immunol*, vol. 13, no. 2, pp. 101–117, 2013, doi: 10.1038/nri3369.

[117] M. Watanabe, S. Celli, F. A. Alkhaleel, and R. J. Hodes, 'Antigen-presenting T cells provide critical B7 co-stimulation for thymic iNKT cell development via CD28-dependent trogocytosis', *Cell Rep*, vol. 41, no. 9, p. 111731, 2022, doi: 10.1016/j.celrep.2022.111731.

[118] S. P. Berzins, F. W. McNab, C. M. Jones, M. J. Smyth, and D. I. Godfrey, ' Long-Term Retention of Mature NK1.1 + NKT Cells in the Thymus ', *The Journal of Immunology*, vol. 176, no. 7, pp. 4059–4065, 2006, doi: 10.4049/jimmunol.176.7.4059.

[119] L. M. Hix, Y. H. Shi, R. R. Brutkiewicz, P. L. Stein, C. R. Wang, and M. Zhang, 'CD1d-expressing breast cancer cells modulate NKT cell-mediated antitumor immunity in a murine model of breast cancer metastasis', *PLoS One*, vol. 6, no. 6, 2011, doi: 10.1371/journal.pone.0020702.

[120] T. Seki, J. Liu, R. R. Brutkiewicz, and M. Tsuji, 'A potent CD1d-binding glycolipid for iNKT-cell-based therapy against human breast cancer', *Anticancer Res*, vol. 39, no. 2, pp. 549–555, 2019, doi: 10.21873/anticanres.13147.

[121] T. Kawano *et al.*, 'Natural killer-like nonspecific tumor cell lysis mediated by specific ligand-activated Vα14 NKT cells', *Proc Natl Acad Sci U S A*, vol. 95, no. 10, pp. 5690–5693, 1998, doi: 10.1073/pnas.95.10.5690.

[122] G. Wingender, P. Krebs, B. Beutler, and M. Kronenberg, 'Antigen-Specific Cytotoxicity by Invariant NKT Cells In Vivo Is CD95/CD178-Dependent and Is Correlated with Antigenic Potency', *The Journal of Immunology*, vol. 185, no. 5, pp. 2721–2729, 2010, doi: 10.4049/jimmunol.1001018.Antigen-specific.

[123] F. Gorini *et al.*, 'Invariant NKT cells contribute to chronic lymphocytic leukemia surveillance and prognosis', *Blood*, vol. 129, no. 26, pp. 3440–3451, 2017, doi: 10.1182/blood-2016-11-751065.

[124] H. Bassiri *et al.*, 'iNKT cell cytotoxic responses control T-lymphoma growth in vitro and in vivo', *Cancer Immunol Res*, vol. 2, no. 1, pp. 59–69, 2014, doi: 10.1158/2326-6066.CIR-13-0104.iNKT.

[125] R. L. Bjordahl, L. Gapin, P. Marrack, and Y. Refaeli, 'INKT cells suppress the CD8+ T cell response to a murine burkitt's-like b cell lymphoma', *PLoS One*, vol. 7, no. 8, 2012, doi: 10.1371/journal.pone.0042635.

[126] S. Fallarini, T. Paoletti, N. Orsi Battaglini, and G. Lombardi, 'Invariant NKT cells increase drug-induced osteosarcoma cell death', *Br J Pharmacol*, vol. 167, no. 7, pp. 1533–1549, 2012, doi: 10.1111/j.1476-5381.2012.02108.x.

[127] L. S. Metelitsa *et al.*, 'Natural Killer T Cells Infiltrate Neuroblastomas Expressing the Chemokine CCL2', *Journal of Experimental Medicine*, vol. 199, no. 9, pp. 1213–1221, 2004, doi: 10.1084/jem.20031462.

[128] A. Heczey *et al.*, 'Anti-GD2 CAR-NKT cells in patients with relapsed or refractory neuroblastoma: an interim analysis', *Nat Med*, vol. 26, no. 11, pp. 1686–1690, 2020, doi: 10.1038/s41591-020-1074-2.

[129] K. M. Dhodapkar *et al.*, 'Invariant natural killer T cells are preserved in patients with glioma and exhibit antitumor lytic activity following dendritic cell-mediated expansion', *Int J Cancer*, vol. 109, no. 6, pp. 893–899, 2004, doi: 10.1002/ijc.20050.

[130] J. Konishi, K. Yamazaki, H. Yokouchi, N. Shinagawa, K. Iwabuchi, and M. Nishimura, 'The characteristics of human NKT cells in lung cancer - CD1d independent cytotoxicity against lung cancer cells by NKT cells and decreased human NKT cell response in lung cancer patients', *Hum Immunol*, vol. 65, no. 11, pp. 1377–1388, 2004, doi: 10.1016/j.humimm.2004.09.003.

[131] N. B. Janakiram *et al.*, 'Loss of natural killer T cells promotes pancreatic cancer in LSL-KrasG12D/+ mice', *Immunology*, vol. 152, no. 1, pp. 36–51, 2017, doi: 10.1111/imm.12746.

[132] S. Nagaraj, C. Ziske, J. Strehl, D. Messmer, T. Sauerbruch, and I. G. H. Schmidt-Wolf, 'Dendritic cells pulsed with alpha-galactosylceramide induce anti-tumor immunity against pancreatic cancer in vivo', *Int Immunol*, vol. 18, no. 8, pp. 1279–1283, 2006, doi: 10.1093/intimm/dxl059.

[133] F. Cortesi *et al.*, 'Bimodal CD40/Fas-Dependent Crosstalk between iNKT Cells and Tumor-Associated Macrophages Impairs Prostate Cancer Progression', *Cell Rep*, vol. 22, no. 11, pp. 3006–3020, 2018, doi: 10.1016/j.celrep.2018.02.058.

[134] M. Bellone *et al.*, 'iNKT cells control mouse spontaneous carcinoma independently of tumor-specific cytotoxic T cells', *PLoS One*, vol. 5, no. 1, 2010, doi: 10.1371/journal.pone.0008646.

[135] P. W. Darcy, L. K. Denzin, and D. B. Sant'Angelo, 'YY1lo NKT cells are dedicated IL-10 producers', *Sci Rep*, vol. 10, no. 1, pp. 1–15, 2020, doi: 10.1038/s41598-020-60229-6.

[136] E. Ambrosino *et al.*, 'Cross-Regulation between Type I and Type II NKT Cells in Regulating Tumor Immunity: A New Immunoregulatory Axis1', *The Journal of Immunology*, 2011.

[137] T. Hattori *et al.*, 'Antitumor effect of whole body hyperthermia with α-galactosylceramide in a subcutaneous tumor model of colon cancer', *International Journal of Hyperthermia*, vol. 23, no. 7, pp. 591–598, 2007, doi: 10.1080/02656730701708328.

[138] J. M. Park, M. Terabe, L. T. van den Broeke, D. D. Donaldson, and J. A. Berzofsky, 'Unmasking immunosurveillance against a syngeneic colon cancer by elimination of CD4+ NKT regulatory cells and IL-13', *Int J Cancer*, vol. 114, no. 1, pp. 80–87, 2005, doi: 10.1002/ijc.20669.

[139] Y. Wang, S. Sedimbi, L. Löfbom, A. K. Singh, S. A. Porcelli, and S. L. Cardell, 'Unique invariant natural killer T cells promote intestinal polyps by suppressing TH1 immunity and promoting regulatory T cells Ying', *Mucosal Immunol*, vol. 11, no. 1, pp. 131–143, 2018, doi: 10.1007/s12026-008-8082-5.Thymus.

[140] Y. Wang, M. S. Bhave, H. Yagita, and S. L. Cardell, 'Natural Killer T-Cell Agonist α-Galactosylceramide and PD-1 Blockade Synergize to Reduce Tumor Development in a Preclinical Model of Colon Cancer', *Front Immunol*, vol. 11, no. October, pp. 1–12, 2020, doi: 10.3389/fimmu.2020.581301.

[141] Q. Xu, J. Li, N. Zhang, L. Zhang, and R. Qian, 'Utilization of invariant natural killer T cells for gastric cancer treatment', *Future Oncology*, vol. 14, no. 20, 2018.

[142] A. M. Melo *et al.*, 'CD1d expression and invariant natural killer T-cell numbers are reduced in patients with upper gastrointestinal cancers and are further impaired by commonly used chemotherapies', *Cancer Immunology, Immunotherapy*, vol. 69, no. 6, pp. 969–982, 2020, doi: 10.1007/s00262-020-02514-x.

[143] M. J. Wolf *et al.*, 'Metabolic activation of intrahepatic CD8+ T cells and NKT cells causes nonalcoholic steatohepatitis and liver cancer via cross-talk with hepatocytes', *Cancer Cell*, vol. 26, no. 4, pp. 549–564, 2014, doi: 10.1016/j.ccell.2014.09.003.

[144] K. Yanagisawa, K. Seino, Y. Ishikawa, M. Nozue, T. Todoroki, and K. Fukao, 'Impaired Proliferative Response of Vα24 NKT Cells from Cancer Patients Against α-Galactosylceramide', *Journal of Immunology*, vol. 168, no. 12, pp. 6494–6499, 2002.

[145] S. Fu *et al.*, 'Impaired lipid biosynthesis hinders anti-tumor efficacy of intratumoral iNKT cells', *Nat Commun*, vol. 11, no. 1, pp. 1–15, 2020, doi: 10.1038/s41467-020-14332-x.

[146] J. Burks, P. B. Olkhanud, and J. A. Berzofsky, 'The role of NKT cells in gastrointestinal cancers', *Oncoimmunology*, vol. 11, no. 1, 2022, doi: 10.1080/2162402X.2021.2009666.

[147] T. Miyagi *et al.*, 'CD1d-mediated stimulation of natural killer T cells selectively activates hepatic natural killer cells to eliminate experimentally disseminated hepatoma cells in murine liver', *Int J Cancer*, vol. 106, no. 1, pp. 81–89, 2003, doi: 10.1002/ijc.11163.

[148] G. Bricard *et al.*, ' Enrichment of Human CD4 + Vα24/Vβ11 Invariant NKT Cells in Intrahepatic Malignant Tumors ', *The Journal of Immunology*, vol. 182, no. 8, pp. 5140–5151, 2009, doi: 10.4049/jimmunol.0711086.

[149] T. Kenna *et al.*, 'NKT Cells from Normal and Tumor-Bearing Human Livers Are Phenotypically and Functionally Distinct from Murine NKT Cells', *The Journal of Immunology*, vol. 171, no. 4, pp. 1775–1779, 2003, doi: 10.4049/jimmunol.171.4.1775.

[150] X. Liu *et al.*, 'NK and NKT cells have distinct properties and functions in cancer', *Oncogene*, vol. 40, no. 27, pp. 4521–4537, 2021, doi: 10.1038/s41388-021-01880-9.

[151] A. Díaz-Basabe *et al.*, 'Human intestinal and circulating invariant Natural Killer T cells are cytotoxic against colorectal cancer cells via the perforin-granzyme pathway', *Mol Oncol*, 2021.

[152] C. Ma *et al.*, 'Gut microbiome–mediated bile acid metabolism regulates liver cancer via NKT cells', *Science (1979)*, vol. 360, no. 6391, 2018, doi: 10.1126/science.aan5931.

[153] K. Bandyopadhyay, I. Marrero, and V. Kumar, 'NKT cell subsets as key participants in liver physiology and pathology', *Cell Mol Immunol*, vol. 13, no. 3, pp. 337–346, 2016, doi: 10.1038/cmi.2015.115.

[154] D. Krijgsman *et al.*, 'Characterization of circulating T-, NK-, and NKT cell subsets in patients with colorectal cancer: the peripheral blood immune cell profile', *Cancer Immunology, Immunotherapy*, vol. 68, no. 6, pp. 1011–1024, 2019, doi: 10.1007/s00262-019-02343-7.

[155] G. Delfanti, P. Dellabona, G. Casorati, and M. Fedeli, 'Adoptive Immunotherapy With Engineered iNKT Cells to Target Cancer Cells and the Suppressive Microenvironment', *Front Med (Lausanne)*, vol. 9, no. May, pp. 1–12, 2022, doi: 10.3389/fmed.2022.897750.

[156] M. S. Cruz, J. P. Loureiro, M. J. Oliveira, and M. F. Macedo, 'The iNKT Cell–Macrophage Axis in Homeostasis and Disease', *Int J Mol Sci*, vol. 23, no. 3, 2022, doi: 10.3390/ijms23031640.

[157] L. Song *et al.*, 'Vα24-invariant NKT cells mediate antitumor activity via killing of tumor-associated macrophages', *Journal of Clinical Investigation*, vol. 119, no. 6, pp. 1524–1536, 2009, doi: 10.1172/JCI37869.

[158] P. Barral *et al.*, 'CD169+ macrophages present lipid antigens to mediate early activation of iNKT cells in lymph nodes', *Nat Immunol*, vol. 11, no. 4, pp. 303–312, 2010, doi: 10.1038/ni.1853.

[159] L. Y. *et al.*, 'CD1d highly expressed on DCs reduces lung tumor burden by enhancing antitumor immunity', *Oncol Rep*, vol. 4, no. 5, pp. 2679–2688, 2019.

[160] C. Ni *et al.*, 'Thymosin alpha1 enhanced cytotoxicity of iNKT cells against colon cancer via upregulating CD1d expression', *Cancer Lett*, vol. 356, no. 2, pp. 579–588, 2015, doi: 10.1016/j.canlet.2014.10.002.

[161] P. Barral *et al.*, 'B cell receptor-mediated uptake of CD1d-restricted antigen augments antibody responses by recruiting invariant NKT cell help in vivo', *Proc Natl Acad Sci U S A*, vol. 105, no. 24, pp. 8345–8350, 2008, doi: 10.1073/pnas.0802968105.

[162] C. de Santo *et al.*, 'Invariant NKT cells modulate the suppressive activity of IL-10-secreting neutrophils differentiated with serum amyloid A', *Nat Immunol*, vol. 11, no. 11, pp. 1039–1046, 2010, doi: 10.1038/ni.1942.

[163] T. Hägglöf *et al.*, 'Neutrophils license iNKT cells to regulate self-reactive mouse B cell responses', *Nat Immunol*, vol. 17, no. 12, pp. 1407–1414, 2016, doi: 10.1038/ni.3583.

[164] A. Thanabalasuriar, A. S. Neupane, J. Wang, M. F. Krummel, and P. Kubes, 'iNKT Cell Emigration out of the Lung Vasculature Requires Neutrophils and Monocyte-Derived Dendritic Cells in Inflammation', *Cell Rep*, vol. 16, no. 12, pp. 3260–3272, 2016, doi: 10.1016/j.celrep.2016.07.052.

[165] G. Wingender *et al.*, 'Intestinal Microbes Affect Phenotypes and Functions of Invariant Natural Killer T cells in Mice', *Gastroenterology*, vol. 143, no. 2, pp. 418–428, 2012, doi: 10.1053/j.gastro.2012.04.017.Intestinal.

[166] C. Burrello *et al.*, 'Mucosa-associated microbiota drives pathogenic functions in IBD-derived intestinal iNKT cells', *Life Sci Alliance*, vol. 2, no. 1, pp. 1–17, 2019, doi: 10.26508/LSA.201800229.

[167] C. Burrello *et al.*, 'Short-term Oral Antibiotics Treatment Promotes Inflammatory Activation of Colonic Invariant Natural Killer T and Conventional CD4+ T Cells', *Front Med (Lausanne)*, vol. 5, no. 21, pp. 1–12, 2018, doi: 10.3389/fmed.2018.00021.

[168] F. Strati *et al.*, 'Antibiotic-associated dysbiosis affects the ability of the gut microbiota to control intestinal inflammation upon fecal microbiota transplantation in experimental colitis models', *Microbiome*, vol. 9, no. 1, pp. 1–15, 2021, doi: 10.1186/s40168-020-00991-x.

[169] E. A. Ivleva and S. I. Grivennikov, 'Microbiota-driven mechanisms at different stages of cancer development', *Neoplasia (United States)*, vol. 32, no. C, p. 100829, 2022, doi: 10.1016/j.neo.2022.100829.

[170] N. Hafsi *et al.*, 'Human Dendritic Cells Respond to Helicobacter pylori, Promoting NK Cell and Th1-Eector Responses In Vitro', *The journal of immunology*, vol. 173, no. 2, pp. 1249–1257, 2004.

[171] Y. Zhang *et al.*, 'Fusobacterium nucleatum promotes colorectal cancer cells adhesion to endothelial cells and facilitates extravasation and metastasis by inducing ALPK1/NF-κB/ICAM1 axis', *Gut Microbes*, vol. 14, no. 1, 2022, doi: 10.1080/19490976.2022.2038852.

[172] E. J. Lim, J. H. Kang, Y. J. Kim, S. Kim, and S. J. Lee, 'ICAM-1 promotes cancer progression by regulating SRC activity as an adapter protein in colorectal cancer', *Cell Death Dis*, vol. 13, no. 4, pp. 1–11, 2022, doi: 10.1038/s41419-022-04862-1.

[173] B. Udayasuryan *et al.*, 'Fusobacterium nucleatum induces proliferation and migration in pancreatic cancer cells through host autocrine and paracrine signaling', *Sci Signal*, vol. 15, no. 756, p. eabn4948, 2022, doi: 10.1126/scisignal.abn4948.

[174] M. A. Casasanta *et al.*, 'Fusobacterium nucleatum host-cell binding and invasion induces IL-8 and CXCL1 secretion that drives colorectal cancer cell migration', *Sci Signal*, vol. 13, no. 641, pp. 1–13, 2020, doi: 10.1126/SCISIGNAL.ABA9157.

[175] A. D. Kostic *et al.*, 'Fusobacterium nucleatum Potentiates Intestinal Tumorigenesis and Modulates the Tumor-Immune Microenvironment', *Cell Host Microbe*, vol. 14, no. 2, pp. 207–215, 2013, doi: 10.1016/j.chom.2013.07.007.

[176] C. A. Brennan *et al.*, 'Fusobacterium nucleatum drives a pro-inflammatory intestinal microenvironment through metabolite receptor-dependent modulation of IL-17 expression', *Gut Microbes*, vol. 13, no. 1, 2021, doi: 10.1080/19490976.2021.1987780.

[177] C. Martin-Gallausiaux, A. Malabirade, J. Habier, and P. Wilmes, 'Fusobacterium nucleatum Extracellular Vesicles Modulate Gut Epithelial Cell Innate Immunity via FomA and TLR2', *Front Immunol*, vol. 11, no. December, pp. 1–15, 2020, doi: 10.3389/fimmu.2020.583644.

[178] C. Gur *et al.*, 'Binding of the Fap2 protein of fusobacterium nucleatum to human inhibitory receptor TIGIT protects tumors from immune cell attack', *Immunity*, vol. 42, no. 2, pp. 344–355, 2015, doi: 10.1016/j.immuni.2015.01.010.

[179] J. B. Lee *et al.*, 'Association between Fusobacterium nucleatum and patient prognosis in metastatic colon cancer', *Sci Rep*, vol. 11, no. 1, pp. 1–9, 2021, doi: 10.1038/s41598-021-98941-6.

[180] Y. Gao *et al.*, 'Fusobacterium nucleatum enhances the efficacy of PD-L1 blockade in colorectal cancer', *Signal Transduct Target Ther*, vol. 6, no. 1, pp. 1–10, 2021, doi: 10.1038/s41392-021-00795-x.

[181] B. A. Helmink, M. A. W. Khan, A. Hermann, V. Gopalakrishnan, and J. A. Wargo, 'The microbiome, cancer, and cancer therapy', *Nat Med*, vol. 25, no. 3, pp. 377–388, 2019, doi: 10.1038/s41591-019-0377-7.

[182] M. Amin *et al.*, *AJCC Cancer Staging Manual 8th edition*. 2017.

[183] Y. H. Xie, Y. X. Chen, and J. Y. Fang, 'Comprehensive review of targeted therapy for colorectal cancer', *Signal Transduct Target Ther*, vol. 5, no. 1, 2020, doi: 10.1038/s41392-020-0116-z.

[184] P. Benatti *et al.*, 'Microsatellite instability and colorectal cancer prognosis', *Clinical Cancer Research*, vol. 11, no. 23, pp. 8332–8340, 2005, doi: 10.1158/1078-0432.CCR-05-1030.

[185] Y. Zhang *et al.*, 'α-GalCer and iNKT cell-based cancer immunotherapy: Realizing the therapeutic potentials', *Front Immunol*, vol. 10, no. JUN, pp. 11–15, 2019, doi: 10.3389/fimmu.2019.01126.

[186] M. Waldowska, A. Bojarska-Junak, and J. Rolinski, 'A brief review of clinical trials involving manipulation of invariant NKT cells as a promising approach in future cancer therapies', *Central European Journal of Immunology*, vol. 42, no. 2, 2017.

[187] V. v. Parekh *et al.*, 'Glycolipid antigen induces long-term natural killer T cell anergy in mice', *Journal of Clinical Investigation*, vol. 115, no. 9, pp. 2572–2583, 2005, doi: 10.1172/JCI24762.

[188] Y. Zhu *et al.*, 'Development of Hematopoietic Stem Cell-Engineered Invariant Natural Killer T Cell Therapy for Cancer', *Cell Stem Cell*, vol. 25, no. 4, pp. 542-557.e9, 2019, doi: 10.1016/j.stem.2019.08.004.

[189] B. J. Wolf, J. E. Choi, and M. A. Exley, 'Novel approaches to exploiting invariant NKT cells in cancer immunotherapy', *Front Immunol*, vol. 9, 2018, doi: 10.3389/fimmu.2018.00384.

[190] A. Rotolo *et al.*, 'Enhanced Anti-lymphoma Activity of CAR19-iNKT Cells Underpinned by Dual CD19 and CD1d Targeting', *Cancer Cell*, vol. 34, no. 4, pp. 596-610.e11, 2018, doi: 10.1016/j.ccell.2018.08.017.

[191] E. Landoni *et al.*, 'A High-Avidity T-cell Receptor Redirects Natural Killer T-cell Specificity and Outcompetes the Endogenous Invariant T-cell Receptor', *Cancer Immunol Res*, vol. 8, no. 1, pp. 57–69, 2020, doi: 10.1158/2326-6066.CIR-19-0134.

[192] Z. M. Jiang *et al.*, 'Development of genetically engineered iNKT cells expressing TCRs specific for the M. tuberculosis 38-kDa antigen', *J Transl Med*, vol. 13, no. 1, pp. 1–10, 2015, doi: 10.1186/s12967-015-0502-4.

[193] G. Delfanti *et al.*, 'TCR-engineered iNKT cells induce robust antitumor response by dual targeting cancer and suppressive myeloid cells', *Sci Immunol*, vol. 7, no. 74, 2022.

[194] C. Becker, M. C. Fantini, and M. F. Neurath, 'High resolution colonoscopy in live mice', *Nat Protoc*, vol. 1, pp. 2900–2904, 2006.

[195] L. van der Maaten and G. Hinton, 'Visualizing Data using t-SNE', *Journal of Machine Learning Research*, vol. 1, pp. 1–25, 2008.

[196] J. Brummelman *et al.*, 'Development , application and computational analysis of high-dimensional fl uorescent antibody panels for single-cell fl ow cytometry', *Nat Protoc*, vol. 14, no. July, pp. 1946–1969, 2019, doi: 10.1038/s41596-019-0166-2.

[197] D. Albanese, P. Fontana, C. de Filippo, D. Cavalieri, and C. Donati, 'MICCA: A complete and accurate software for taxonomic profiling of metagenomic data', *Sci Rep*, vol. 5, pp. 1–7, 2015, doi: 10.1038/srep09743.

[198] Q. Wang, G. M. Garrity, J. M. Tiedje, and J. R. Cole, 'Naïve Bayesian classifier for rapid assignment of rRNA sequences into the new bacterial taxonomy', *Appl Environ Microbiol*, vol. 73, no. 16, pp. 5261–5267, 2007, doi: 10.1128/AEM.00062-07.

[199] T. Z. DeSantis *et al.*, 'NAST: A multiple sequence alignment server for comparative analysis of 16S rRNA genes', *Nucleic Acids Res*, vol. 34, no. WEB. SERV. ISS., pp. 394–399, 2006, doi: 10.1093/nar/gkl244.

[200] P. J. McMurdie and S. Holmes, 'Phyloseq: An R Package for Reproducible Interactive Analysis and Graphics of Microbiome Census Data', *PLoS One*, vol. 8, no. 4, 2013, doi: 10.1371/journal.pone.0061217.

[201] P. J. McMurdie and S. Holmes, 'Waste Not, Want Not: Why Rarefying Microbiome Data Is Inadmissible', *PLoS Comput Biol*, vol. 10, no. 4, 2014, doi: 10.1371/journal.pcbi.1003531.

[202] V. Bianchi *et al.*, 'Integrated systems for NGS data management and analysis: Open issues and available solutions', *Front Genet*, vol. 7, no. MAY, pp. 1–8, 2016, doi: 10.3389/fgene.2016.00075.

[203] M. I. Love, W. Huber, and S. Anders, 'Moderated estimation of fold change and dispersion for RNA-seq data with DESeq2', *Genome Biol*, vol. 15, no. 12, pp. 1–21, 2014, doi: 10.1186/s13059-014-0550-8.

[204] B. T. Sherman *et al.*, 'DAVID: a web server for functional enrichment analysis and functional annotation of gene lists (2021 update)', *Nucleic Acids Res*, vol. 50, no. W1, pp. W216–W221, 2022, doi: 10.1093/nar/gkac194.

[205] Y. Hao *et al.*, 'Integrated analysis of multimodal single-cell data', *Cell*, vol. 184, no. 13, pp. 3573-3587.e29, 2021, doi: 10.1016/j.cell.2021.04.048.

[206] C. Hafemeister and R. Satija, 'Normalization and variance stabilization of single-cell RNA-seq data using regularized negative binomial regression', *Genome Biol*, vol. 20, no. 1, pp. 1–15, 2019, doi: 10.1186/s13059-019-1874-1.

[207] K. Pelka *et al.*, 'Spatially organized multicellular immune hubs in human colorectal cancer', *Cell*, vol. 184, no. 18, pp. 4734-4752.e20, 2021, doi: 10.1016/j.cell.2021.08.003.

[208] I. Korsunsky *et al.*, 'Fast, sensitive and accurate integration of single-cell data with Harmony', *Nat Methods*, vol. 16, no. 12, pp. 1289–1296, 2019, doi: 10.1038/s41592-019-0619-0.

[209] F. Veglia *et al.*, 'Analysis of classical neutrophils and polymorphonuclear myeloid-derived suppressor cells in cancer patients and tumor-bearing mice', *Journal of Experimental Medicine*, vol. 218, no. 4, 2021, doi: 10.1084/JEM.20201803.

[210] S. Tiberti *et al.*, 'GZMKhigh CD8+ T effector memory cells are associated with CD15high neutrophil abundance in non-metastatic colorectal tumors and predict poor clinical outcome', *Nat Commun*, vol. 13, no. 1, 2022, doi: 10.1038/s41467-022-34467-3.

[211] M. A. Murphy, J. S. Evans, and A. Storfer, 'Quantifying Bufo boreas connectivity in Yellowstone National Park with landscape genetics', *Ecology*, vol. 91, no. 1, pp. 252–261, 2010, doi: 10.1890/08-0879.1.

[212] C. Faccani *et al.*, 'Workflow for high-dimensional flow cytometry analysis of T cells from tumor metastases', *Life Sci Alliance*, vol. 5, no. 10, pp. 1–18, 2022, doi: 10.26508/lsa.202101316.

[213] Y. Wang *et al.*, 'Tumor-derived GM-CSF promotes inflammatory colon carcinogenesis via stimulating epithelial release of VEGF', *Cancer Res*, vol. 74, no. 3, pp. 716–726, 2014, doi: 10.1158/0008-5472.CAN-13-1459.

[214] F. Amicarella *et al.*, 'Dual role of tumour-infiltrating T helper 17 cells in human colorectal cancer', *Gut*, vol. 66, no. 4, pp. 692–704, 2017, doi: 10.1136/gutjnl-2015-310016.

[215] I. Ballesteros *et al.*, 'Co-option of Neutrophil Fates by Tissue Environments', *Cell*, vol. 183, no. 5, pp. 1282-1297.e18, 2020, doi: 10.1016/j.cell.2020.10.003.

[216] K. Liu *et al.*, 'Increased Neutrophil Aging Contributes to T Cell Immune Suppression by PD-L1 and Arginase-1 in HIV-1 Treatment Naïve Patients', *Front Immunol*, vol. 12, no. August, pp. 1–12, 2021, doi: 10.3389/fimmu.2021.670616.

[217] A. v. Belikov, B. Schraven, and L. Simeoni, 'T cells and reactive oxygen species', *J Biomed Sci*, vol. 22, no. 1, pp. 1–11, 2015, doi: 10.1186/s12929-015-0194-3.

[218] E. L. Yarosz and C. H. Chang, 'Role of reactive oxygen species in regulating T cell-mediated immunity and disease', *Immune Netw*, vol. 18, no. 1, pp. 1–15, 2018, doi: 10.4110/in.2018.18.e14.

[219] E. Cremonesi *et al.*, 'Gut microbiota modulate T cell trafficking into human colorectal cancer', *Gut*, vol. 67, no. 11, pp. 1984–1994, 2018, doi: 10.1136/gutjnl-2016-313498.

[220] Q. Lin *et al.*, 'Invariant natural killer T cells minimally influence gut microbiota composition in mice', *Gut Microbes*, vol. 14, no. 1, 2022, doi: 10.1080/19490976.2022.2104087.

[221] T. Selvanantham *et al.*, 'NKT Cell–Deficient Mice Harbor an Altered Microbiota That Fuels Intestinal Inflammation during Chemically Induced Colitis', *The Journal of Immunology*, vol. 197, no. 11, pp. 4464–4472, 2016, doi: 10.4049/jimmunol.1601410.

[222] B. Chen, M. Khodadoust, C. Long Liu, A. Newman, and A. Alizadeh, 'Profiling tumor infiltrating immune cells with CIBERSORT', *Methods Mol Biol*, vol. 1711, no. 1, pp. 243–259, 2018, doi: 10.1007/978-1-4939-7493-1.

[223] F. Avila Cobos, J. Vandesompele, P. Mestdagh, and K. de Preter, 'Computational deconvolution of transcriptomics data from mixed cell populations', *Bioinformatics*, vol. 34, no. 11, pp. 1969–1979, 2018, doi: 10.1093/bioinformatics/bty019.

[224] F. Avila Cobos, J. Alquicira-Hernandez, J. E. Powell, P. Mestdagh, and K. de Preter, 'Benchmarking of cell type deconvolution pipelines for transcriptomics data', *Nat Commun*, vol. 11, no. 1, 2020, doi: 10.1038/s41467-020-19015-1.

[225] G. J. Sutton *et al.*, 'Comprehensive evaluation of deconvolution methods for human brain gene expression', *Nat Commun*, vol. 13, no. 1, pp. 1–18, 2022, doi: 10.1038/s41467-022-28655-4.

[226] J. J. O. Konek *et al.*, 'Mouse and human iNKT cell agonist β-mannosylceramide reveals a distinct mechanism of tumor immunity', *Journal of Clinical Investigation*, vol. 121, no. 28, pp. 683–694, 2011, doi: 10.1172/JCI42314.Previous.

[227] B. Routy *et al.*, 'Gut microbiome influences efficacy of PD-1-based immunotherapy against epithelial tumors', *Science (1979)*, vol. 359, no. 6371, pp. 91–97, 2018, doi: 10.1126/science.aan3706.

[228] V. Gopalakrishnan *et al.*, 'Gut microbiome modulates response to anti-PD-1 immunotherapy in melanoma patients', *Science (1979)*, vol. 359, no. 6371, pp. 97–103, 2018, doi: 10.1126/science.aan4236.

[229] M. Vétizou *et al.*, 'Anticancer immunotherapy by CTLA-4 blockade relies on the gut microbiota', *Science (1979)*, vol. 350, no. 6264, pp. 1079–1084, 2015, doi: 10.1126/science.aad1329.

JCC OXFORD

IL10 Secretion Endows Intestinal Human iNKT Cells with Regulatory Functions Towards Pathogenic T Lymphocytes

Claudia Burrello,[a,§,#] Francesco Strati,[a,§] Georgia Lattanzi,[a,b,†] Angelica Diaz-Basabe,[a,b,†] Erika Mileti,[a] Maria Rita Giuffrè,[a] Gianluca Lopez,[c] Fulvia Milena Cribiù,[c] Elena Trombetta,[d] Marinos Kallikourdis,[e,f] Marco Cremonesi,[f] Francesco Conforti,[g] Fiorenzo Botti,[g,h] Laura Porretti,[d] Maria Rescigno,[e] Maurizio Vecchi,[g,i] Massimo C. Fantini,[j] Flavio Caprioli,[g,i] Federica Facciotti[a,k]

[a]Department of Experimental Oncology, European Institute of Oncology IRCCS, Milan, Italy
[b]Department of Oncology and Hemato-oncology, Università degli Studi di Milano, Milan, Italy
[c]Pathology Unit, Fondazione IRCCS Cà Granda, Ospedale Maggiore Policlinico, Milan, Italy
[d]Clinical Chemistry and Microbiology Laboratory Fondazione IRCCS Ca' Granda Ospedale Maggiore Policlinico, Milan, Italy
[e]Department of Biomedical Sciences, Humanitas University, Pieve Emanuele, Milan, Italy
[f]Laboratory of Adaptive Immunity, IRCCS Humanitas Research Hospital, Milan, Italy
[g]Gastroenterology and Endoscopy Unit, Fondazione IRCCS Cà Granda, Ospedale Maggiore Policlinico, Milan, Italy
[h]General and Emergency Surgery Unit, Fondazione IRCCS Ca' Granda, Ospedale Maggiore Policlinico, Milan, Italy
[i]Department of Pathophysiology and Transplantation, Università degli Studi di Milano, Milan, Italy
[j]Department of Medical Science and Public Health, University of Cagliari, Cagliari, Italy
[k]Department of Biotechnology and Biosciences, University of Milan-Bicocca, Milan, Italy

Corresponding author: Dr Federica Facciotti, Department of Experimental Oncology, European Institute of Oncology IRCCS, Via Adamello 16, 20135, Milan, Italy. Email: Federica.facciotti@ieo.it
§These authors contributed equally to this work.
†These authors contributed equally to this work.
#Current address: Division of Tumor Biology and Immunology, Netherlands Cancer Institute, Amsterdam, The Netherlands.

Abstract

Background and Aims: Invariant natural killer T [iNKT] cells perform pleiotropic functions in different tissues by secreting a vast array of pro-inflammatory and cytotoxic molecules. However, the presence and function of human intestinal iNKT cells capable of secreting immunomodulatory molecules such as IL-10 has never been reported so far. Here we describe for the first time the presence of IL10-producing iNKT cells [NKT10 cells] in the intestinal lamina propria of healthy individuals and of Crohn's disease [CD] patients.

Methods: Frequency and phenotype of NKT10 cells were analysed *ex vivo* from intestinal specimens of Crohn's disease [n = 17] and controls [n = 7]. Stable CD-derived intestinal NKT10 cell lines were used to perform *in vitro* suppression assays and co-cultures with patient-derived mucosa-associated microbiota. Experimental colitis models were performed by adoptive cell transfer of splenic naïve CD4+ T cells in the presence or absence of IL10-sufficient or -deficient iNKT cells. *In vivo* induction of NKT10 cells was performed by administration of short chain fatty acids [SCFA] by oral gavage.

Results: Patient-derived intestinal NKT10 cells demonstrated suppressive capabilities towards pathogenic CD4+ T cells. The presence of increased proportions of mucosal NKT10 cells associated with better clinical outcomes in CD patients. Moreover, an intestinal microbial community enriched in SCFA-producing bacteria sustained the production of IL10 by iNKT cells. Finally, IL10-deficient iNKT cells failed to control the pathogenic activity of adoptively transferred CD4+ T cells in an experimental colitis model.

Conclusions: These results describe an unprecedentd IL10-mediated immunoregulatory role of intestinal iNKT cells in controlling the pathogenic functions of mucosal T helper subsets and in maintaining the intestinal immune homeostasis.

Key Words: Crohn's disease; IL10; iNKT cells; SCFA; microbiota

Mucosal Overexpression of Thymic Stromal Lymphopoietin and Proinflammatory Cytokines in Patients With Autoimmune Atrophic Gastritis

Marco Vincenzo Lenti, MD[1,*], Federica Facciotti, PhD[2,3,*], Emanuela Miceli, MD[1], Alessandro Vanoli, PhD[4], Giulia Fornasa, PhD[5], Edith Lahner, PhD[6], Ilaria Spadoni, PhD[7], Paolo Giuffrida, PhD[1], Giovanni Arpa, MD[4], Alessandra Pasini, MD[1], Laura Rovedatti, MD[1], Flavio Caprioli, PhD[8], Cristina Travelli, PhD[9], Georgia Lattanzi, PhD[2], Laura Conti, MD[6], Catherine Klersy, MD[10], Maurizio Vecchi, MD[8], Marco Paulli, MD[4], Bruno Annibale, PhD[6], Gino Roberto Corazza, MD[1], Maria Rescigno, PhD[5,7] and Antonio Di Sabatino, MD[1]

INTRODUCTION: The immune mechanisms underlying human autoimmune atrophic gastritis (AAG) are poorly understood. We sought to assess immune mucosal alterations in patients with AAG.

METHODS: In 2017–2021, we collected gastric corpus biopsies from 24 patients with AAG (median age 62 years, interquartile range 56–67, 14 women), 26 age-matched and sex-matched healthy controls (HCs), and 14 patients with *Helicobacter pylori* infection (HP). We investigated the lamina propria mononuclear cell (LPMC) populations and the mucosal expression of thymic stromal lymphopoietin (TSLP) and nicotinamide phosphoribosyltransferase (NAMPT). *Ex vivo* cytokine production by organ culture biopsies, under different stimuli (short TSLP and zinc-l-carnosine), and the gastric vascular barrier through plasmalemma vesicle-associated protein-1 (PV1) were also assessed.

RESULTS: In the subset of CD19+ LPMC, CD38+ cells (plasma cells) were significantly higher in AAG compared with HC. *Ex vivo* production of tumor necrosis factor (TNF)-α, interleukin (IL)-15, and transforming growth factor β1 was significantly higher in AAG compared with HC. At immunofluorescence, both IL-7R and TSLP were more expressed in AAG compared with HC and HP, and short TSLP transcripts were significantly increased in AAG compared with HC. In the supernatants of AAG corpus mucosa, short TSLP significantly reduced TNF-α, while zinc-l-carnosine significantly reduced interferon-γ, TNF-α, IL-21, IL-6, and IL-15. NAMPT transcripts were significantly increased in AAG compared with HC. PV1 was almost absent in AAG, mildly expressed in HC, and overexpressed in HP.

DISCUSSION: Plasma cells, proinflammatory cytokines, and altered gastric vascular barrier may play a major role in AAG. TSLP and NAMPT may represent potential therapeutic targets, while zinc-l-carnosine may dampen mucosal inflammation.

[1]First Department of Internal Medicine, IRCCS San Matteo Hospital Foundation, University of Pavia, Pavia, Italy; [2]Department of Experimental Oncology, IRCCS European Institute of Oncology, Milan, Italy; [3]Department of Biotechnology and Biosciences, University of Milano-Bicocca, Milan, Italy; [4]Unit of Anatomic Pathology, IRCCS San Matteo Hospital Foundation, University of Pavia, Pavia, Italy; [5]IRCCS Humanitas Research Hospital, Rozzano, Milan, Italy; [6]Department of Medical-Surgical Sciences and Translational Medicine, Sant'Andrea Hospital, University La Sapienza, Rome, Italy; [7]Humanitas University, Department of Biomedical Sciences, Pieve Emanuele, Milan, Italy; [8]Gastroenterology and Endoscopy Unit, IRCCS Ca' Granda Hospital Foundation, University of Milan, Milan, Italy; [9]Department of Pharmaceutical Sciences, University of Pavia, Pavia, Italy; [10]Clinical Epidemiology & Biometry, IRCCS San Matteo Hospital Foundation, Pavia, Italy. **Correspondence:** Antonio Di Sabatino, MD. E-mail: a.disabatino@smatteo.pv.it.
*Marco Vincenzo Lenti and Federica Facciotti contributed equally to this article.
Received February 22, 2022; accepted June 6, 2022; published online June 13, 2022

Appendix III

Review

Microbiota-targeted therapies in inflammation resolution

Francesco Strati [a,b], Georgia Lattanzi [a], Chiara Amoroso [c], Federica Facciotti [a,b,*]

[a] *Department of Experimental Oncology, European Institute of Oncology IRCCS, Milan, Italy*
[b] *Department of Biotechnology and Biosciences, University of Milano-Bicocca, Milan, Italy*
[c] *Gastroenterology and Endoscopy Unit, Fondazione IRCCS Cà Granda, Ospedale Maggiore Policlinico, Milan, Italy*

ARTICLE INFO

ABSTRACT

Gut microbiota has been shown to systemically shape the immunological landscape, modulate homeostasis and play a role in both health and disease. Dysbiosis of gut microbiota promotes inflammation and contributes to the pathogenesis of several major disorders in gastrointestinal tract, metabolic, neurological and respiratory diseases. Much effort is now focused on understanding host-microbes interactions and new microbiota-targeted therapies are deeply investigated as a means to restore health or prevent disease.

This review details the immunoregulatory role of the gut microbiota in health and disease and discusses the most recent strategies in manipulating individual patient's microbiota for the management and prevention of inflammatory conditions.

1. Introduction

The dualistic crosstalk between the microbiota and the immune system starts before birth and it is shaped throughout life as a consequence of geographic, cultural and dietary habits as well as individual's genetic background. For this reason, each individual harbors its own normobiotic microbiota, making difficult the identification of a fixed health-associated microbial ecology. The alteration of the gut microbiota composition leads to a condition called "dysbiosis". Dysbiotic events occur throughout life (*i.e.* upon antibiotic usage, as a consequence of infections, or upon drugs administration). However, microbiota's resilience restores the normobiotic state, possibly aided by the immune system. Though, if repeated dysbiosis-leading events occur and the newly-shaped microbiota diverges too much from the healthy status, then microbiota-modifying interventions are necessary to restore normobiosis. Interestingly, dysbiotic individuals vary more in microbial community composition than healthy individuals [1]. This concept reminds of the Anna Karenina's incipit: 'All happy families look alike; each unhappy family is unhappy in its own way'. The original cause of dysbiosis induces different types of microbiome instability. Upon these premises and according to the nature of dysbiosis, different therapeutic approaches aimed at restoring the normobiosis can be envisaged. When health-associated bacteria are depleted, as observed in autoimmune diseases, supplementation of missing bacteria may be a solution. Similarly, *Clostridium (C.) difficile*-induced colitis is efficiently treated by completely reshuffling the microbial composition *via* fecal transplant. On the contrary, if the microbial dysbiosis is associated with the enrichment of specific pathogens, antimicrobials such as antibiotics, bacteriocins and bacteriophages may be used. Another potential strategy is represented by probiotics, living microorganisms which can

---

Human intestinal and circulating invariant natural killer T cells are cytotoxic against colorectal cancer cells via the perforin–granzyme pathway

Angélica Díaz-Basabe[1,2] (iD), Claudia Burrello[1] (iD), Georgia Lattanzi[1,2], Fiorenzo Botti[3,4], Alberto Carrara[3,4], Elisa Cassinotti[3], Flavio Caprioli[3,5] and Federica Facciotti[1] (iD)

1 Department of Experimental Oncology, IEO European Institute of Oncology IRCCS, Milan, Italy
2 Department of Oncology and Hemato-oncology, Università degli Studi di Milano, Milan, Italy
3 Department of Pathophysiology and Transplantation, Università degli Studi di Milano, Milan, Italy
4 Department of Surgery, Fondazione IRCCS Cà Granda, Ospedale Maggiore Policlinico, Milan, Italy
5 Gastroenterology and Endoscopy Unit, Fondazione IRCCS Cà Granda, Ospedale Maggiore Policlinico, Milan, Italy

Invariant natural killer T (iNKT) cells are lipid-specific T lymphocytes endowed with cytotoxic activities and are thus considered important in antitumor immunity. While several studies have demonstrated iNKT cell cytotoxicity against different tumors, very little is known about their cell-killing activities in human colorectal cancer (CRC). Our aim was to assess whether human iNKT cells are cytotoxic against colon cancer cells and the mechanisms underlying this activity. For this purpose, we generated stable iNKT cell lines from peripheral blood and colon specimens and used NK-92 and peripheral blood natural killer cells as cell-mediated cytotoxicity controls. *In vitro* cytotoxicity was assessed using a panel of well-characterized human CRC cell lines, and the cellular requirements for iNKT cell cytotoxic functions were evaluated. We demonstrated that both intestinal and circulating iNKT cells were cytotoxic against the entire panel of CRC lines, as well as against freshly isolated patient-derived colonic epithelial cancer cells. Perforin and/or granzyme inhibition impaired iNKT cell cytotoxicity, whereas T-cell receptor (TCR) signaling was a less stringent requirement for efficient killing. This study is the first evidence of tissue-derived iNKT cell cytotoxic activity in humans, as it shows that iNKT cells depend on the perforin–granzyme pathway and both adaptive and innate signal recognition for proper elimination of colon cancer cells.

1. Introduction

Colorectal cancer (CRC) is the third-most common cancer worldwide and the fourth cancer type for mortality [1]. Surgery, chemotherapy, and radiotherapy are currently the most frequently used therapeutic approaches for metastatic and nonmetastatic diseases. Targeted therapies with monoclonal antibodies directed against growth and angiogenic factors have been effectively included in the therapeutic options for CRC patients [1]. More recently, immunotherapy has gained consideration for CRC treatment thanks to the advent of technologies such as immune checkpoint inhibition [2–4] and CAR-T technology [5–9]. Alongside CD8+

Appendix V

Microbiome

RESEARCH   **Open Access**

Antibiotic-associated dysbiosis affects the ability of the gut microbiota to control intestinal inflammation upon fecal microbiota transplantation in experimental colitis models

Francesco Strati[1]* , Meritxell Pujolassos[2], Claudia Burrello[1], Maria Rita Giuffrè[1], Georgia Lattanzi[1], Flavio Caprioli[3,4], Jacopo Troisi[2,5†] and Federica Facciotti[1*†]

Abstract

Background: The gut microbiota plays a central role in host physiology and in several pathological mechanisms in humans. Antibiotics compromise the composition and functions of the gut microbiota inducing long-lasting detrimental effects on the host. Recent studies suggest that the efficacy of different clinical therapies depends on the action of the gut microbiota. Here, we investigated how different antibiotic treatments affect the ability of the gut microbiota to control intestinal inflammation upon fecal microbiota transplantation in an experimental colitis model and in ex vivo experiments with human intestinal biopsies.

Results: Murine fecal donors were pre-treated with different antibiotics, i.e., vancomycin, streptomycin, and metronidazole before FMT administration to colitic animals. The analysis of the gut microbiome, fecal metabolome, and the immunophenotyping of colonic lamina propria immune cells revealed that antibiotic pre-treatment significantly influences the capability of the microbiota to control intestinal inflammation. Streptomycin and vancomycin-treated microbiota failed to control intestinal inflammation and were characterized by the blooming of pathobionts previously associated with IBD as well as with metabolites related to the presence of oxidative stress and metabolism of simple sugars. On the contrary, the metronidazole-treated microbiota retained its ability to control inflammation co-occurring with the enrichment of *Lactobacillus* and of innate immune responses involving iNKT cells. Furthermore, ex vivo cultures of human intestinal lamina propria mononuclear cells and iNKT cell clones from IBD patients with vancomycin pre-treated sterile fecal water showed a Th1/Th17 skewing in CD4^{+} T-cell populations; metronidazole, on the other hand, induced the polarization of iNKT cells toward the production of IL10.

(Continued on next page)

---

* Correspondence: francesco.strati@ieo.it; federica.facciotti@ieo.it
†Jacopo Troisi and Federica Facciotti contributed equally to this work.
[1]Department of Experimental Oncology, IEO European Institute of Oncology IRCCS, Milan, Italy
Full list of author information is available at the end of the article

Article

Persistence of Anti-SARS-CoV-2 Antibodies in Non-Hospitalized COVID-19 Convalescent Health Care Workers

Margherita Bruni [1,†], Valentina Cecatiello [1,†], Angelica Diaz-Basabe [1,2,†], Georgia Lattanzi [1,2,†], Erika Mileti [1,†], Silvia Monzani [1,†], Laura Pirovano [1,†], Francesca Rizzelli [1,†], Clara Visintin [1,†], Giuseppina Bonizzi [1], Marco Giani [3], Marialuisa Lavitrano [3], Silvia Faravelli [4], Federico Forneris [4], Flavio Caprioli [5,6], Pier Giuseppe Pelicci [1,2], Gioacchino Natoli [1], Sebastiano Pasqualato [1,‡], Marina Mapelli [1,‡] and Federica Facciotti [1,*,‡]

[1] Department of Experimental Oncology, European Institute of Oncology IRCCS, via Adamello 16, 20139 Milan, Italy; margherita.bruni@ieo.it (M.B.); valentina.cecatiello@ieo.it (V.C.); angelica.diazbasabe@ieo.it (A.D.-B.); georgia.lattanzi@ieo.it (G.L.); erika.mileti@ieo.it (E.M.); silvia.monzani@ieo.it (S.M.); laura.pirovano@ieo.it (L.P.); francesca.rizzelli@ieo.it (F.R.); claraemilia.visintin@ieo.it (C.V.); giuseppina.bonizzi@ieo.it (G.B.); piergiuseppe.pelicci@ieo.it (P.G.P.); gioacchino.natoli@ieo.it (G.N.); sebastiano.pasqualato@ieo.it (S.P.); marina.mapelli@ieo.it (M.M.)
[2] Department of Oncology and Hemato-Oncology, University of Milan, via Festa del Perdono 7, 20122 Milan, Italy
[3] School of Medicine and Surgery, University of Milano-Bicocca, via Cadore 48, 20900 Monza, Italy; marco.giani@unimib.it (M.G.); marialuisa.lavitrano@unimib.it (M.L.)
[4] The Armenise-Harvard Laboratory of Structural Biology, Department of Biology and Biotechnology "L. Spallanzani", University of Pavia, via Ferrata 9, 27100 Pavia, Italy; silvia.faravelli1@gmail.com (S.F.); federico.forneris@unipv.it (F.F.)
[5] Gastroenterology and Endoscopy Unit, Fondazione IRCCS Ca' Granda Ospedale Policlinico Milano, Via F. Sforza 35, 20135 Milan, Italy; flavio.caprioli@unimi.it
[6] Department of Pathophysiology and Transplantation, University of Milan, Via F. Sforza 35, 20135 Milan, Italy
[*] Correspondence: federica.facciotti@ieo.it
[†] Authors have contributed equally.
[‡] Authors have contributed equally.

check for updates

Abstract: Although antibody response to SARS-CoV-2 can be detected early during the infection, several outstanding questions remain to be addressed regarding the magnitude and persistence of antibody titer against different viral proteins and their correlation with the strength of the immune response. An ELISA assay has been developed by expressing and purifying the recombinant SARS-CoV-2 Spike Receptor Binding Domain (RBD), Soluble Ectodomain (Spike), and full length Nucleocapsid protein (N). Sera from healthcare workers affected by non-severe COVID-19 were longitudinally collected over four weeks, and compared to sera from patients hospitalized in Intensive Care Units (ICU) and SARS-CoV-2-negative subjects for the presence of IgM, IgG and IgA antibodies as well as soluble pro-inflammatory mediators in the sera. Non-hospitalized subjects showed lower antibody titers and blood pro-inflammatory cytokine profiles as compared to patients in Intensive Care Units (ICU), irrespective of the antibodies tested. Noteworthy, in non-severe COVID-19 infections, antibody titers against RBD and Spike, but not against the N protein, as well as pro-inflammatory cytokines decreased within a month after viral clearance. Thus, rapid decline in antibody titers and in pro-inflammatory cytokines may be a common feature of non-severe SARS-CoV-2 infection, suggesting that antibody-mediated protection against re-infection with SARS-CoV-2 is of short duration. These results suggest caution in using serological testing to estimate the prevalence of SARS-CoV-2 infection in the general population.

International Journal of
Molecular Sciences

MDPI

Review

Gut Microbiota Manipulation as a Tool for Colorectal Cancer Management: Recent Advances in Its Use for Therapeutic Purposes

Federica Perillo [1,†], Chiara Amoroso [1,†], Francesco Strati [1,*], Maria Rita Giuffrè [1], Angélica Díaz-Basabe [1,2], Georgia Lattanzi [1,2] and Federica Facciotti [1,*]

[1]   Department of Experimental Oncology, IEO European Institute of Oncology IRCCS, 20139 Milan, Italy; federica.perillo@ieo.it (F.P.); chiara.amoroso@ieo.it (C.A.); MariaRita.giuffre@ieo.it (M.R.G.); angelicajulieth.diazbasabe@ieo.it (A.D.-B.); georgia.lattanzi@ieo.it (G.L.)
[2]   Department of Oncology and Hemato-Oncology, Università degli Studi di Milano, 20135 Milan, Italy
*   Correspondence: francesco.strati@ieo.it (F.S.); federica.facciotti@ieo.it (F.F.)
†   These authors equally contributed.

check for updates

Abstract: Colorectal cancer (CRC) is a multifaceted disease influenced by both environmental and genetic factors. A large body of literature has demonstrated the role of gut microbes in promoting inflammatory responses, creating a suitable microenvironment for the development of skewed interactions between the host and the gut microbiota and cancer initiation. Even if surgery is the primary therapeutic strategy, patients with advanced disease or cancer recurrence after surgery remain difficult to cure. Therefore, the gut microbiota has been proposed as a novel therapeutic target in light of recent promising data in which it seems to modulate the response to cancer immunotherapy. The use of microbe-targeted therapies, including antibiotics, prebiotics, live biotherapeutics, and fecal microbiota transplantation, is therefore considered to support current therapies in CRC management. In this review, we will discuss the importance of host–microbe interactions in CRC and how promoting homeostatic immune responses through microbe-targeted therapies may be useful in preventing/treating CRC development.

Keywords: colorectal cancer; gut microbiome; live biotherapeutic products

Appendix VIII

OXFORD

JCC

Original Article

Immunological Variables Associated With Clinical and Endoscopic Response to Vedolizumab in Patients With Inflammatory Bowel Diseases

Marina Coletta,[a,†] Moira Paroni,[b,c,†] Maria Francesca Alvisi,[d]
Matilde De Luca,[d] Eliana Rulli,[d] Stefano Mazza,[a] Federica Facciotti,[e,©]
Georgia Lattanzi,[e] Francesco Strati,[e] Sergio Abrignani,[b,f]
Massimo Claudio Fantini,[g] Maurizio Vecchi,[a,h] Jens Geginat,[b]
Flavio Caprioli[a,h,©]

[a]Gastroenterology and Endoscopy Unit, Fondazione IRCCS Ca' Granda, Ospedale Maggiore Policlinico, Milan, Italy [b]Istituto Nazionale di Genetica Molecolare 'Enrica ed Romeo Invernizzi' [INGM], Milan, Italy [c]Department of Biosciences, Università degli Studi di Milano, Milan, Italy [d]Oncology Department, Istituto di Ricerche Farmacologiche Mario Negri IRCCS, Milan, Italy [e]Department of Experimental Oncology, IEO European Institute of Oncology IRCCS, Milan, Italy [f]Department of Clinical Sciences and Community Health, Università degli Studi di Milano, Milan, Italy [g]Department of Systems Medicine, Università di Roma Tor Vergata, Rome, Italy [h]Department of Pathophysiology and Transplantation, Università degli Studi di Milano, Milan, Italy

[†]MC and MP contributed equally to this paper.

Corresponding author: Prof. Flavio Caprioli, MD PhD, Department of Pathophysiology and Transplantation, Università degli Studi di Milano, Via F. Sforza 35, 20122 Milan, Italy. Email: flavio.caprioli@unimi.it and Dr Jens Geginat, Istituto Nazionale di Genetica Molecolare "Enrica ed Romeo Invernizzi" INGM, Via Francesco Sforza, 35, 20122 Milan, Italy. Email: geginat@ingm.org

Conference presentation: Digestive Disease Week 2019, San Diego, CA.

Abstract

Background and Aims: Vedolizumab [VDZ] is a monoclonal antibody directed against the $\alpha 4\beta 7$ integrin heterodimer, approved for patients with inflammatory bowel diseases [IBD]. This study aimed at identifying immunological variables associated with response to vedolizumab in patients with ulcerative colitis [UC] and Crohn's disease [CD].

Methods: This is a phase IV explorative prospective interventional trial. IBD patients received open-label VDZ at Weeks 0, 2, 6, and 14. Patients with a clinical response at Week 14 were maintained with VDZ up to Week 54. At Weeks 0 and 14, their peripheral blood was obtained and endoscopy with biopsies was performed. The Week 14 clinical response and remission, Week 54 clinical remission, and Week 14 endoscopic response were evaluated as endpoints of the study. The expression of surface markers, chemokine receptors, and $\alpha 4\beta 7$ heterodimer in peripheral blood and lamina propria lymphocytes was assessed by flow cytometry. A panel of soluble mediators was assessed in sera at baseline and at Week 14 by 45-plex.

Results: A total of 38 IBD patients [20 UC, 18 CD] were included in the study. At Week 14, the clinical response and remission rates were 87% and 66%, respectively. Higher baseline levels of circulating memory Th1 cells were strongly associated with clinical response at Week 14 [$p = 0.0001$], whereas reduced baseline levels of lamina propria memory Th17 and Th1/17 cells were associated with endoscopic response. Immunological clusters were found to be independently associated with vedolizumab outcomes at multivariable analysis. A panel of soluble markers, including IL17A, TNF, CXCL1, CCL19 for CD and G-CSF and IL7 for UC, associated with vedolizumab-induced Week 54 clinical remission.

Acknowledgements

The success of this PhD project did not depend exclusively on my efforts, but it relied on the help of many others.

I want to express my deep gratitude to my supervisor, Dr. Federica Facciotti, who gave me the opportunity to work in an extremely fascinating project. Besides that, I want to thank Federica for showing me how strong, passionate and enthusiastic someone can be and for always encouraging, supporting and critically questioning me. Thank you for pushing me to constantly improve my skills and my knowledge and for having trusted me since the beginning.

I want to thank all my colleagues who contributed to the work and helped me along this journey. A big thanks goes to Dr. Francesco Strati for all the critical discussions we had since the first day he arrived and for the constant support and all the invaluable advices he gave me. Thanks to all the other members of the Facciotti lab, present and past ones, for their team-work, their help and their real friendship.

Furthermore, I would like to thank our collaborators at the IRCCS Policlinico Ospedale Maggiore, Milan. The Surgery Unit and Prof. Luigi Boni, the Gastroenterology Unit and Prof. Flavio Caprioli, the Pathology Unit and Dr. Michele Ghidini of the Oncology Unit. I would like to thank also our collaborator at the Bios$^+$ Institute in Bellinzona, Prof. Giandomenica Iezzi for helping me in setting the *in vivo* orthotopical model of cancer. They were all essentials for the translational and clinical relevance of this project.

Moreover, I would like to express my appreciation to my PhD advisors: Prof. Peter J. Kuppen (Leiden University Medical Centre, Leiden) and Dr. Silvia Marsoni (FIRC Institute of Molecular Oncology, Milan). They supported me during these years with useful insights and valuable comments.

Finally, a big thank you to the Scellerati who shared with me these magical crazy years, to my friends and to my family who walked beside me along the way of this tortuous journey. Thank you for your continuous understanding, your loughs and your love.